Evolution of Late Cenozoic Minibasins and Growth Faulting, Green Canyon Area, Northwestern Gulf of Mexico

---

A Thesis

Presented to

the Faculty of the Department of Earth and Atmospheric Sciences

University of Houston

In Partial Fulfillment

of the Requirements for the Degree

Master of Science

By

Selin Akhun

May 2014

Evolution of Late Cenozoic Minibasins and Growth Faulting, Green Canyon Area, Northwestern Gulf of Mexico

_____

Selin Akhun

APPROVED:

_____

Dr. Michael A. Murphy

_____

Dr. Paul Mann

_____

Dr. Pete Emmet

_____

Dean, College of Natural Sciences and Mathematics

Evolution of Late Cenozoic Minibasins and Growth Faulting, Green Canyon Area, Northwestern Gulf of Mexico

---

An Abstract of a Thesis

Presented to

the Faculty of the Department of Earth and Atmospheric Sciences

University of Houston

In Partial Fulfillment

of the Requirements for the Degree

Master of Science

By

Selin Akhun

May 2014

ABSTRACT

The northern margin of the Gulf of Mexico has a complex geologic history involving growth faulting, the emplacement of allochthonous salt bodies and the evolution of small-scale Neogene depocenters overlying the mobile salt bodies (called ‘minibasins’). My study area is located in the northwestern Gulf of Mexico and lies along the continental shelf edge. The presence of salt welds on many seismic profiles indicates that high rates of sedimentation during the Pliocene and Pleistocene likely caused mobilization and complete evacuation of an allochthonous Miocene salt sheet. This movement is interpreted to have caused the formation of minibasins overlying the salt and many basinward-dipping growth faults in the study area.

I interpreted faults, salt structures and sedimentary rocks using high resolution seismic reflection data covering an area of 2,800 km^2 in the northwestern Gulf of Mexico. Throw-depth plots are created to clarify the growth history of selected faults. Time-structure maps were generated to understand salt-sediment-fault kinematic interaction. Finally, isopach maps were generated to understand the effect of faulting and salt movement in sediment thickness.

Three different fault families have been identified: (1) basinward-dipping growth faults family, (2) landward-dipping growth faults, and the (3) radial faults located within the sediments overlying rising salt diapirs. The observation that most of the faults sole into a salt structure implies that the kinematics of faulting and salt movement are linked. For

basin-bounding faults, I suggest that these faults formed in response to the salt flowage away from the center of the minibasin and that this flowage has led to syn-depositional, minibasin subsidence.

Time-structure maps indicate the presence of fault linkages and relay ramps along normal faults in the northern part of the study area which means that these faults are soft-linked and that they act as a system.

Interpreted seismic sections and time-structure maps show that salt flows both laterally or downdip so does not exhibit a primary flow direction. I conclude that the gentle slope of the continental shelf slope initiated salt flowage but sedimentary loading keeps the fault system active and is also the primary cause controlling salt evacuation in the study area.

ACKNOWLEDGEMENTS

I would like to express my gratitude to my supervisor Michael Murphy for the useful comments, remarks and engagement through the learning process of this master thesis. Furthermore I would like to thank my committee members Paul Mann and Pete Emmet who have willingly shared their precious time for providing me useful suggestions on the way.

To all my friends who have lent a hand to complete this thesis, especially to Ozbil Yapar for sharing this research experience with me.

The help of so many wonderful people and organizations mentioned and not mentioned here was instrumental to this research. I heartily thank everyone who directly and indirectly helped me in my research.

Finally my most important acknowledgments are towards my family who have been the single biggest motivating force in my life. I thank my beloved husband Suleyman, and my mother for their encouragement, my father who took the lead to heaven before the compilation of this work for his guidance and my dear sons Selim and Cihangir who enlighten my days with their precious smiles. This dissertation is dedicated to them.

Contents

CHAPTER 1: INTRODUCTION

1.1 Significance of the Study

Minibasins are a basin type commonly found in mobile salt environments, are generally sub-circular in shape, and only a few tens of kilometers in diameter. The term 'minibasin' was first used by Worrall and Snelson (1989) as they described the interaction between Cenozoic growth faulting and salt movement in the northern Gulf of Mexico basin. Minibasins form from sediment loading of an underlying, mobile salt layer (Shoup and Karlo, 1993). Jackson and Talbot (1991) refined the term "minibasin" as "a syn-kinematic basin subsiding into a relatively thick, allochthonous or autocthonous salt". In many cases, the downdip margin of minibasins are bounded by a counter-regional fault while the updip margin and sides are generally bordered by growth faults or salt domes and salt ridges, sometimes with strike-slip displacement. It is believed that most minibasin subsidence is a result of the density inversion caused by the loading of thick sedimentary fill although Hudec et al. (2009) have proposed that a density-driven mechanism might not be the only cause that triggers a minibasin to subside.

Minibasins are common features on the Louisiana shelf and slope that are critical for petroleum production because most of the major hydrocarbon traps are found in shelf minibasins (Sumner et al., 1991). Because of their structural, stratigraphic and economic importance, it is important to understand the evolution and interaction of minibasins with their mobile salt substrate and bounding fault systems.

This study focuses on minibasins, faulting and salt movement using 3D seismic seismic reflection data in the northwestern Gulf of Mexico near the continental shelf/slope boundary. This study is important because Plio-Pleistocene turbidites found in great thicknesses within minibasins provide the main producing reservoirs in this part of the Gulf of Mexico. Minibasin subsidence history also affects the maturity of possible hydrocarbon source rocks and the evolution of the bounding growth faults may impact the reservoir seals.

1.2 Geologic Setting of the Study Area

The Gulf of Mexico basin is a roughly circular basin that is 1600 km in diameter with shallow and intertidal areas (< 20 m deep) covering 38% of its area. The continental shelf (20-180 m) comprises 22% of its area, the continental slope (180-3000 m) comprises 20% of its area, and the abyssal areas (> 3000 m) constitute the its remaining 20% of area (Gore, 1992). The modern shelf edge, as shown by a pronounced increase in its basinward gradient, generally occurs at a water depth of 100–120 m.

The tectonic evolution of the Gulf of Mexico began with intracontinental rifting between the Yucatan block and North America in the Middle Jurassic. (230 Ma, Salvador, 1991). During late Callovian-early Oxfordian time, intermittent flooding of seawater into the low-lying rifted area caused the formation of extensive salt deposits known as Louann salt. The absence of major rivers emptying to these restricted salty areas and the presence of arid to semi-arid climate in the area were additional causes for the deposition of the salt

at the base of the Gulf of Mexico stratigraphic section (Salvador, 1991). Deposition of salt in the rift basin occurred before the advent of seafloor spreading (Bird et al., 2005) and continued until the Kimmeridgian. Following the restricted marine conditions, an increasingly large and deep body of water with normal salinity replaced the shallow hypersaline water bodies from which the thick Callovian salt sequence was produced (Salvador, 1987). Continental rifting in the basin lasted about 70 my and resulted in anti-clockwise rotation of the Yucatan block. The opening of the basin took place during the counterclockwise rotation of the Yucatan Peninsula block away from the northern Gulf of Mexico. The timing of the onset of this rotation is thought to be late Callovian-early Oxfordian. This rotation and southward movement of the Yucatan block caused regional extension and initiated the 'drift' or passive margin stage of the basin margins along with the formation of a central band of oceanic crust formed during the Kimmeridgian (Salvador, 1991). Rifting resulted in the splitting of the Louann salt deposits in two parts now located in the US part of the northern gulf and in the Mexican part of the southern gulf (Buffler and Thomas 1994) (Fig. 1.1).

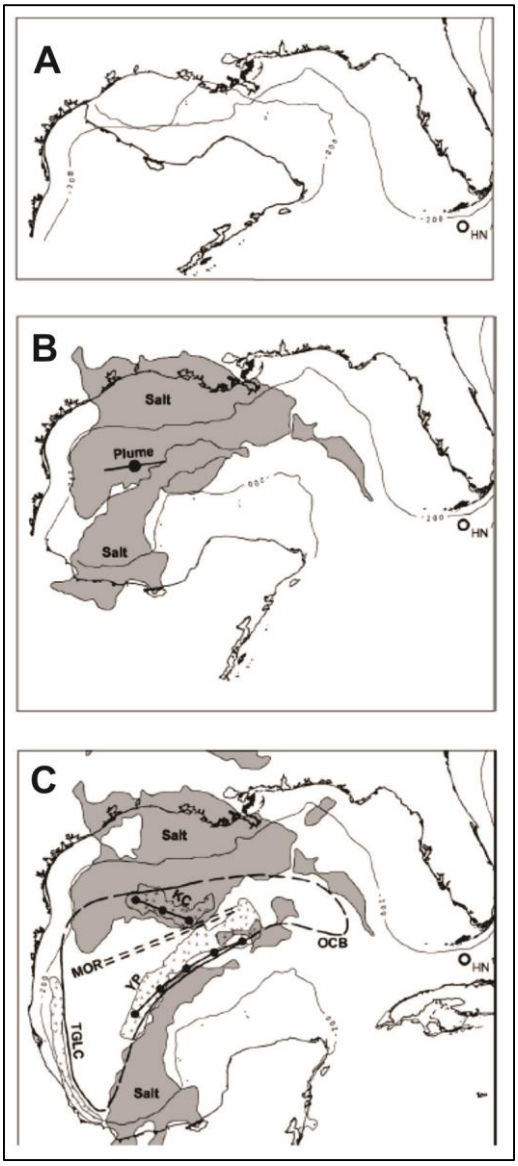

Figure 1.1: A. Initial Jurassic pre-rift position of Yucatan Peninsula; B. Jurassic rotation, continental crust extension and seafloor spreading; C. Rotation and present position achieved (from Bird et al., 2005).

By the cessation of seafloor spreading in Berriasian time, the Yucatan platform had reached its present-day position. Total subsidence of 5-7 km in the basin resulted from subsidence caused by crustal stretching, cooling of oceanic crust and sedimentary loading (Sawyer et al., 1991). The current 10-20 km basement depth below sea level of the crust

was attained by the sedimentary loading which continued through the Holocene (Galloway, 2008).

During the stable tectonic conditions of the Cretaceous and Cenozoic, sediment loading stimulated the movement of Louann salt and the development of growth fault systems bounding major depocenters. In the northern parts of the Gulf Coast, the tilting of Upper Jurassic evaporites by the end of the Late Cretaceous gave rise to the large-scale downslope movement of the salt by gravity and the formation of the first salt diapirs. The movement of the salt during the Middle and Late Eocene caused the formation of a large salt sheet covered by a thick sequence of terrigeneous sediments. During Miocene, the terrigeneous sediments' depocenters moved to the Louisiana sector of the continental margin and this shift caused the formation of a new salt sheet that covered a large area of the shelf and continental slope. An increasing amount of sediment accumulation gave rise to the creation of diverse salt structures at the Miocene/Pliocene boundary about 5 Ma (Konyukhov, 2008).

Tectonic stability resulted in the persistence of the environments of deposition and the lithologic composition of the passive margin sedimentary sequence from the late Jurassic to present. According to Salvador (1991) three lithofacies provinces can be identified in the Gulf of Mexico, and they correspond to the following depositional environments; (1) in the Florida and Yucatan platforms, carbonates and lesser amounts of evaporites predominate the sedimentary section, (2) in the area of the Isthmus of Tehuantepec and in east-central Mexico, carbonates and fine-grained terrigeneous clastics are the most important deposits, and also lesser amounts of coarse grained clastics exist in

the Miocene successions, and (3) from northeastern Mexico to Alabama, including Texas-Louisiana continental slope and continental shelf, coarse-grained terrigeneous clastics are dominant and signify the importance of the large fluvial systems that drain into the northern part of the Gulf of Mexico.

Eight large river systems controlled the sedimentation in the Louisiana continental shelf and slope in the area of my study area: the Norma, Rio Grande, Carriso, Corsar, Houston, Red River and Central and Eastern branches of Mississippi River (Konyukhov, 2008). The Mississippi River provided the major source of terrigeneous clastics since Late Jurassic (Bryant et al., 1991) along with the Red River and Tennessee Rivers (Galloway et al., 2011).

During the Cenozoic the large volume of terrigeneous clastic sediments entering to the basin from north and west changed the structural and stratigraphic framework of my area. The vast sediment volumes resulted in rapid basinward migration of shoreline deposition across the shelves (Galloway et al., 2011) (Fig. 1.2). Large loads of coarse-grained clastics deposited on an unstable base of abnormally pressured salt are responsible for downslope salt movement. This movement deformed sediments above the salt and initiated the listric normal faults in the continental shelf. Evacuation and advance of salt sheets also created accommodation space in the form of minibasins on the shelf and slope areas (Fig. 1.3).

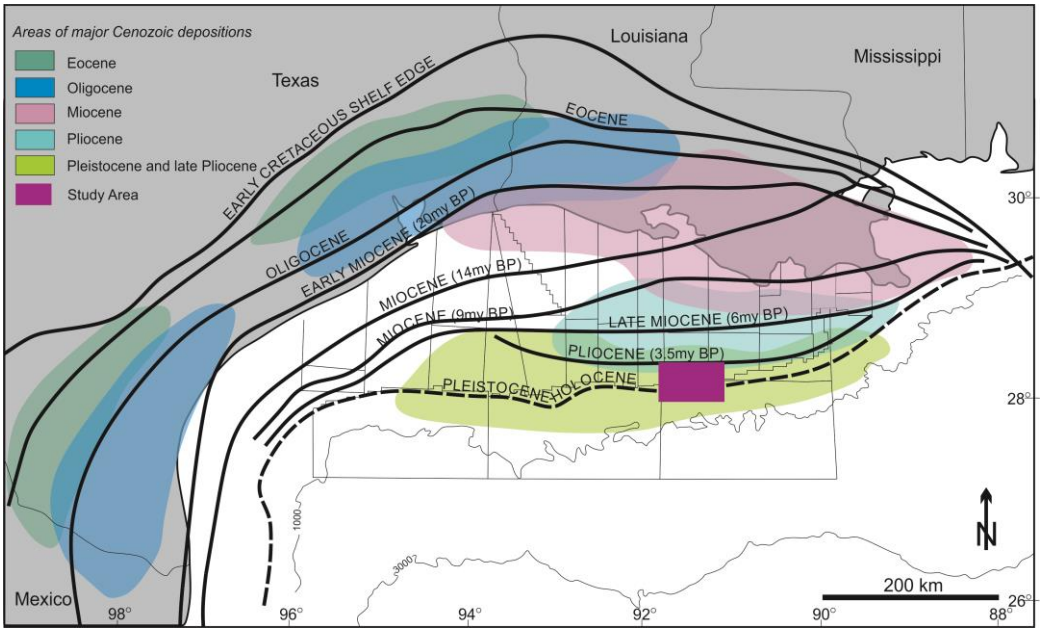

Figure 1.2: Paleoshelf edges in the Northern Gulf of Mexico basin, distribution of major Cenozoic depocenters, and location of study area (purple box) (modified after Martin, 1977, and Galloway et al., 2011).

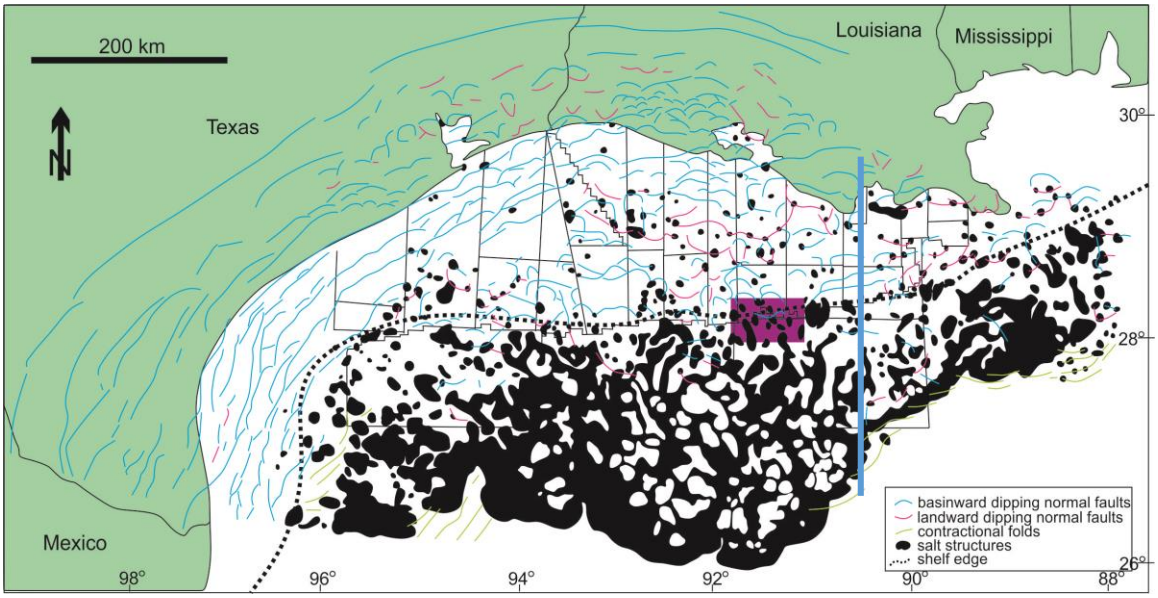

Figure 1.3: Tectonic map of the northern Gulf of Mexico (modified after Diegel et al., 1995). Purple area shows the location of my thesis study area straddling the shelf break (dotted line)**.** Note that most salt has been evacuated from north of the shelf break by sediment loading of the shelf.

1.3 Depositional Environment and Facies

Pleistocene depositional history in the study area are dominated by three major rivers: Red, Mississippi and Tennessee (Fig. 1.4). Through time, Mississippi became the only sediment source as Tennessee and Red rivers changed their axes and were captured by the incised Mississippi valley (Fig. 1.5). The primary agent that reorganized the drainage system of North America during Pleistocene period were mountain glaciers and the continental ice sheet (Galloway et al., 2011). Moreover, the study area is locally influenced by subsurface salt deformation that influenced the spatial and temporal distribution of lithofacies (Rowan and Weimer, 1998).

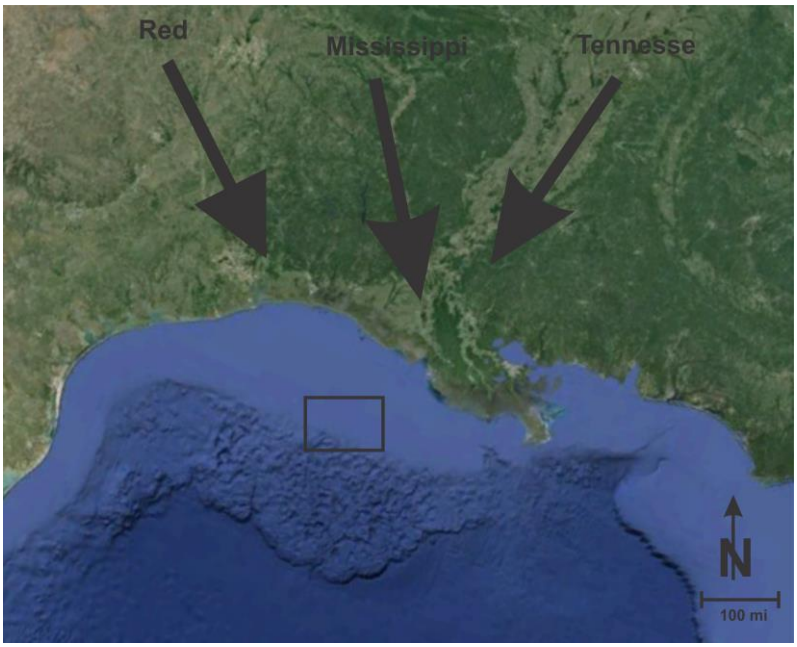

Figure 1.4: Three important rivers that provide sediments to the study area. The Red and Tennessee Rivers were captured in the offshore area by the Mississippi River's incised valleys.

Depositional phases in the study area can be divided in three different phases: (1) prodelta phase, (2) proximal phase, and (3) fluvial phase. The prodelta is situated beyond the delta front and its facies includes bathyal and outer neritic shales and turbidites, Also distal deltaic sands are deposited during the prodelta phase in the study area. During the proximal deltaic phase, mainly shelf margin delta-derived sand, silt and clay are deposited. During the fluvial phase shallow-marine deltaic and fluvial sands and neritic shales are deposited during sea level rise.

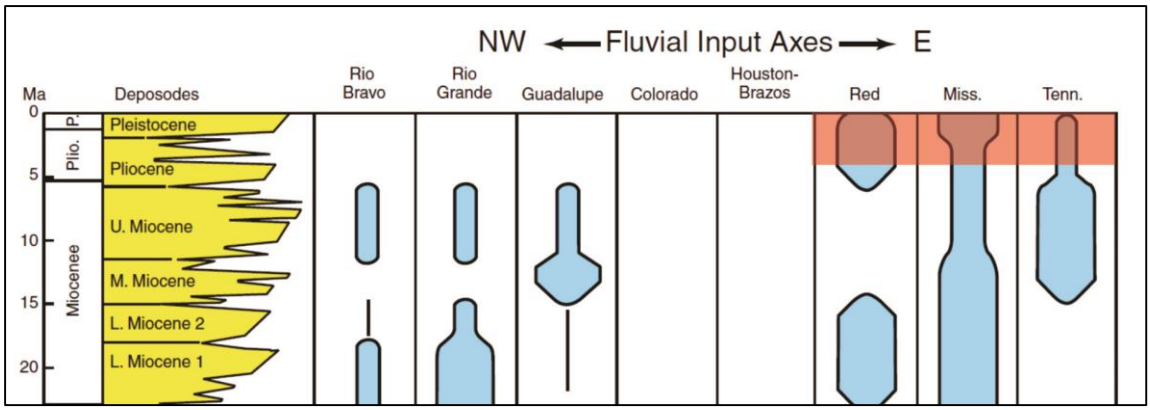

Figure 1.5: Basin fluvial input axes of Gulf of Mexico. Last three rivers (Red, Tennessee and Mississippi) are responsible for the sediment supply in the study area. The width of the blue bar indicates the relative contributions of the rivers from the late Miocene to Pleistocene (modified from Galloway et al., 2011).

Two transgressive surfaces and one high amplitude event were mapped in order to understand the evolution of the study area. The high amplitude event is the youngest surface and older transgressive surfaces are Plac A, Plac B with ages of 0.46 and 0.65 Ma, respectively. The surfaces are named after the index fossils found in these transgressive shale sections (Alexander and Fleming, 1995). A stratigraphic column was created using

the transgressive surfaces defined by Alexander and Flemings (1995) and five gamma ray logs located in the study area (Fig. 1.6). Five well logs are provided from OWL 7 Database (Table 1.1).

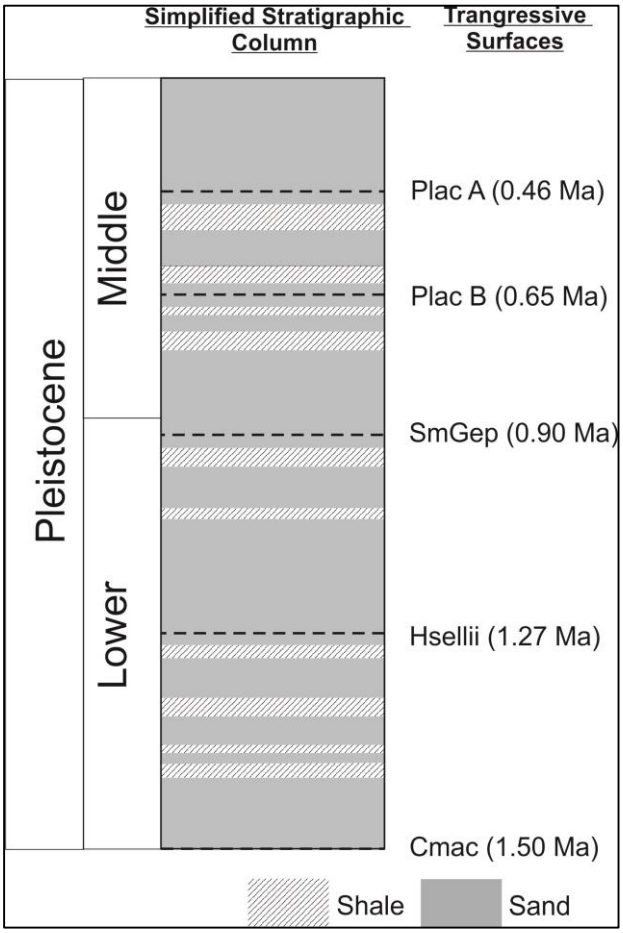

Figure 1.6: Simplified stratigraphic column of the study area. Transgressive surfaces are used to interpret seismic cross sections and generate isopach and time-structure maps.

Table 1.1: Well and well log types used in this study. Well data are provided from OWL 7 Database

Well (Lease Block Name-Block Number)	Well Log Type
EW 977	Gamma Ray
EI 386	Gamma Ray
GC 50	Gamma Ray
GC 95	Gamma Ray
GC 99	Gamma Ray

1.4 Study Area

The study area is situated in northern Gulf of Mexico and straddles the shelf break separating the Louisiana continental slope and shelf. The Texas Louisiana shelf width ranges from 32 to 90 km and is deeply incised by Wisconsinian age channels now filled with sediments. The large amount of sediment caused the shelf to be faulted and the underlying salt to be remobilized as salt diapirs (Bryant et al., 1991). The Texas-Louisiana slope is bordered by the shelf break to the north and by Sigsbee Escarpment on the south. The bathymetry of the slope is highly dominated by salt activity and the salt activity give rise to formation of complex faults on the slope (Ewing, 1991). The morphology of the area is controlled by sea-level fluctuations during the Pleistocene, the high rate sedimentation of the Mississippi, Red and Tennessee Rivers, and deformation related with salt movement. This complex situation gave rise to unusually thick sediment accumulation (Coleman et al., 1991; Galloway et al., 2011).

The study area includes southern part of Eugene Island, Ewing Bank and northern part of the Green Canyon area with detailed bathymetric maps of the study area showing water depths of 100 to 700 m (Fig. 1.7). According to Diegel et al. (1995) tectonostratigraphic provinces, the study area lies at the boundary of the Pliocene-Pleistocene detachment and Tabular Salt Minibasin provinces (Diegel et al., 1995) (Fig. 1.7, 1.8). Pliocene-Pleistocene detachment province is dominated by salt withdrawal fault systems where organized or disorganized growth faults are soling into a salt weld which has been described in previous studies in other areas as a characteristic discontinuous, high-amplitude zone of seismic reflections caused by remnant salt preserved along the welds (Jackson and Cramez, 1989). Basinward-dipping listric growth faults sliding on the salt welds carries a large amount of extension on the outer shelf and this extension is compensated by the withdrawal of underlying, tabular salt that was originally present near seafloor (Diegel et al., 1995).

The tabular Salt-Minibasin province is bounded by Sigsbee Escarpment to the south and by Louisiana shelf margin on the north (Fig. 1.7). The location and bathymetry of the slope is highly influenced by the salt tectonics and large amount of sedimentary loading: for example, there is little salt beneath the continental shelf because it has been evacuated by sediment loading. Allochthonous salt sheets evacuated from beneath the shelf now underlie the slope and abyssal plain. The dominant features of the Louisiana slope are minibasins that are surrounded by isolated salt bodies and/or arcuate growth fault systems (Fig. 1.7). In general, minibasins bounded by growth faults dominate the upper slope while minibasins bounded by isolated salt bodies controls the lower slope (Diegel et al., 1995).

The study area is dominated by: (1) growth faults activated by the gravity-driven deformation as the sedimentary overburden spreads under its own weight and slides basinward on salt detachments (e.g., Jackson and Galloway, 1984; Worrall and Snelson, 1989; Wu et al., 1990; Diegel et al., 1995; Peel et al., 1995), (2) complex salt bodies with variable morphology which are believed to be the parts of an allochthonous salt sheet that was remobilized in the latest Miocene (West, 1989; Seni, 1992; Rowan, 1993), and (3) minibasins with different geometries and having Plio-Pleistocene thickness up to 6000 m (Rowan, 1993).

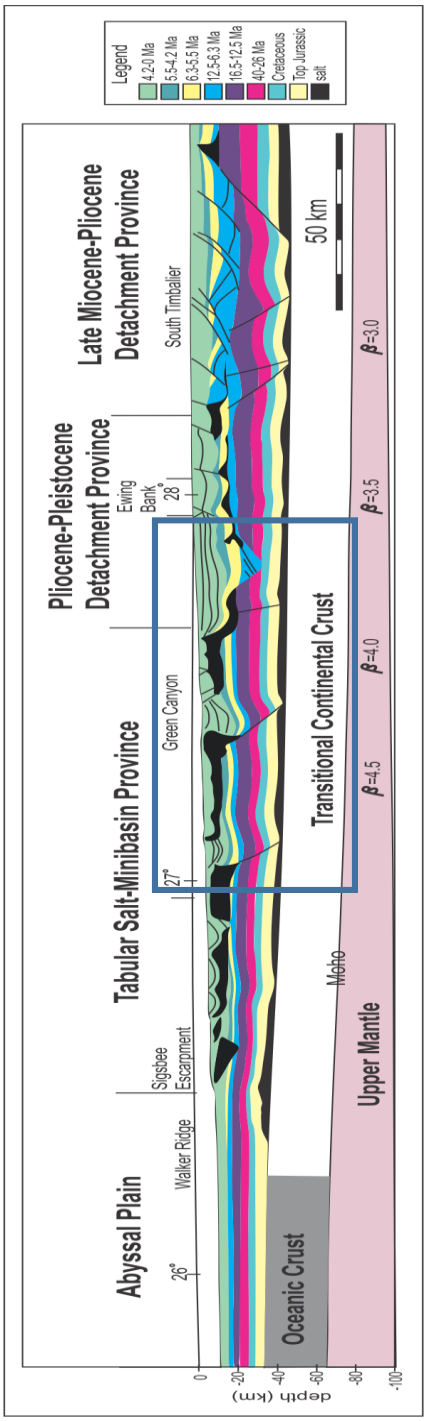

Figure 1.7: N-S regional depth cross section across the northern Gulf of Mexico basin from abyssal plain to Late Miocene-Pliocene detachment province. The study area lies between Tabular Salt-Minibasin province and Pliocene-Pleistocene detachment province (map modified and simplified after McBride 1998) (blue box represents the location of the study area) (the location of the profile is given in Fig. 1.3 (blue line)).

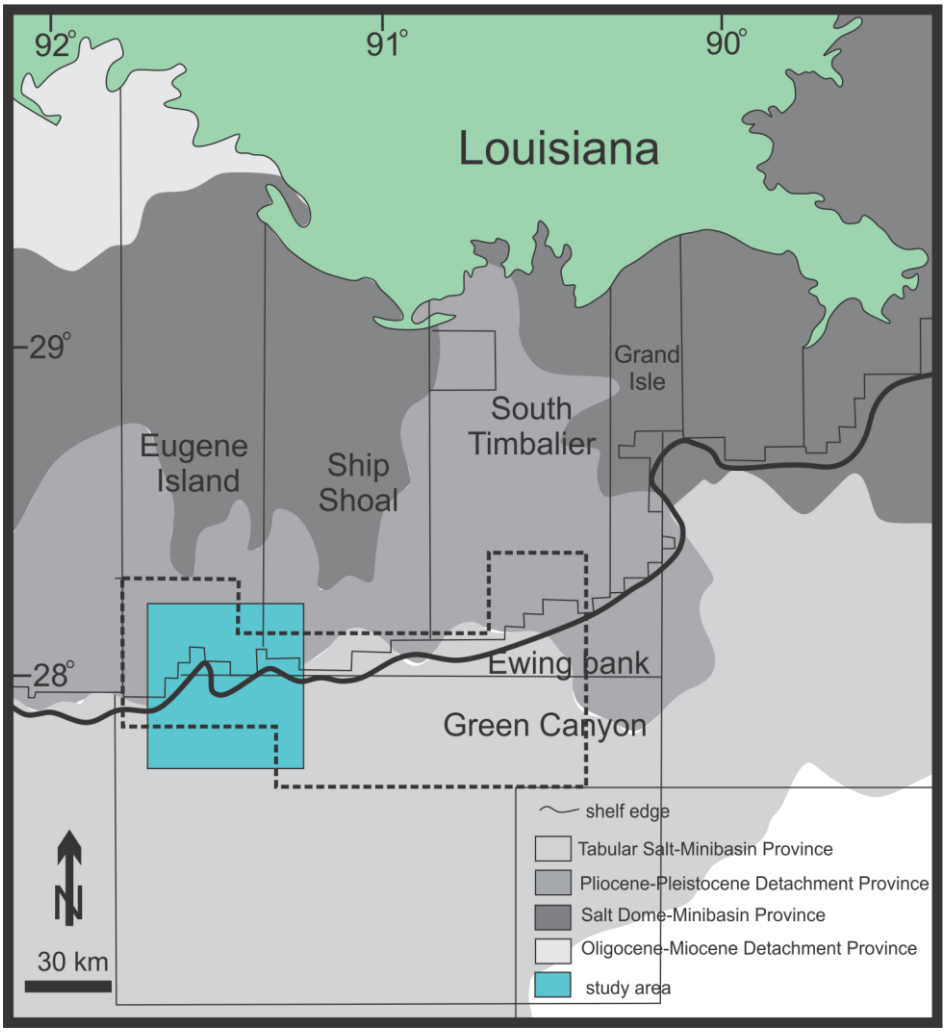

Figure 1.8: Regional map showing tectonostratigraphic provinces defined by Diegel et al., 1995 and the location of the study area (shown in blue). The dash line represents the study area of Alexander and Flemings, 1995 and Rowan and Weimer, 1998).

1.5 Previous Studies of the Thesis Area

Eugene Island and Green Canyon are among the most studied areas in Gulf of Mexico after the discovery of the giant Eugene Island Field 330 in 1971. The presence of a mobile salt substrate, high sedimentation rates related to the presence of large river systems, and growth faulting on both the shelf and slope (Fig. 1.7) make the study area a

natural laboratory to study the causal relationships between structure and sedimentation. Lack of active, crustal tectonic activity isolates the effects of basinward, gravity-driven movements.

Rowan, (1993) described a method for the sequentially restoring cross sections in areas of salt-related deformation and applied this technique to an interpreted seismic profile from the eastern Green Canyon/Ewing Bank area. He suggested that the subsidence is 1760 m over the last 5.5 Ma; the rate of subsidence was not constant during this time interval in Ewing Bank-Green Canyon area; the net measured extension is 16.4 % in the study area; and that the area of salt is decreased by 27 %.

Diegel et al., (1995) divided northern Gulf of Mexico basin into eight different regions to explain the complex Cenozoic structural evolution. Following Diegel et al. (1995), the current study area lies between Tabular Salt Minibasin and Pliocene-Pleistocene detachment provinces. Rowan and Ratliff, (2012) summarized the historical development of ideas, methods and applications of restoration in salt basins using cross sections from Louisiana coast and deepwater Gulf of Mexico to explain potential pitfalls of this method. Alexander and Flemings, (1995) documented the spatial and temporal distributions of reservoir sands within the context of an evolving Pliocene-Pleistocene salt-withdrawal shelf minibasin. They concluded that the stacking pattern and geologic evolution of the minibasin appear to be similar to that in other Gulf of Mexico minibasins formed by progradational deltaic deposition above a mobile salt substrate.

In their stratigraphic study, Weimer et al. (1998) described Pliocene-Pleistocene turbidite systems in Green Canyon and Ewing Bank areas and found that sand supply in minibasins is controlled by abrupt decreases in the bathymetric gradient. Rowan and Weimer (1998) concluded that there is a reciprocal relation between sedimentation and salt deformation in the northern Gulf of Mexico. Using palinspastic and depositional environment maps, they suggested four different types of minibasins based on different stacking patterns of tectonostratigraphic packages: (1) BW_lL: deep bowl overlain by a landward-thickening wedge and then a layer, (2) BW_bL: a deep bowl overlain by a basinward-thickening wedge and then a layer, (3) W_lL: adjacent landward-thickening wedges overlain by a layer, and (4) TW_bL: a deep trough overlain by a basinward-thickening wedge and then a layer.

Rowan et al. (1998) evaluated the evolution and geometry of a minibasin-bounding growth fault array and distinguished three different types of faults: (1) growth faults with throw increasing downward, (2) compensation faults with closed tip lines, and (3) composite faults combining elements of both growth and compensation faults. They highlighted the presence of isolated faults linking with basin-bounding growth faults in the Eugene Island 330 field.

In their structural study, Rowan et al., (1999) classified extensional, contractional and strike-slip faults in the northern Gulf of Mexico. They suggested that the fault families and fault welds are kinematically linked to one another during basinward translation, basin subsidence into the underlying salt layer, or folding.

McBride (1998) utilized a 590-km-long cross section across the north-central Gulf of Mexico basin from east-central Louisiana to the abyssal plain to illustrate the complex history and relation of sedimentation and salt movement. He concluded that the deformation history is mainly controlled by gravity and the progradation of Cenozoic sediments over mobile salt. After sequential restoration of cross sections in Ewing Bank and northern Green Canyon areas, McBride et al., (1998) stated that salt movement creates space for continued sedimentary loading and that the absorption of much extension and contraction is accommodated by the geometry of salt body which is continuously changing. Yapar, (2013) used the northern part of the same data set I am using to investigate the interaction between faulting, salt and sedimentation. He concluded that salt movement and faults are kinematically linked in his study area.

1.6 Objectives of this Thesis

The complex interaction of salt tectonics with sedimentation and faulting in the northwestern Gulf of Mexico produced a variety of structural styles that control differing depositional environments. The overall objective of this study is to understand the relationship between salt movement, sediment accumulation in overlying minibasins, and faulting because minibasins are high-fidelity recorders of these structural processes. The following are the specific objectives addressed in this research:

1. Define regional and local fault systems related to salt movement during the period from late Pleistocene to present;

2. Analyze in detail the kinematic evolution of the salt layer and overlying faults and basins through interpretation of faults and growth strata in the study area. Construction of fault maps at different depth help to understand how faults and basins change with depth;
3. Investigate the spatial, temporal, and causal relationships between faults, mobile salt bodies and minibasin strata. Do faults allow sedimentation, does sedimentation allow faulting, does salt movement allow sedimentation, and does sedimentation trigger salt movement?

1.7 Methods and Workflow

Figure 1.8 summarizes the workflow used in this study. Data loading and preparation is the first step in order to interpret seismic time-depth cross sections and time slices. Secondly, seismic interpretation is performed for faults, horizons and salt. Finally, maps are generated in order to understand the relation between salt movement, faulting, and minibasin formation.

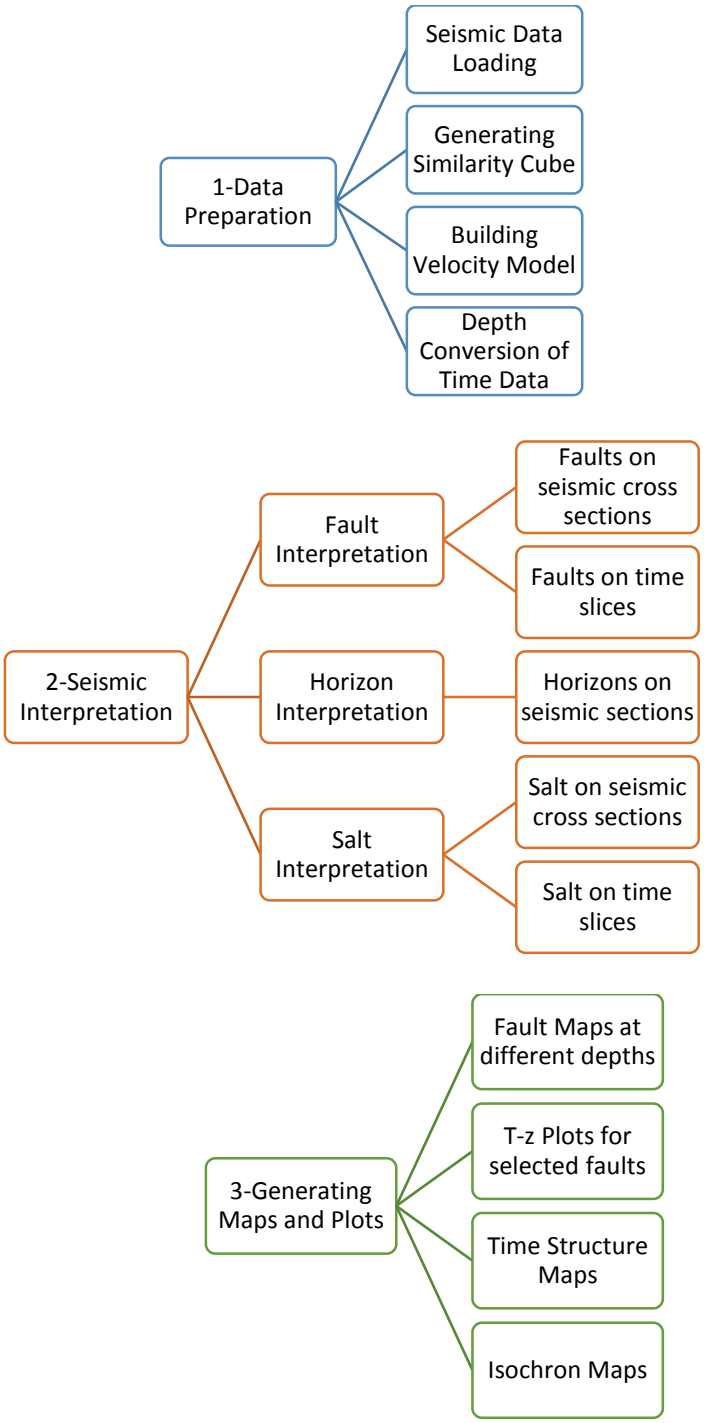

Figure 1.8: The workflow followed during the study. Seismic data is interpreted using both time slices and cross sections and four different type of maps were generated in order to understand the evolution in the study area.

CHAPTER 2: DATA AND METHODOLOGY

2.1 Seismic Data and Wells Used in the Study

The 3D seismic dataset used for this study includes the northeastern portion of an approximately 8000 km^2 Kirchhoff prestack time migrated seismic survey acquired by Petroleum Geo-Services (PGS) in 1995-1996 and kindly provided by PGS for research purposes to the University of Houston. The record time is 12 seconds two-way travel time with a sample rate of 4 milliseconds (ms) but only 8 seconds of data are used for this study. The vertical resolution is 3 m near the surface with a dominant frequency of 50 Hz and 150 m at 6400 m with a dominant frequency equal to 12 Hz. The lateral resolution is approximately equal to the inline and crossline spacing of 25 m and 37.5 m respectively. The acquisition parameters are summarized below:

Table 2.1. Acquisition parameters of the study area

Acquisition Parameters	
Shooting directing	E-W
Configuration	2 sources-3 streamers
Maximum offset	6000 m
Channels	240
Shotpoint interval	31.25 m per array
Group interval	25 m
CMP bin dimension	12.5 x 40 m
Nominal fold	48

The horizons were interpreted using paleontological data obtained from the website of the Bureau of Safety and Environmental Enforcement (http://www.bsee.gov/) along with published work in the area by Alexander and Flemings (1995) and Rowan and Weimer (1998). The seismic amplitude cube was used to interpret horizons and generate fault heave maps. Another usage of the amplitude cube was to locate minibasins in the study area. A similarity cube was generated according to the seismic data frequency spectrum and was used to locate and map faults and salt diapirs in the study area (Fig. 2.1). The similarity attribute is a useful attribute to use to locate faults and channel because it is sensitive to discontinuities.

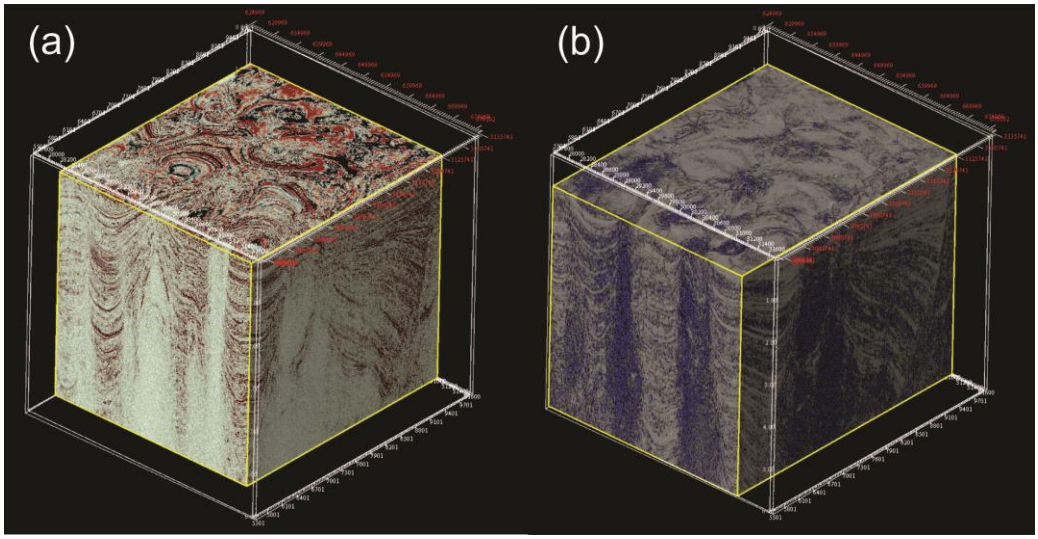

Figure 2.1: (a) Amplitude cube used to map horizons and generate fault heave maps, (b) similarly cube used to map faults and salt diapirs (seismic data cube provided courtesy of PGS).

2.2 Time to Depth Conversion

The accuracy of fault maps is essential for any fault study like this one. To perform displacement measurements, seismic data was converted from travel time to depth. Depth conversion in this study is carried out using velocity surveys retrieved from the Bureau of Safety and Environmental Enforcement web site (http://www.bsee.gov/) and 35 velocity wells are used to generate linear velocity function of the study area (Figs. 2.2 and 2.3). The velocity function is best constrained for depths shallower than 3 km, where most of the interpretation of the seismic cube was concentrated.

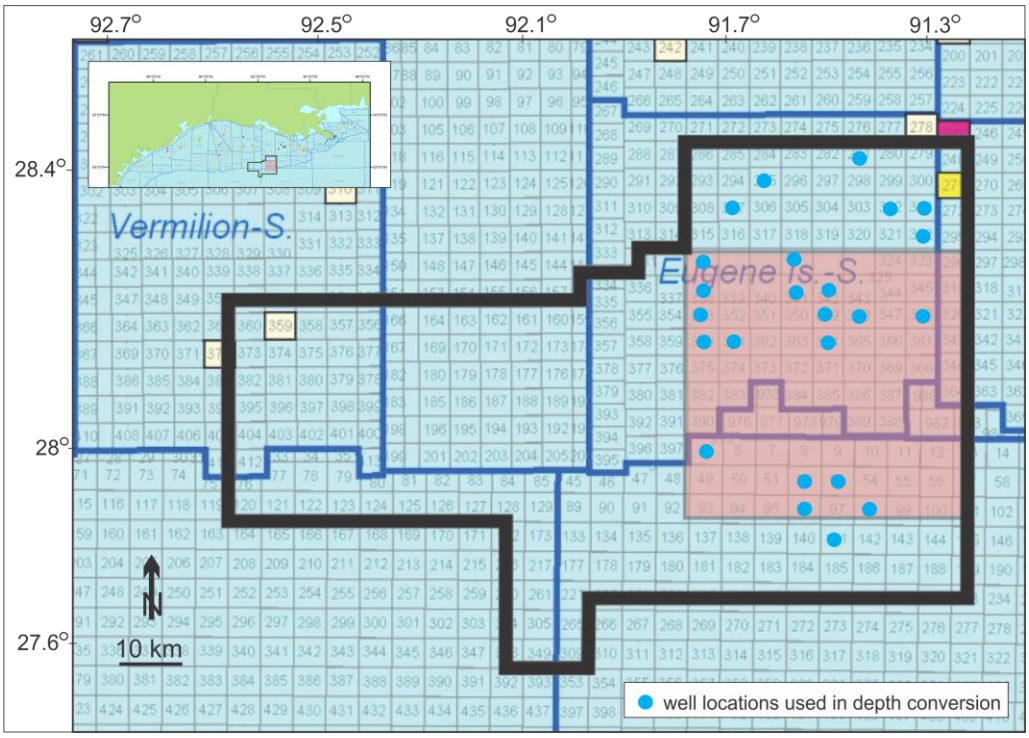

Figure 2.2: Location of the seismic data and well locations used in depth conversion (pink area represents the part of the seismic data interpreted for this study).

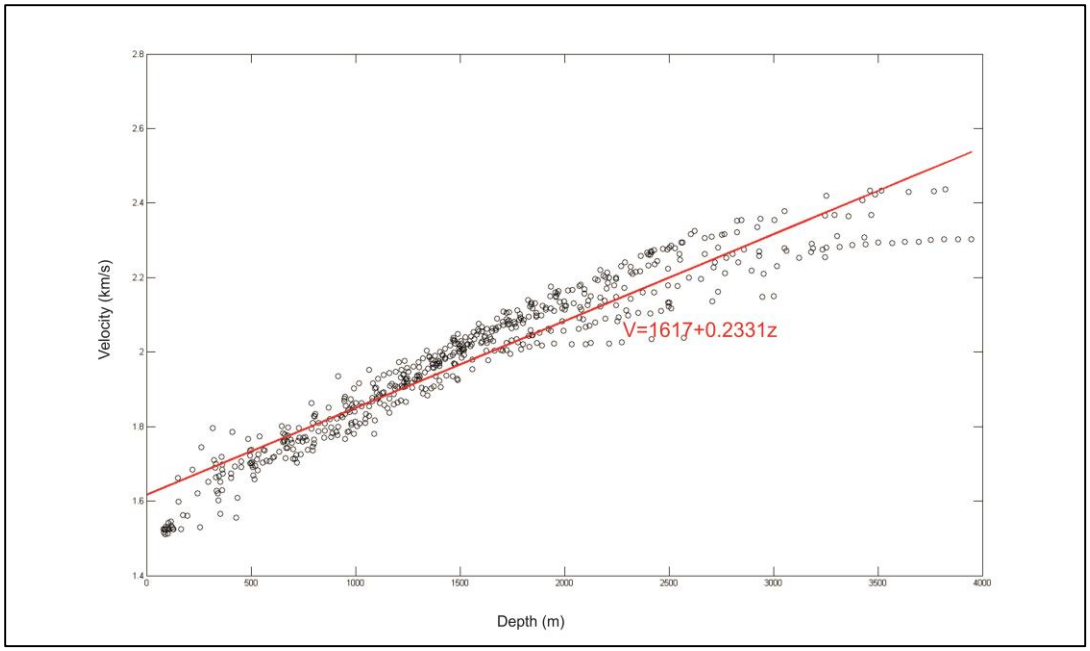

Figure 2.3: Linear velocity function of the study area retrieved from 35 different velocity surveys.

CHAPTER 3: INTERPRETATION

3.1 Faults

3.1.1 Fault Interpretation in Map View

The study area has a complex fault distribution. Thirty faults are mapped using IHS Kingdom Suite software on similarity attribute time slices. First, the seismic cube is used to identify faults in cross sections and similarity time slices are interpreted to generate a fault map of the study area. In addition to fault map generation, similarity time slices provide information about the accuracy of fault interpretation because the similarity attribute is sensitive to discontinuities. Similarity time slices are generated for slices at 0.5 sec, 0.7 sec, 0.9 sec and 1.1 sec to see the continuation of faulting with depth.

Faults are analyzed in map view for the four different time slices mentioned above. In the time slice at 0.5 sec, forty faults are interpreted (Fig. 3.1). In the time slice at 0.7 sec, forty-one faults are interpreted (Fig. 3.2). In the time slice at 0.9 sec, forty four faults are interpreted and finally in the time slice at 1.1 sec, forty six faults are interpreted (Figs. 3.3, 3.4).

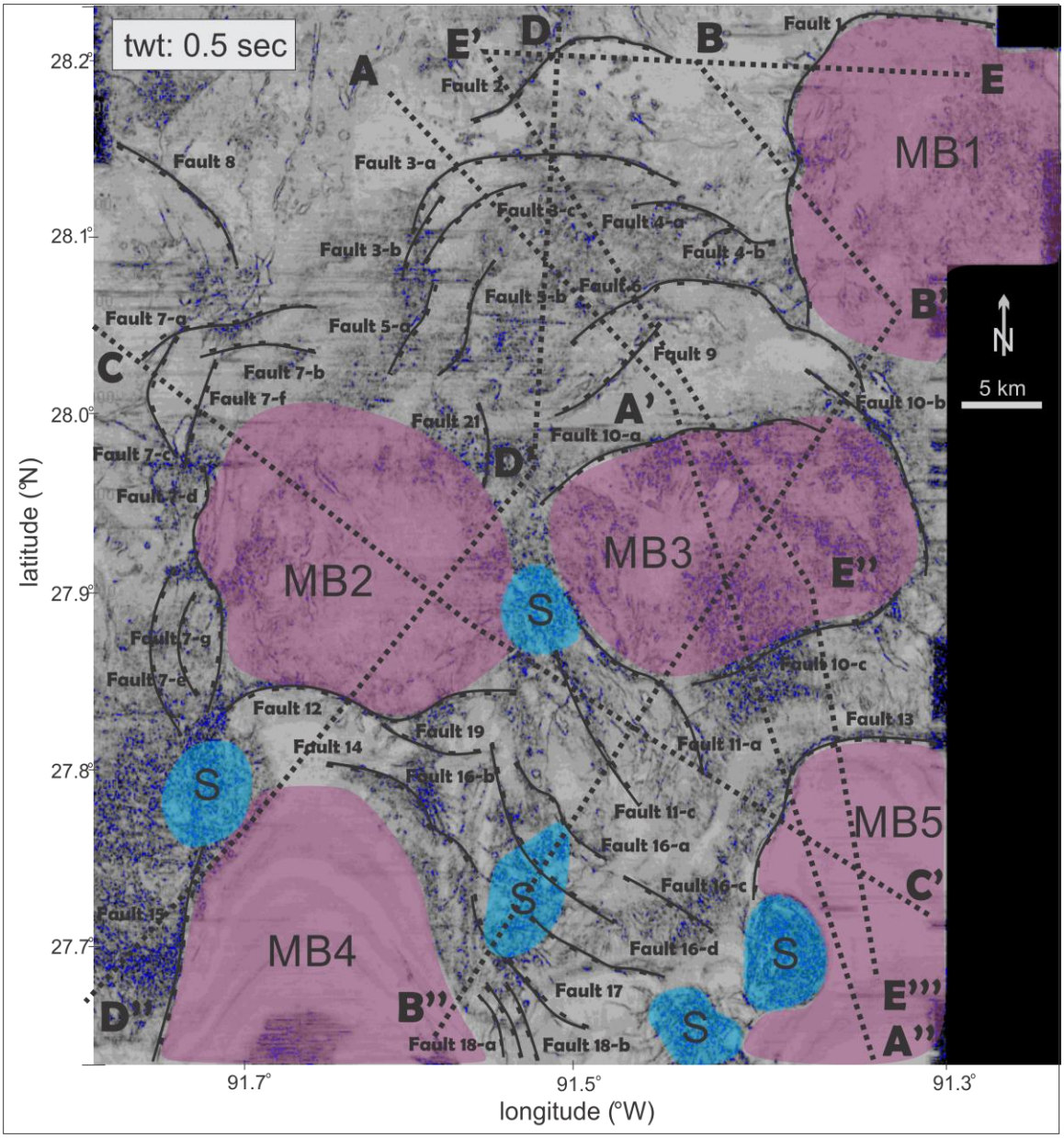

Figure 3.1. Fault map of the study area at 0.5 sec. in the similarity cube. Pink areas are minibasins and blue areas salt diapirs. Dashed lines are the location of interpreted seismic cross sections. Blue reflections are either salt bodies or sand deposited in a high-energy environment.

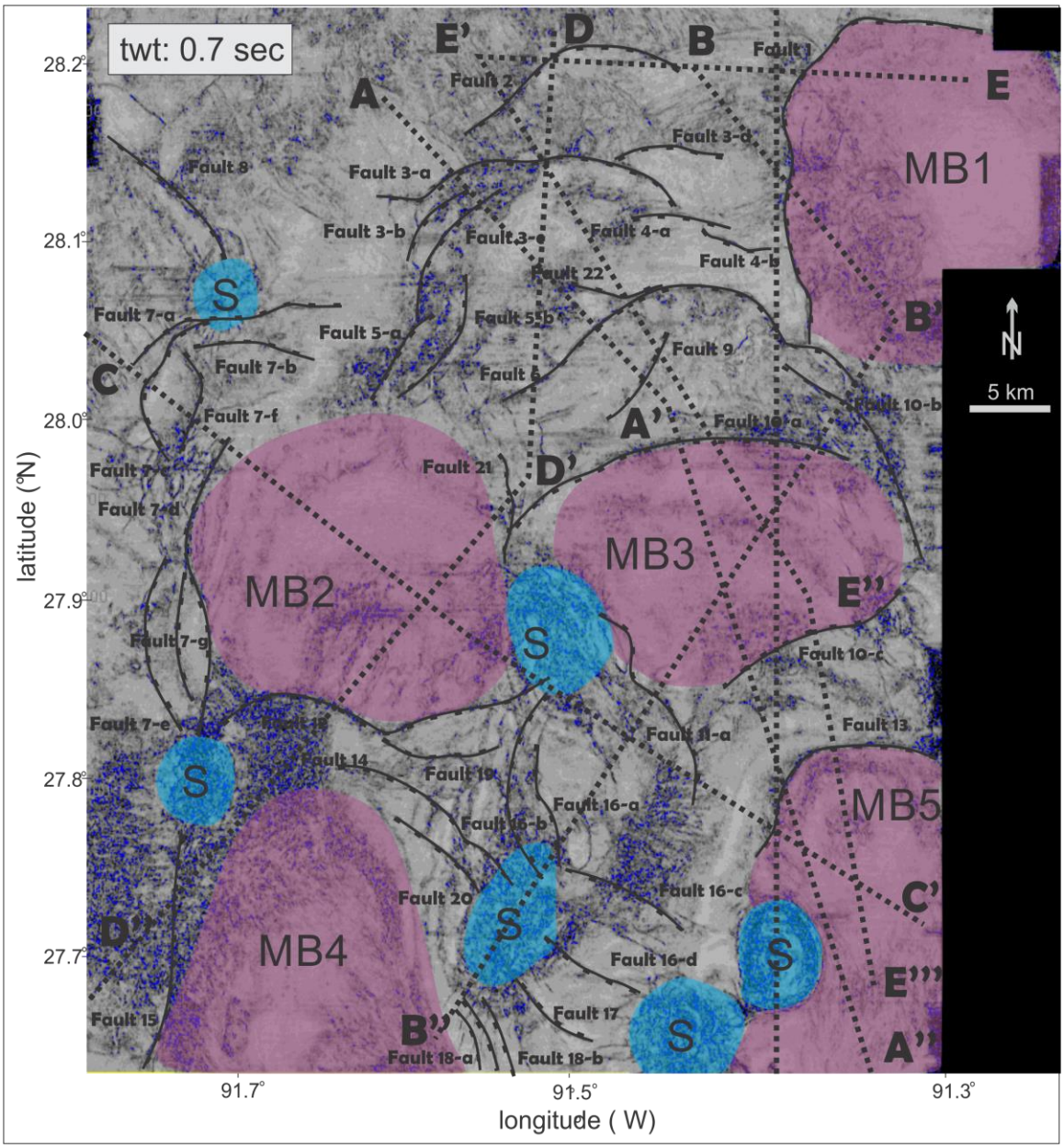

Figure 3.2. Fault map of the study area at 0.7 sec in the similarity cube. Pink areas are minibasins and blue areas are salt diapirs. Dashed lines are the location of interpreted seismic cross sections.

Fault 1, Fault 7-d, Fault 10-a, Fault 10-b, Fault 10-c, Fault 12, Fault 13 and Fault 15 are basin-bounding faults. Fault 10-c is a north-northwest-dipping listric normal fault. Fault 7-d separates Minibasin 2 and Minibasin 4 so it is a basin-bounding fault for both minibasins. The rest of basin-bounding faults are arcuate, listric growth faults (Fig. 3.1-4) that dip basinward (Fig. 3.1-4).

Fault 3-a, Fault 3-b, Fault 3-c, Fault 4-a, Fault 4-b, Fault 5-a, Fault 6 and Fault 22 are basinward-dipping, listric growth faults that are soling into an allochthonous salt layer (Fig. 3.1-4). These faults are called a 'roller fault family' after Rowan et al., 1999. In map view, the strike of roller faults are roughly parallel to the regional strike of the slope and they form elongate arrays even though single faults are locally more arcuate in map view (Fig. 3.1-4).

Fault 2 is an arcuate south-southeast-dipping normal fault. Fault 8 is a southwest-dipping normal fault. Fault 7-a and Fault 7-b are north-northwest-dipping normal fault. Fault 7-c and 7-f are east-dipping, arcuate normal faults. Fault 7-d is dipping west and Fault 7-e and Fault 7-g are dipping east and they form a small graben with Fault 7-d near Minibasin 2 (Fig. 3.1-4).

Fault 11-a is a southwest-dipping normal fault. Fault 11-b and Fault 11-c are northeast-dipping normal faults and both are counter-regional faults. Fault 11-a and Fault 11-b create a graben at the southwestern edge of Minibasin 3. Fault 16-a and Fault 16-c are dipping southwest and they are both basinward-dipping normal faults. Fault 16-b is dipping northeast and is a counter-regional dipping normal fault and Fault 16-d is a basinward-dipping normal fault

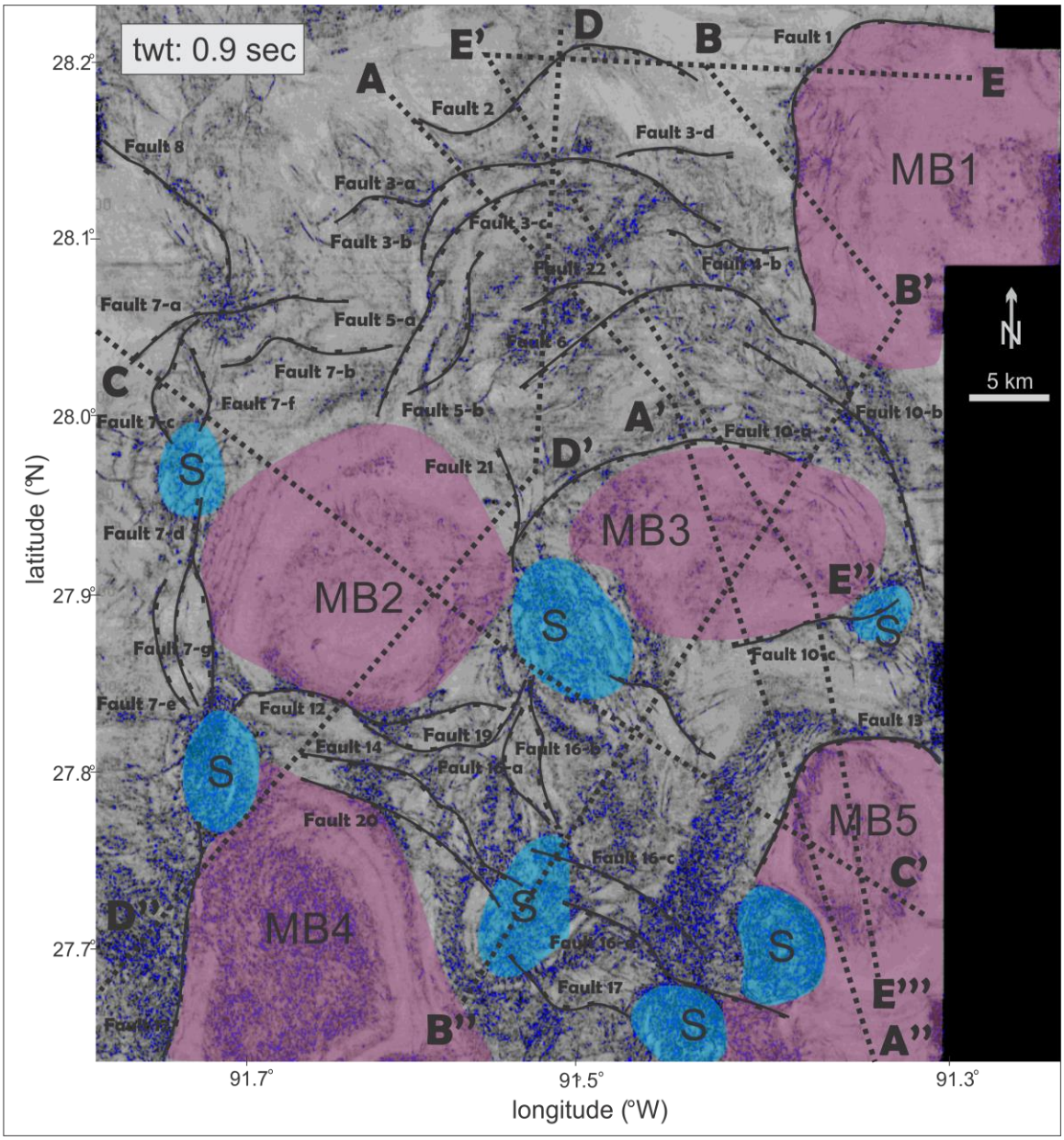

Figure 3.3. Fault map of the study area at 0.9 sec in the similarity cube. Pink areas are minibasins and blue areas are salt diapirs. Dashed lines are the location of interpreted seismic cross sections. Note that the traces of faults lengthen at these greater depths.

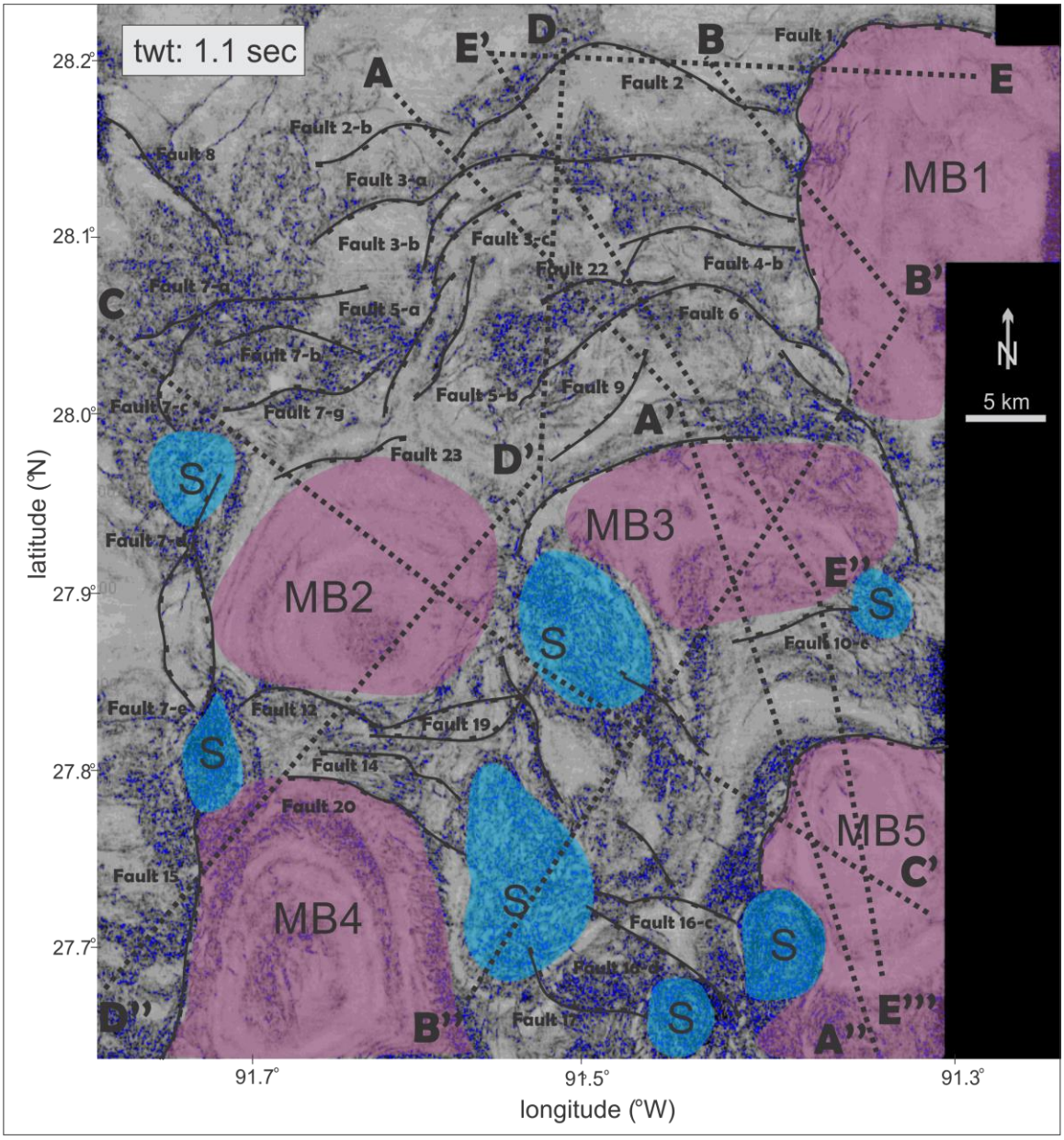

Figure 3.4. Fault map of the study area at 1.1 sec. Pink areas are minibasins and blue areas are salt diapirs. Dashed lines are the location of interpreted seismic cross sections. At this depth, the northern part of the study area has a more complex fault distribution.

Fault 18-a and Fault 18-b are southwest-dipping normal faults situated near a salt diapir. This type of faults are called ‘crestal faults’ by Rowan et al., (1999). Fault 19 is a landward-dipping normal fault that forms a graben with basin-bounding Fault 12. Fault 17 is a northeast-dipping normal fault situated at the top of salt diapir located in the southern part of the study area (Fig. 3.4). Fault 21 is a west-dipping normal fault situated between Minibasin 2 and Minibasin 3. Fault 9 is a northwest-dipping normal fault situated in the northern part of the study area, at the south of the roller fault family. Fault 14 is a southwest-dipping normal fault situated between Minibasin 2 and Minibasin 4 (Fig. 3.1-4). Fault 23 is a basinward-dipping normal fault situated at the northern edge of the Minibasin 2.

3.2 Minibasins

Five minibasins are identified in the study area (Fig. 3.5). Although the data extent allow us to interpret only two minibasins both in their E-W and N-S directions, the characteristics of all five minibasins will be evaluated in this chapter. All minibasins in the study area are underlain by either a salt weld or an allochthonous salt layer. This allochthonous salt layer is thought to have moved during Miocene time from the autochthonous Jurassic salt layer (Rowan, 1993). Minibasin 1 located in the north-eastern edge of the study area is 16 km wide and 4.9 km deep. It is bounded by the same normal fault to the north and south and by the same normal fault to the west (Fig. 3.5). I have no data along the eastern margins of the minibasins. Minibasins 2 and 3 are located in the middle part of the study area. The data extent allows to map both these minibasins in three dimensions. Minibasin 2 is 5.6 km deep and 17.5 km wide while Minibasin 3 is 5.1 km

deep and 18.6 km wide. Minibasin 2 has a symmetric circular shape while Minibasin 3 has a more elliptical shape on different time sections obtained from the seismic data (Fig. 3.5). In the west Minibasin 2 is bordered by normal faults dipping in opposite directions from the basin.

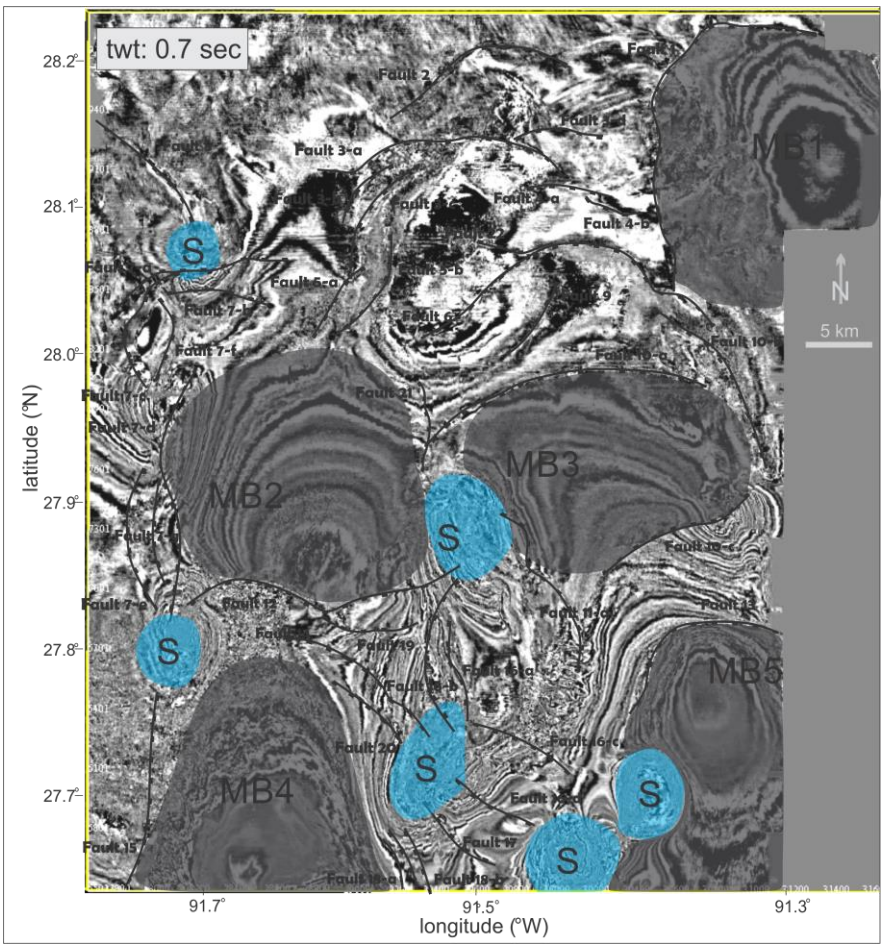

Figure 3.5: Location of minibasins in the study area (in gray). Only the full extent of MB2 and MB3 can be interpreted. MB1, MB2 and MB3 are continental shelf minibasins whereas MB4 and MB5 are continental slope minibasins.

There is a large passive diapir between Minibasin 2 and Minibasin 3 defining the eastern edge of Minibasin 2 and the western edge of Minibasin 3. Minibasin 3 is bounded

by a roller fault family to the north (Fig. 3.6). A salt diapir is located at the eastern edge of Minibasin 3. All three minibasins listed above are defined as continental shelf minibasins usually bordered by large fault families such as roller faults or crestal faults and are all filled with Pliocene-Pleistocene sediments. (Alexander and Flemings, 1995). Salt movement and increased sedimentary loading are interpreted as the main cause for the minibasin formation in the continental shelf-slope area. Huge sedimentary loads coming from the coastal zone results in the relatively quick evacuation of underlying salt and this rapid escape creates more accommodation space that promotes more faulting.

Minibasin 4 and 5 are located in the continental slope near the shelf edge. Minibasin 4 is 18.3 km wide and 6.2 km deep. A large normal fault is situated at the western edge of minibasin whereas the eastern edge is bordered by a salt diapir (Fig. 3.5). Minibasin 5 is 17.4 km wide and 6.4 km deep. The seismic data covers a small part of this basin so characterization of this basin is incomplete. This minibasin is bordered by salt diapir to the west and a normal fault is located at the northern edge of the basin. This basin is similar to continental shelf minibasin with their asymmetric shape and presence of faults at their edge.

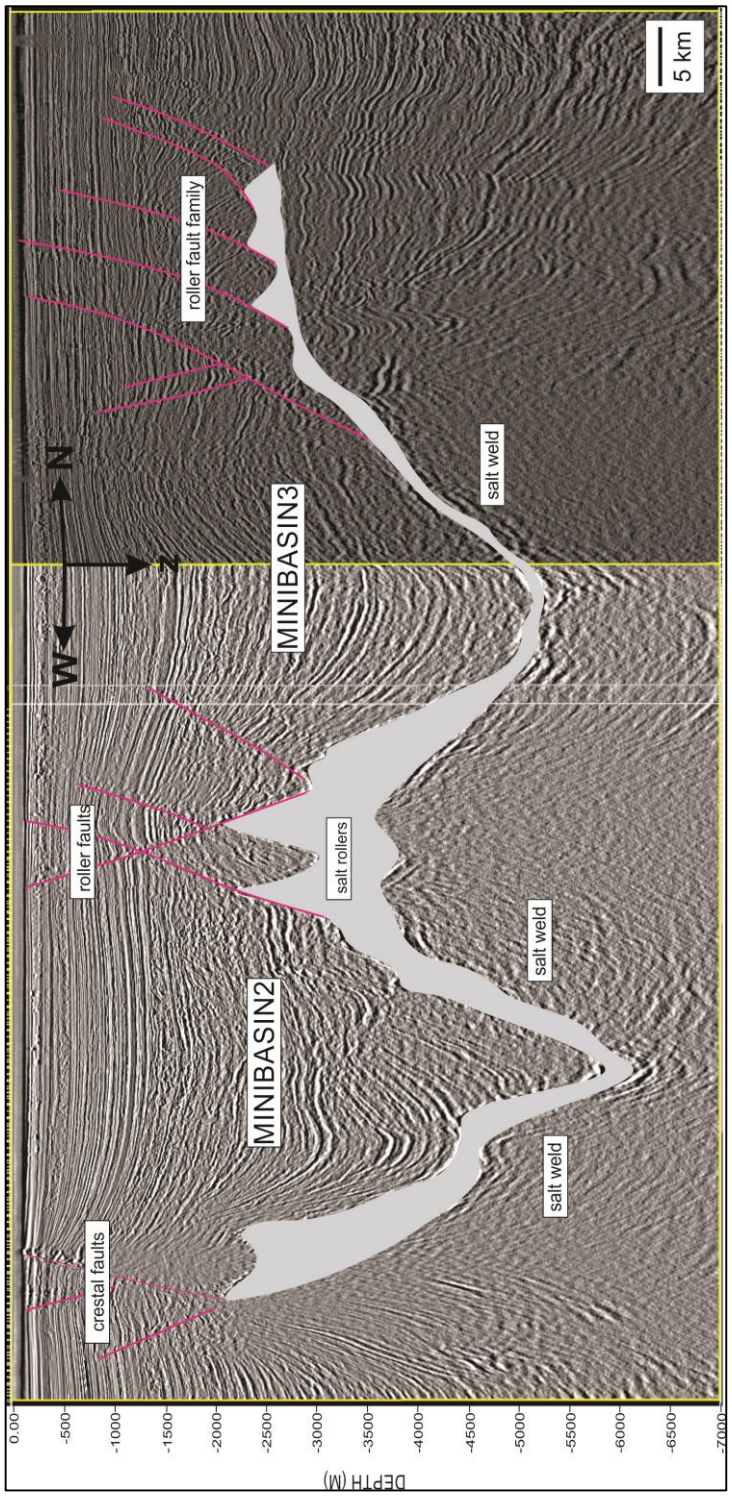

Figure 3.6: 2-D view of the Minibasin 2 and Minibasin 3. Minibasin 3 is bordered from north by faults soling into a salt detachment surface. There is a salt diapir bounding the western edge of Minibasin 2 and some crestal faults are formed because of the diapir rising.

3.3 Salt Structures

Salt systems in the study area include salt rollers, diapirs and salt welds. These systems are interpreted to be kinematically linked to each other and to subsalt and suprasalt strata. Faults and minibasins are two other components related to salt systems in the study area.

Salt diapirs are usually located at the edge of minibasins and near or on the continental slope. They are characterized with weak or absent reflections in seismic data (Fig. 3.7 and 3.8). In time slices, diapirs have circular or elliptical shapes and their width varies from 3.5 to 6.5 km (Fig. 3.5). Only one diapir situated in the southeastern area reaches the surface whereas other diapirs are buried under the younger strata of the study area. The diapir formation starts with a mound stage where salt flowage begins and it creates a differential subsidence and it continues with the dome stage where the sedimentary loading causes salt flowage from the basin flanks to the basin center and finally induces the salt mass to rise vertically. In the study area diapirs do not have a symmetrical shape which indicates different sediment accumulation rates on each side of the basin (Fig. 3.7).

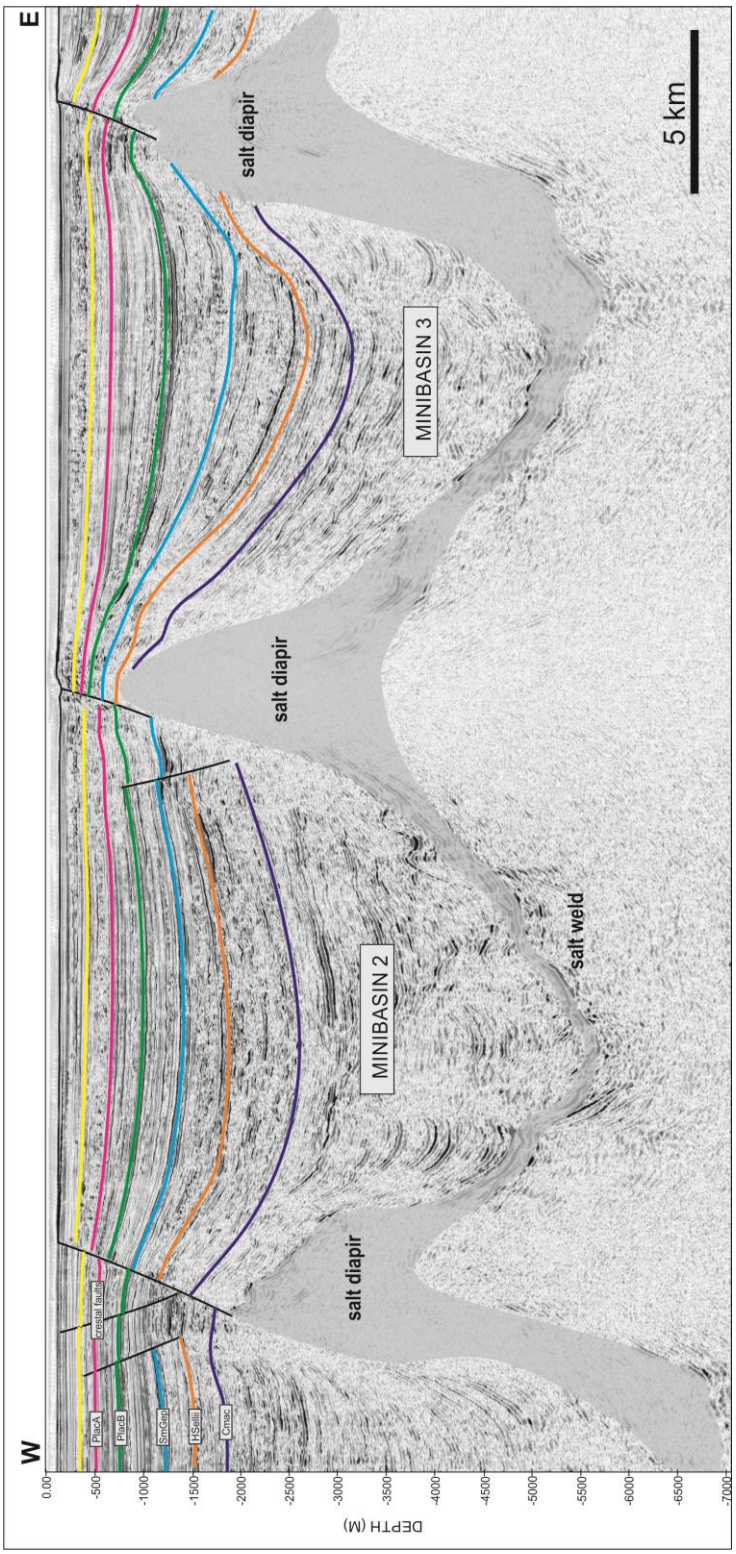

Figure 3.7: Crossline 7454 showing salt structures and Minibasins. Sedimentary loading caused salt to move away from the depocenters which resulted in the formation of salt diapirs.

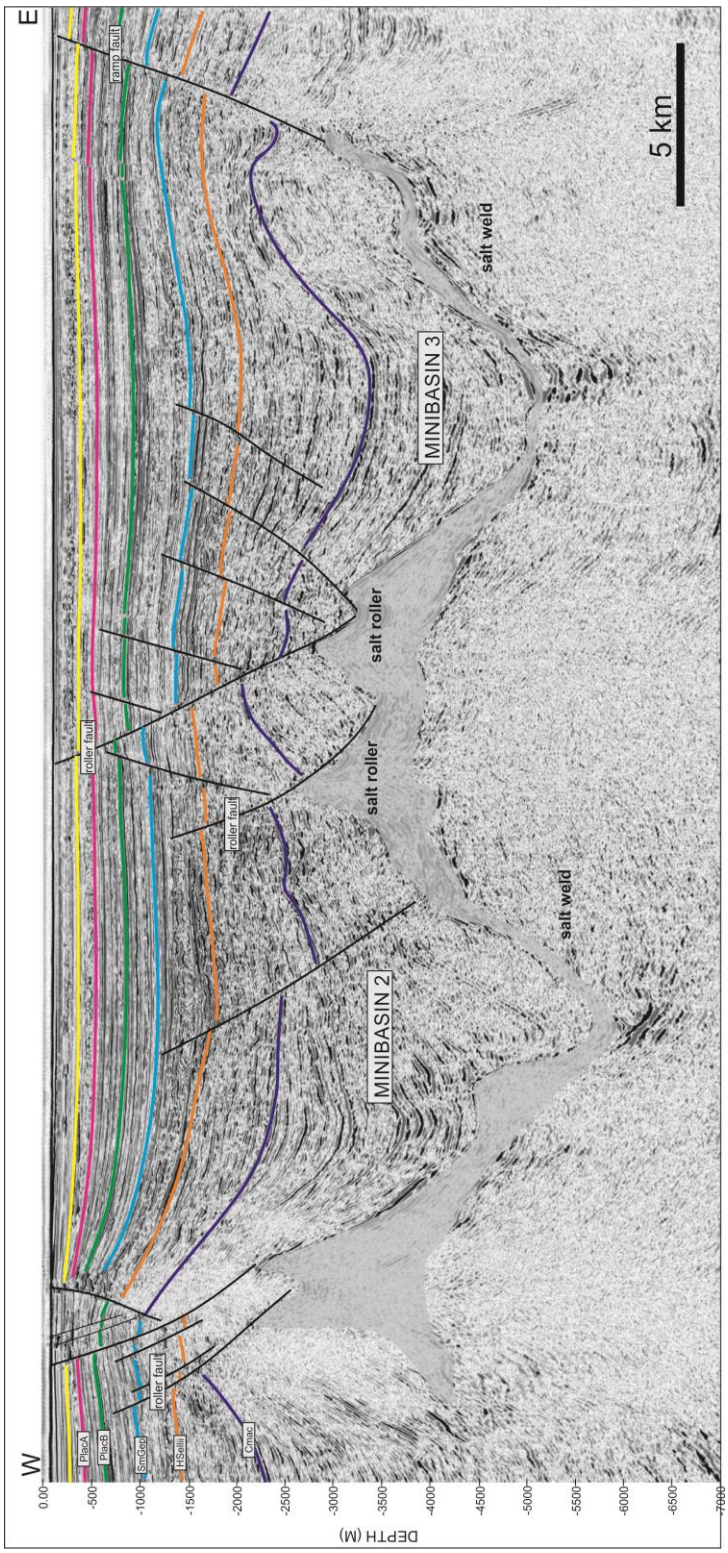

Figure 3.8: Crossline 7715 showing salt rollers and minibasins. Salt rollers are recognizable by their triangular shape and they are related to the listric faulting in the study area.

Salt welds-fault welds are the second more common salt structures in the study area. A salt weld is a surface that separates two strata that once separated by a salt layer and now they are in contact (Rowan et al., 1999). The existence of a salt weld indicates that a salt layer was once present where the weld exists. A fault weld is a fault surface or fault zone joining strata originally separated by autochthonous or allochthonous salt. The presence of allochthonous salt layers and high sedimentation rate in the Northern Gulf of Mexico allow salt to move continuously and create salt welds. Salt welds in the study area are mostly situated beneath minibasins, whereas fault welds are mostly observed in the northern part of the study area where listric faults are present and sole into a thin salt layer (Fig. 3.8). Usually a salt or fault weld creates an apparent angular unconformity between the upper and lower strata but it is important to note that this contact is not formed as an unconformity from erosion or non-deposition but rather by the movement of allochthonous salt. In Figure 3.8, the unconformity between suprasalt and subsalt strata is caused by the downdip movement of an allochthonous salt body induced by high sedimentation and subsequent faulting. In Figure 3.8, 6,000 m of sediments is interpreted as a point load that caused the salt to move away from the center of the minibasin. This movement is interpreted to have culminated with the formation of a salt weld now observed beneath the minibasin (Fig. 3.8).

Salt rollers are the third dominant salt structure observed in the study area. A salt roller is a low-amplitude, asymmetrical structure where one side of the salt body is bounded by a normal fault (Park, 1997). The presence of salt rollers indicates regional, thin-skinned extension perpendicular to the strike of the salt rollers. In the study area salt rollers are

spatially-related with listric growth faults and are recognized by their triangular shapes (Fig. 3.8).

3.4 Fault, Salt and Minibasin Relationships Seen in Seismic Cross Sections

Five seismic amplitude cross sections are used to illustrate fault, sediment, salt and minibasin interactions in the study area. The locations of cross sections are shown in figures 3.1-4. The interpretation of these cross sections demonstrates the complex interaction of faulting, salt, sediment and minibasin strata within the study area. In every cross section the nature of fault, its related structures, horizon changes, and salt structures are evaluated. Uninterpreted seismic sections are displayed for comparison to the interpreted lines.

3.4.1 Cross Section AA''

The length of the cross section AA' is 53.7 km and it consists of two segments. The first segment is oriented N42W and the second segment is oriented N163E (Figs. 3.9 and 3.10).

3.4.1.1 Faults

Fault 2 is a basinward-dipping normal fault. The hanging wall of the fault has a prominent landward-tilted rollover monocline containing expanded growth sections where the displacement increases with depth and the growth strata thicken landward.

Fault 3-a is a basinward-dipping arcuate normal fault. The greater thickness in the hanging wall indicates the synsedimentary growth nature of the fault. The thickness of strata in the hanging wall remains constant and the bounding normal fault soles into a salt roller. The age of the older strata (Cmac) indicates that the main period of salt withdrawal occurred during the Pleistocene.

Fault 3-c is a basinward-dipping, arcuate normal fault. This fault contains a triangular salt roller in its footwall. Fault displacement increases downward and the strata thickness increases landward and toward its footwall (Fig. 3.10). The hanging wall has a prominent, landward-tilted monocline that is best seen in deformation of the older strata.

Fault 6 is a basinward-dipping, arcuate normal fault that soles into a salt roller. The strata in the hanging wall thicken landward and this landward thickening is greatest for the older Cmac strata. The increase of the displacement with depth shows the synsedimentary nature of this fault.

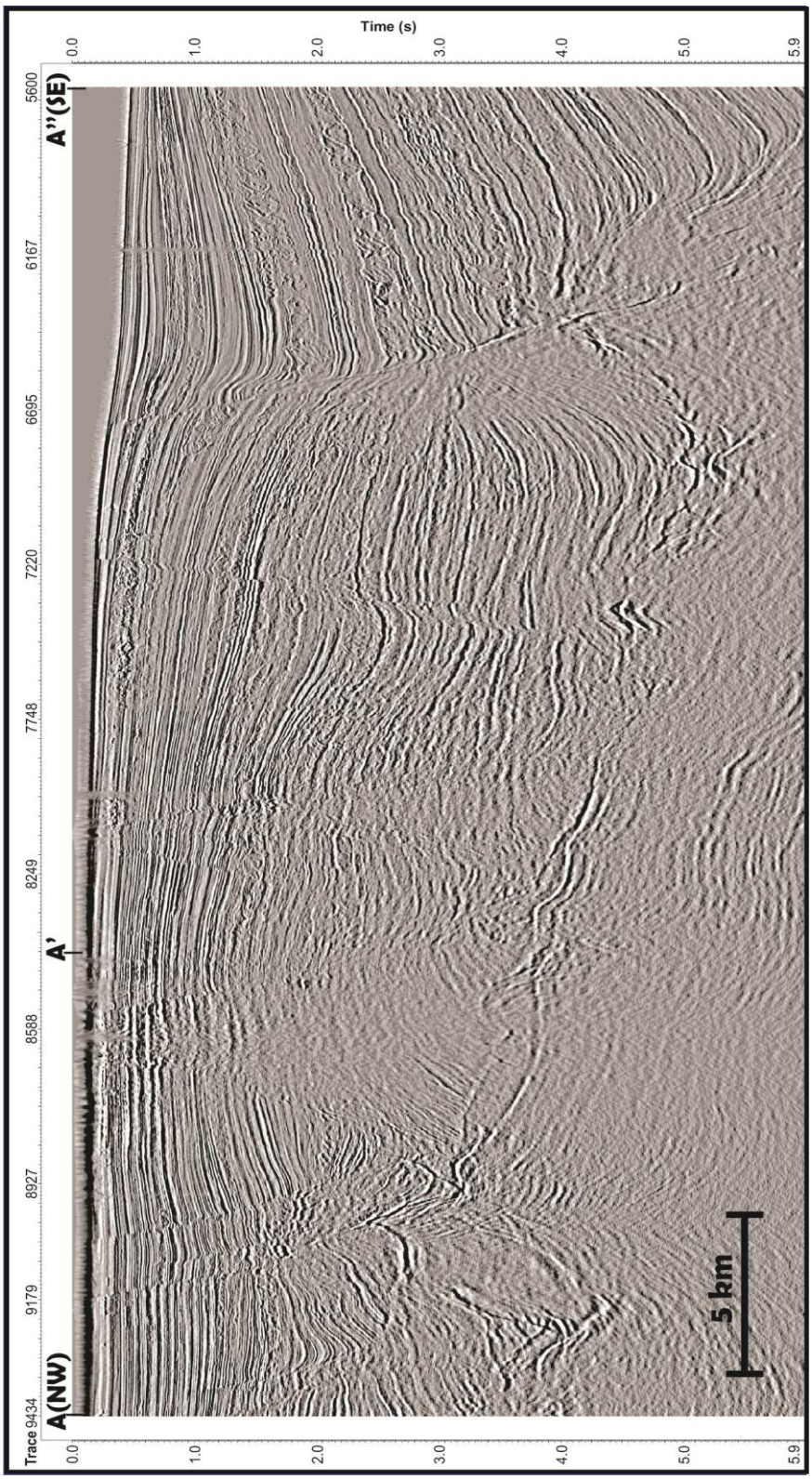

Figure 3.9: Uninterpreted seismic section of arbitrary line AA''.

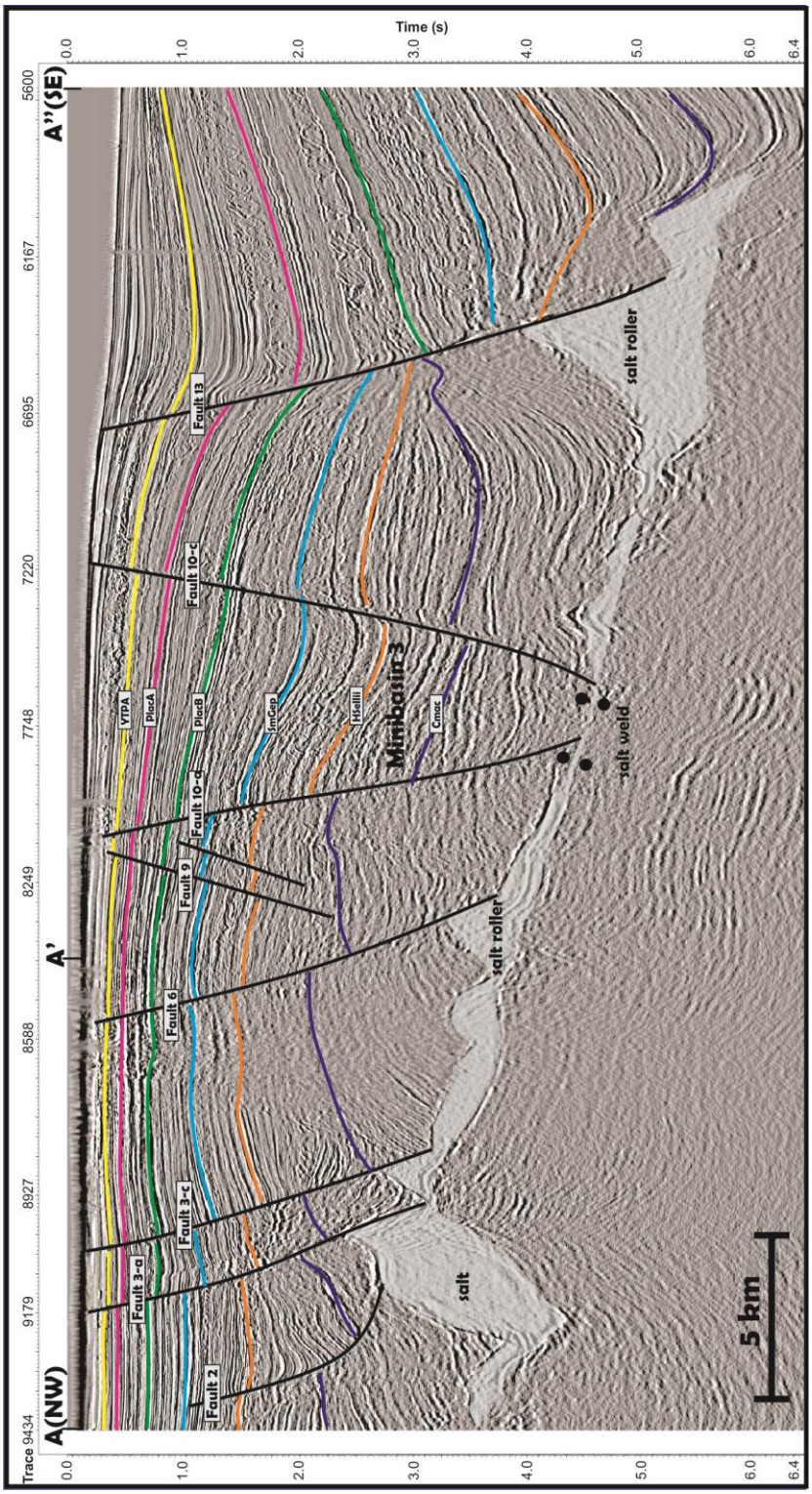

Figure 3.10: Interpreted seismic section of arbitray line AA'' showing deepening salt from north to south because of increasing sediment thickness. Growth faults sole into the salt layer and salt movement causes formation of salt rollers in the foot wall of growth faults.

Fault 9 is a planar, landward-dipping normal fault that does not link with a salt layer or salt structure; therefore, it does not appear to be related to salt movement. The thickness of strata remains the same in both the hanging wall and footwall. Fault 9 and another planar fault situated to the southeast of this fault can be described as antithetic faults since their sense of displacement is opposite to the regional, basinward displacement trend.

Fault 10-a is a basinward-dipping, arcuate normal fault bounding the northern edge of Minibasin 3 and soling into a salt weld. The sedimentary thickness in this minibasin caused the evacuation of salt away from the center of the minibasin and the nucleation of this basin bonding fault. Because fault displacement increases downward, the thickness of the strata is greater in the hanging wall.

Fault 10-c is another basin-bounding fault seen in cross section that is a landward-dipping, arcuate normal fault. This fault forms the southern edge of Minibasin 3. The strata on the hanging wall thickens basinward and fault displacement increases with depth. This fault soles into a salt weld and salt withdrawal was active during the Pleistocene because of the age of the oldest deformed strata.

Fault 13 is a basinward-dipping arcuate normal fault with a large, triangular salt roller in its footwall. The large size of the salt roller can be explained because of its greater depth than the other salt rollers seen on the same cross section. Greater depth means more salt evacuation from this area. The basin-bounding fault coincides with the shelf edge. A landward-dipping monocline is observed in the hanging wall of the fault and displacement increases downward.

3.4.1.2 Horizons

The thickness of the interpreted horizons increases basinward. The older strata Cmac and Hsellii are influenced by the salt movement in the study area which means in addition to faulting, the salt movement causes the deformation of these older strata.

3.4.1.3 Salt structures

Salt rollers are the dominant salt structure in this cross section. There are six faults soling into salt and forming salt rollers or salt welds depending on the salt volume prior to faulting. The salt sheet is allochthonous and the age of the older strata in the cross section indicates that salt is withdrawn during the Pleistocene.

3.4.1.4 Minibasins

Minibasin 3 and Minibasin 5 are the two Minibasins in this cross section. Minibasin 3 is tilted basinward whereas Minibasin 5 is tilted landward. The sediment loading in the Minibasin 3 caused the salt to escape away from the center of the Minibasin leaving behind a salt weld. Minibasin 5 is deeper than Minibasin 3 and the extent of the seismic cube makes impossible to analyze it further.

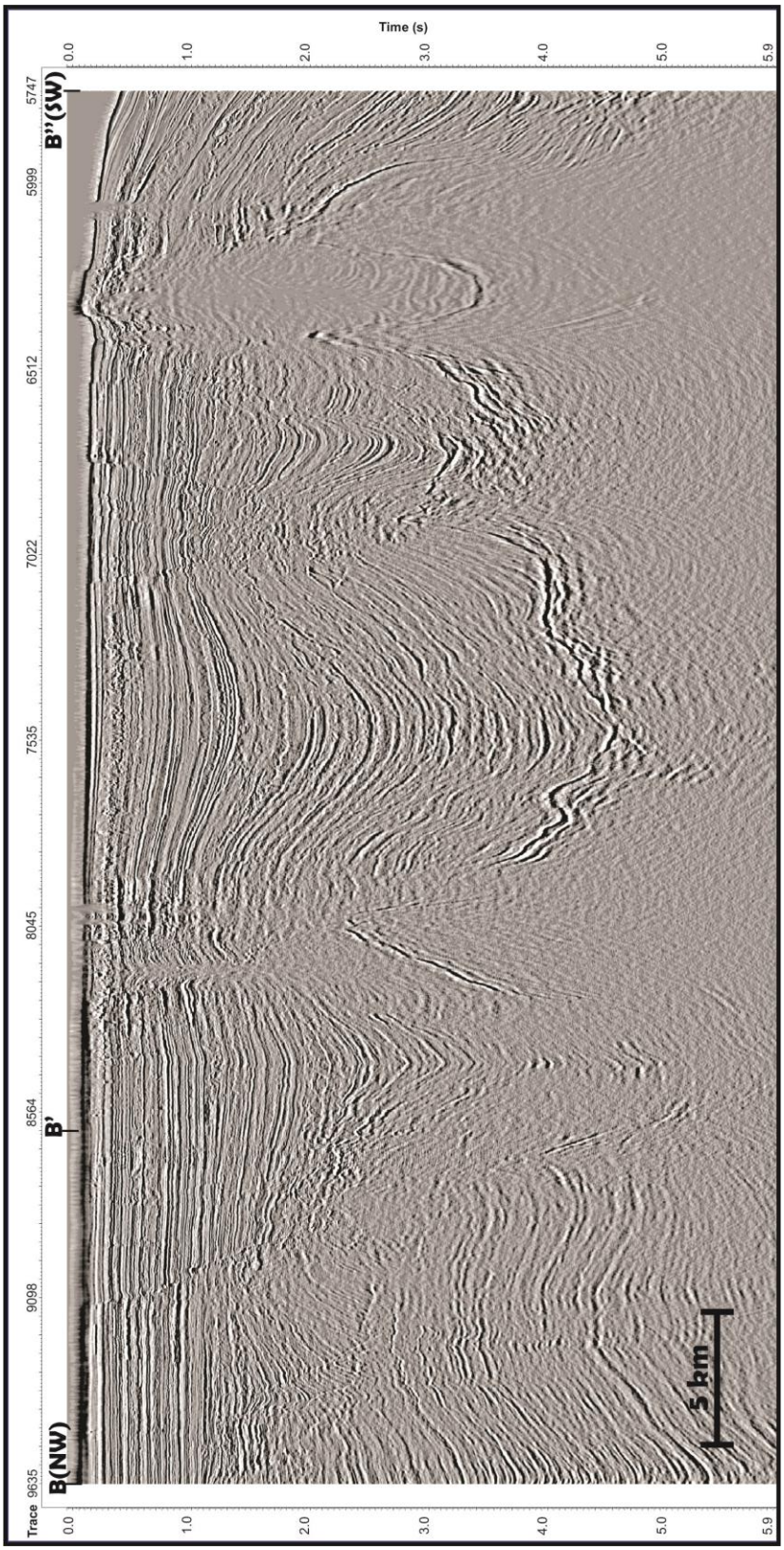

Figure 3.11: Uninterpreted seismic section of arbitrary line BB’’.

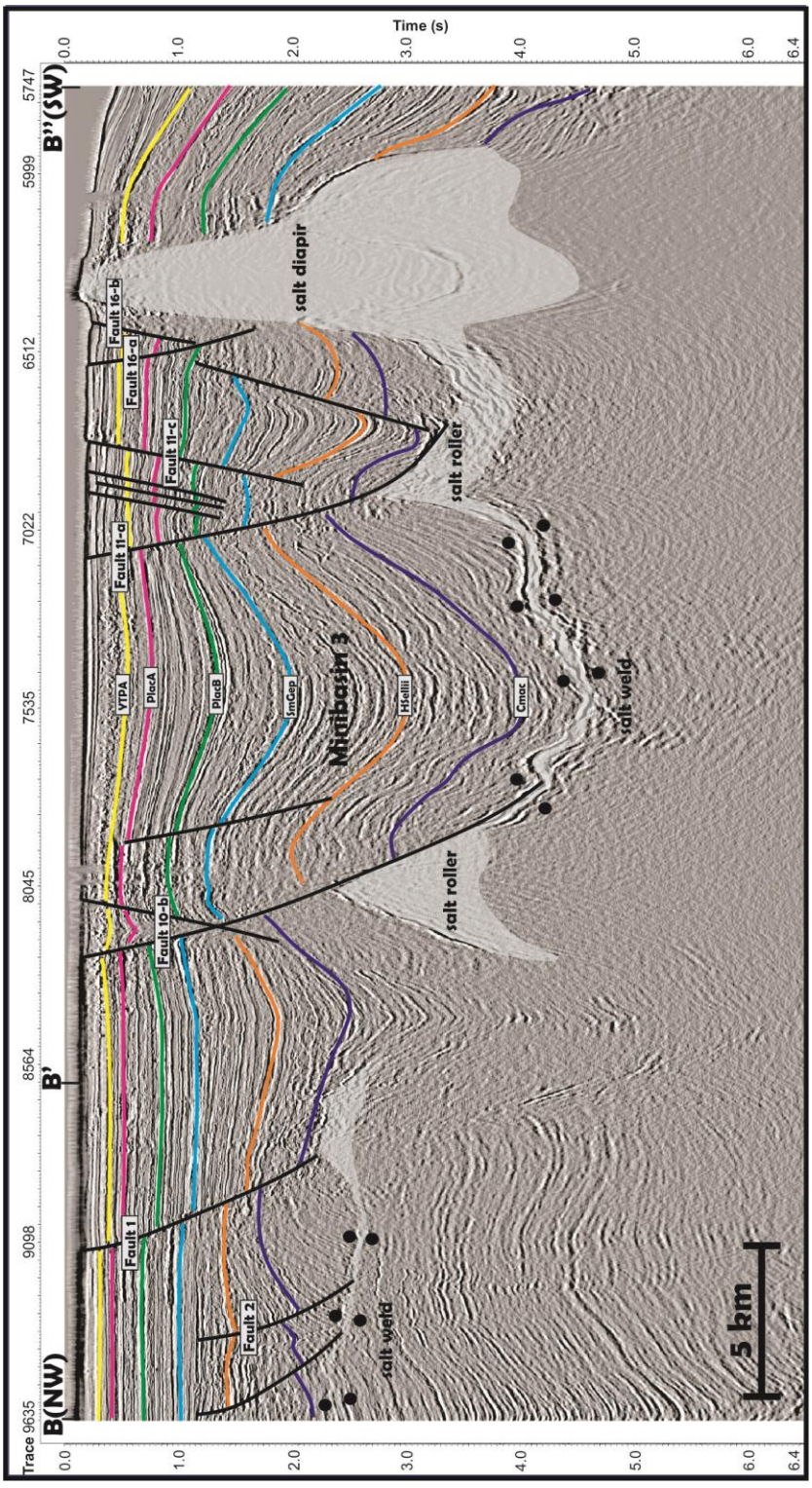

Figure 3.12: Interpreted seismic section of arbitrary line BB''. Two different salt layer exist in this cross section. There is salt diapir coming to the surface which separate roughly the continental slope and continental shelf.

3.4.2 Cross Section BB''

The length of the cross section BB' is 48.6 km and it consists of two segments. The first segment is oriented N39W and the second segment is oriented N142W.

3.4.2.1 Faults

Fault 2 is a basinward-dipping normal fault. The hanging wall of the fault has a prominent landward-tilted rollover monocline. The hanging wall has expanded growth sections where the displacement increases with depth and strata thicken landward.

Fault 6 is a basinward-dipping, arcuate normal fault soling into a large, triangular salt roller. The strata in the hanging wall thickens landward and this landward thickening is the greatest for the older Cmac strata. Increasing displacement with depth shows the synsedimentary nature of the fault. In addition, the southeastern edge of this fault borders Minibasin 3 on its northeastern edge.

Fault 10-b is a basinward-dipping, planar normal fault. The displacement remains constant along the fault and deposition of sediments caused the strata of the hanging wall to be thicker.

Fault 11-a is a basinward-dipping, arcuate normal fault. Although the fault is dipping south, it borders the southern edge of Minibasin 3. The fault soles into salt and the age of the oldest strata indicates that the salt withdrawal occurred during the Pleistocene.

Fault 11-c is a landward-dipping, planar normal fault. The displacement increases downward and the hanging wall strata are thicker than the footwall strata showing the synsedimentary nucleation of the fault. The fault is synthetic with Fault 11-b but antithetic with the regional, basinward dips of most normal faults in the area.

Fault 16-a is a planar, basinward-dipping normal fault. This fault forms a small graben near a salt diapir situated to the southwest. There is no change in the displacement with depth and the thickness in the hanging wall and footwall remains the same.

Fault 16-b is a landward-dipping, planar fault that is antithetic to Fault 16-a and forms the southern edge of the small graben near a large salt diapir.

3.4.2.2 Horizons

Sediment thickness increases from northwest to southwest. The horizon thickness more influenced by extensive faulting in the southern part of the cross section.

3.4.2.3 Salt Structures

Salt diapirs, salt rollers, and salt welds are the dominant salt structures in the cross section (Fig.3.12). Deposition of sediments in the minibasins caused salt to move away from the center of the minibasin and resulted in the formation of a salt weld. This type of salt weld is called a ‘bowl weld’ because of its shape.

The weld situated in the northwestern part of the cross section is called ‘roho weld’. Roho weld is a type of weld into which a family of roller faults root. A salt diapir is situated in the southwestern part of the cross section. The diapir seems to be generated from the allochthonous salt (Fig. 3.12). Salt welds join post-salt and infra-salt sediments that were once separated by an allochthonous salt sheet and the weld.

3.4.2.4 Minibasins

Minibasin 3 is bounded by two faults. Even though Fault 11-a is dipping away from the basin, it still creates enough relief to produce a suitable environment for sediments to be deposited.

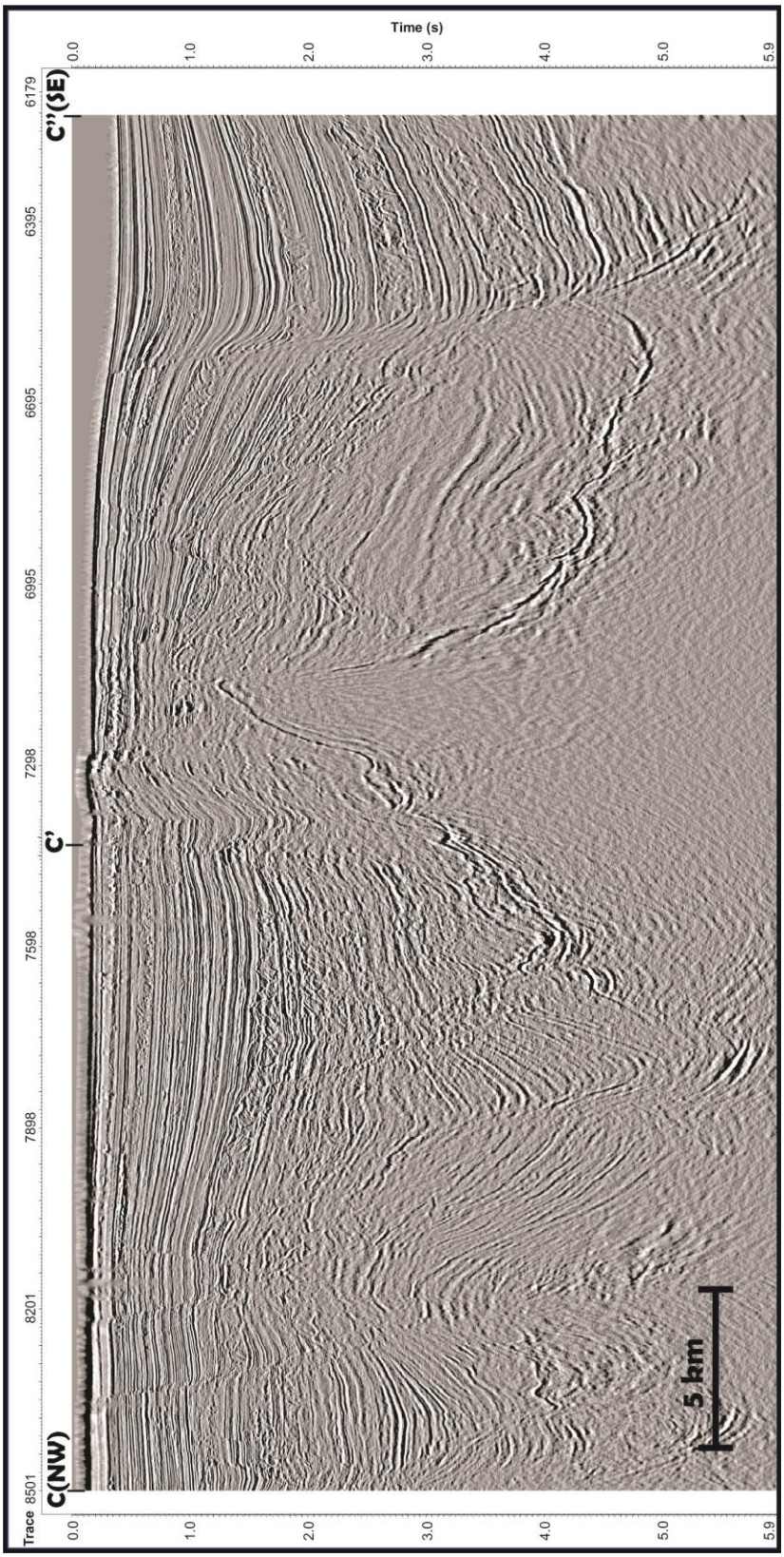

Figure 3.13: Uninterpreted seismic section of arbitrary line CC''.

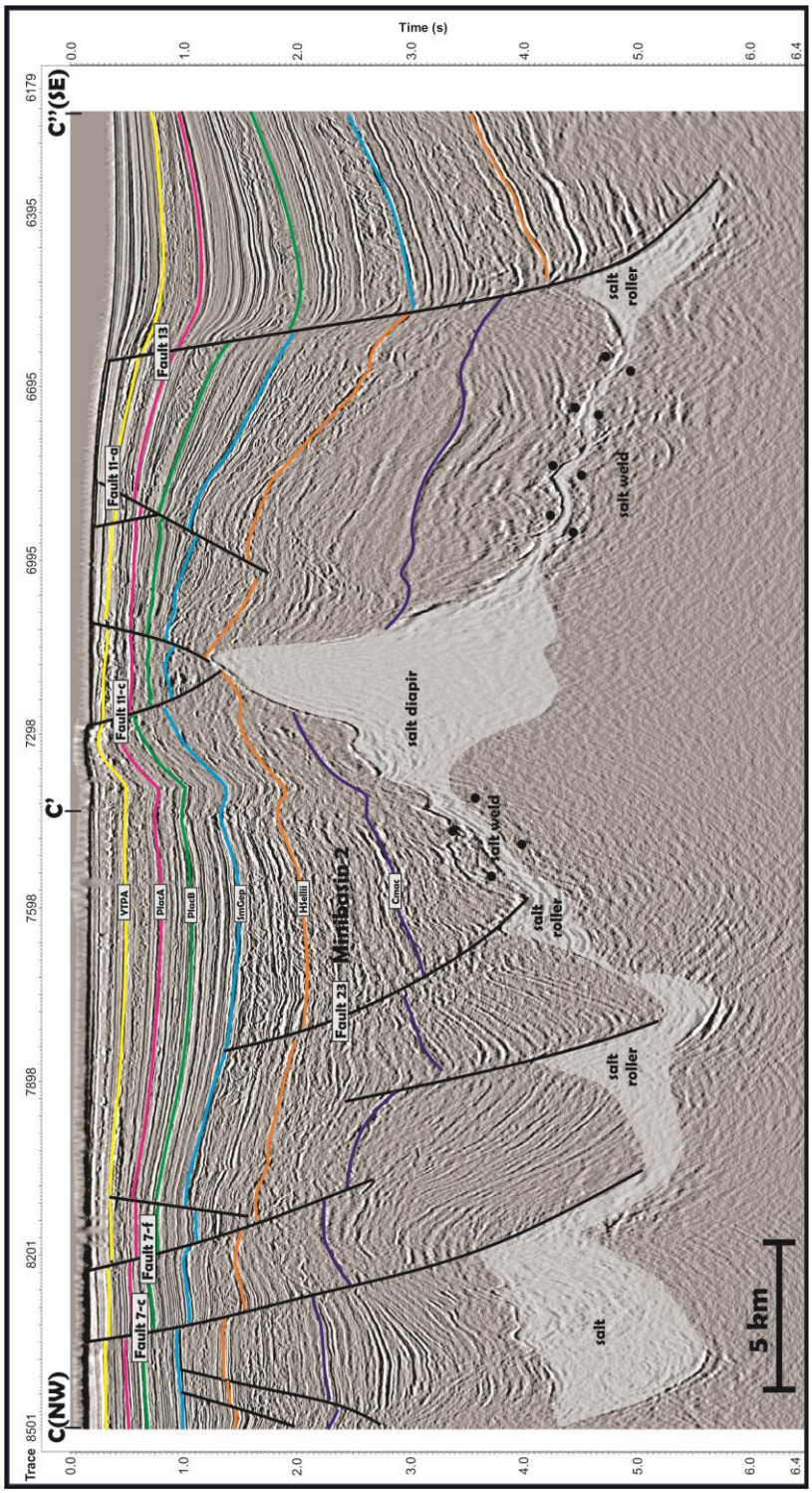

Figure 3.13: Interpreted seismic section of arbitrary line CC''. The deeper parts of Minibasin 2 are faulted as a result of salt movement and sediment loading. In addition to active faults, deeper faults that sole into salt are also seen on the cross section.

3.4.3 Cross Section CC''

The length of the cross section is 29 km and it consists of two segments. The first segment is oriented N44W and the second segment is oriented N53W.

3.4.3.1 Faults

Fault 7-c is a basinward-dipping, arcuate normal fault. The displacement increases downward but the strata thickness remains constant in the hanging wall. This fault soles into a salt sheet.

Fault 7-f is a basinward-dipping planar normal fault. It borders Minibasin 2 to the northwest along with Fault 7-c.

Fault 23 is a basinward-dipping, arcuate normal fault. The fault has growth strata from the top of the salt to the HSellii horizon. This means that the fault was active from the emplacement of the allochthonous salt to the deposition of H.Sellii transgressive shales. The displacement increases with depth with the tilted strata thickening landward.

Fault 11-c is a landward-dipping, planar normal fault.

Fault 11-a is a landward-dipping, arcuate normal fault. The hanging wall strata thickens basinward and displacement increases downward. These characteristics show the growth nature of the fault.

Fault 13 is a basinward-dipping, arcuate normal fault. This fault has a large triangular salt roller in its footwall. The size of the salt roller can be explained by its depth

being greater than the other salt rollers in the cross section. Greater depth means more salt evacuation to this point. The fault is a basin bounding fault and it coincides with shelf edge where the slope starts to increase. There is a landward dipping monocline in the hanging wall of the fault and the displacement increases downward.

3.4.3.2 Horizons

Sedimentary thickness increases from north (landward) to south (basinward).. The two oldest strata - Cmac and Hsellii (Fig. 3.13) are folded showing that they were deformed by salt movement. Sedimentary thickness is greatest at the south of the cross section because of the increasing slope (transition from continental shelf to continental slope) and the presence of a large growth fault.

3.4.3.3 Salt Structures

Salt roller, salt weld and salt diapirs are the dominant structures in the cross section (Fig. 3.13). The salt diapir remains attached to the allochthonous salt layer (mother layer). The salt diapir formed during sedimentary loading and density instability. As sediments get thicker, they become denser and the salt moves away to the area where the sedimentary thickness is less and the diapir continues to rise until the mother salt layer is exhausted. Salt welds are situated near the salt diapir where the sedimentary thickness is the greatest. Salt welds and salt diapir act together as a closed system in the cross section (Fig. 3.13). Salt welds are where the diapir was fed once and now they are the remains of the evacuated salt layers.

3.4.3.4 Minibasins

The downdip margin of Minibasin 2 is bounded by a salt diapir and the updip margin is bordered by a growth fault (Fault 7-c). Faulting and salt movement caused the minibasin to be asymmetrical in its sediment thickness. The updip half of the minibasin has thicker sediments compared to the downdip half because of its extensive faulting in the updip half of the minibasin.

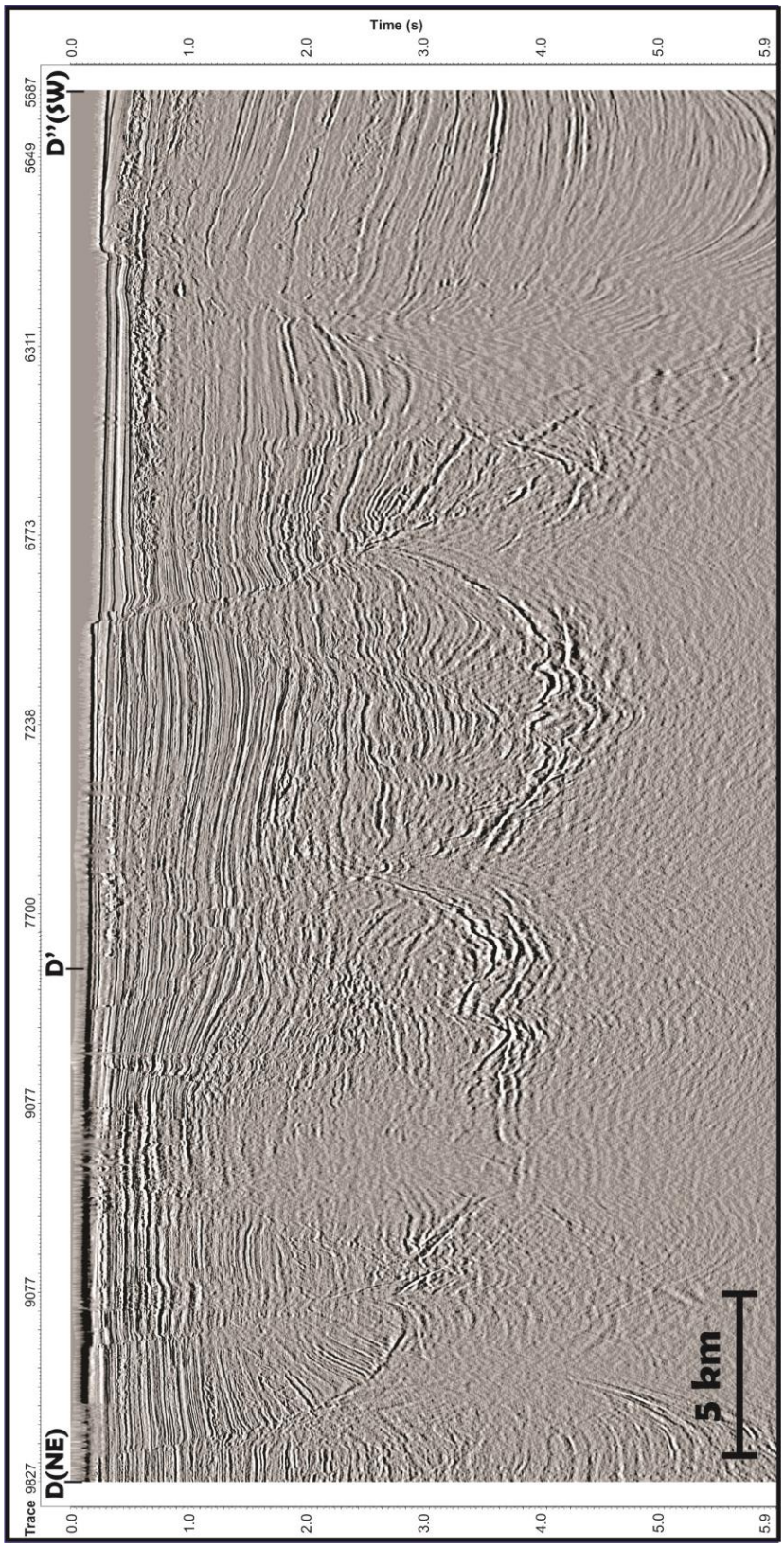

Figure 3.14: Uninterpreted seismic section of arbitrary line DD''.

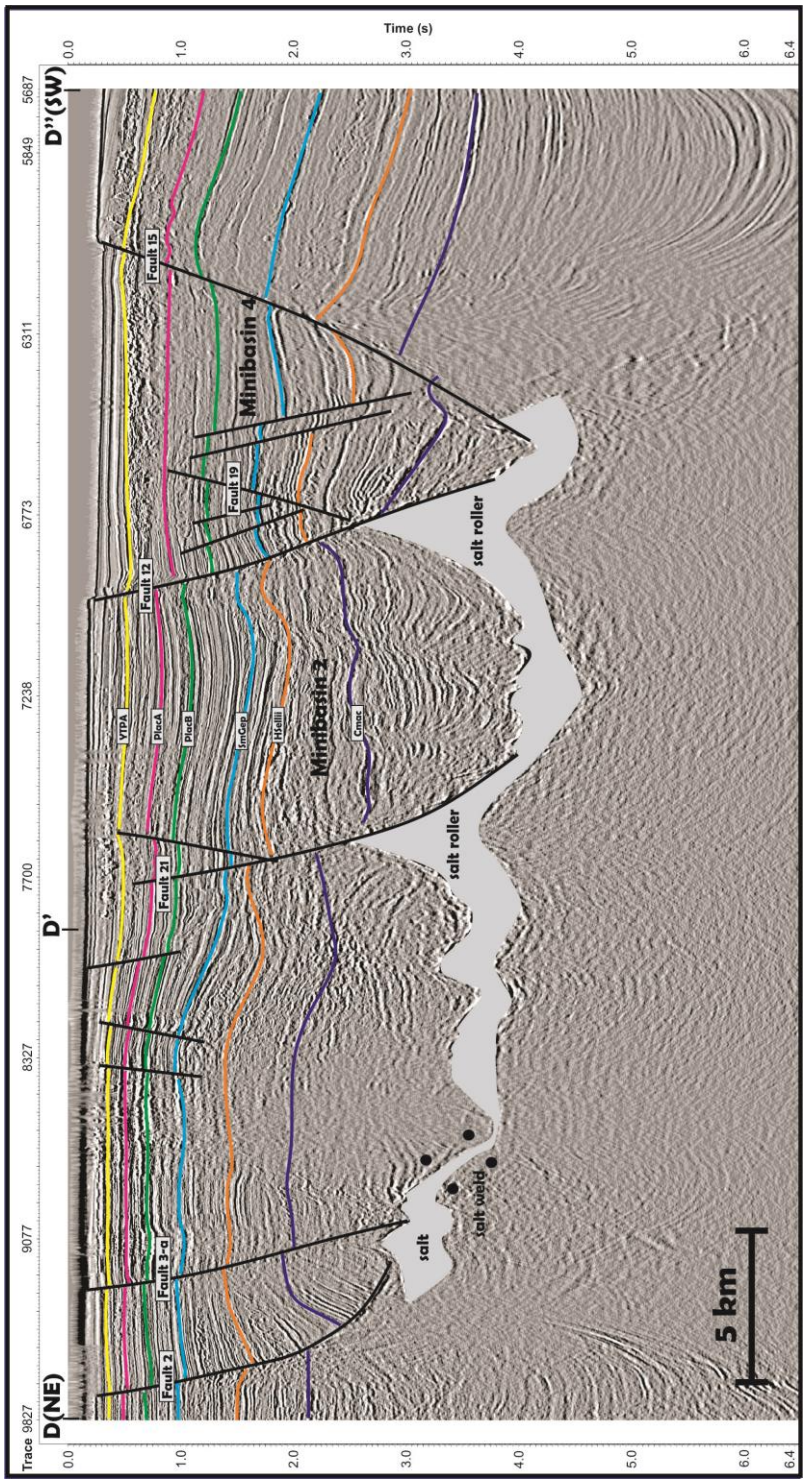

Figure 3.15: Interpreted seismic section of arbitrary line DD''. Minibasin 2 and Minibasin 4 are visible in the cross section. Although Fault 12 is dipping away from Minibasin 2, it forms the southern edge of the basin.

3.4.4 Cross Section DD''

The length of the cross section is 51.7 km and it consists of two segments. The first segment is oriented N12E and the second segment is oriented N126W.

3.4.4.1 Faults

Fault 2 is a basinward-dipping normal fault. The hanging wall of the fault has a prominent landward-tilted, rollover monocline. The hanging wall has expanded growth sections where the displacement increases with depth and the strata thicken landward.

Fault 3-a is a basinward-dipping arcuate normal fault. The greater thickness in the hanging wall indicates the synsedimentary growth nature of the fault. The thickness of strata in the hangingwall remains constant and the fault soles into a salt roller. The age of the older strata (Cmac) indicates that salt withdrawal occurred during the Pleistocene.

Fault 21 is a basinward-dipping, arcuate normal fault. This fault soles into a salt roller and the displacement increases with depth. The sedimentary thickness is greater in the hanging wall. The increase of the displacement with depth and sedimentary thickness in the hanging wall indicate the syn-sedimentary nature of this growth fault.

Fault 12 is a basinward-dipping arcuate normal fault and forms the southern edge of the Minibasin 2 and the northern edge of Minibasin 4. The displacement increases downward and the sedimentary thickness in the hanging wall is greater compared to the footwall. The fault soles into a salt roller.

Fault 19 is a landward-dipping, planar normal fault. This fault is an antithetic fault of fault 12.

Fault 15 is a basinward-striking, strike-slip fault bordering the western edge of Minibasin 4 and soling into a salt roller. The fact that this fault soles into salt layer shows that faulting and salt deformation are kinematically linked.

3.4.4.2 Horizons

The sedimentary thickness increases from northeast to southwest. Older strata (Cmac and Hsellii) are highly influenced by salt movement. The salt withdrawal and high sedimentary input caused these strata to deform.

3.4.4.3 Salt Structures

A Salt roller is the only prominent salt structure in the cross section (Fig. 3.15). Salt flowage is caused by the seaward tilting of the basin and is responsible for the formation of salt rollers in the cross section.

3.4.4.4 Minibasins

Minibasin 3 is bounded by Fault 21 from northeast and by Fault 12 to the southwest. The basin is underlain by a mobile salt layer. The asymmetric shape of the minibasin is

caused by two, bounding faults dipping in the same direction. Minibasin 4 is bordered by Fault 12 to the northeast and by Fault 15 to the southwest.

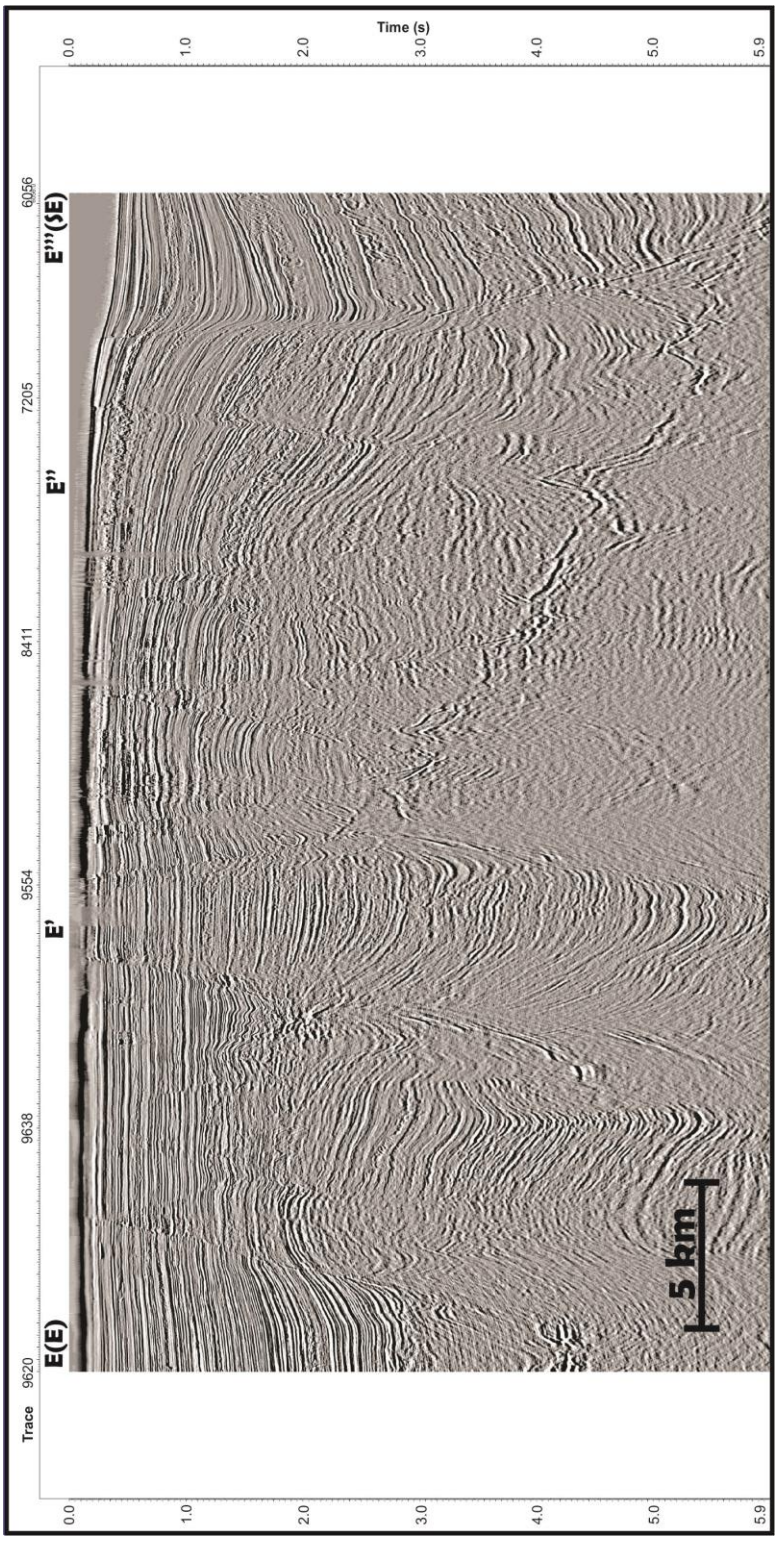

Figure 3.16: Uninterpreted seismic section of arbitrary line EE’’’. Basinward-dipping salt layer is the most prominent reflector.

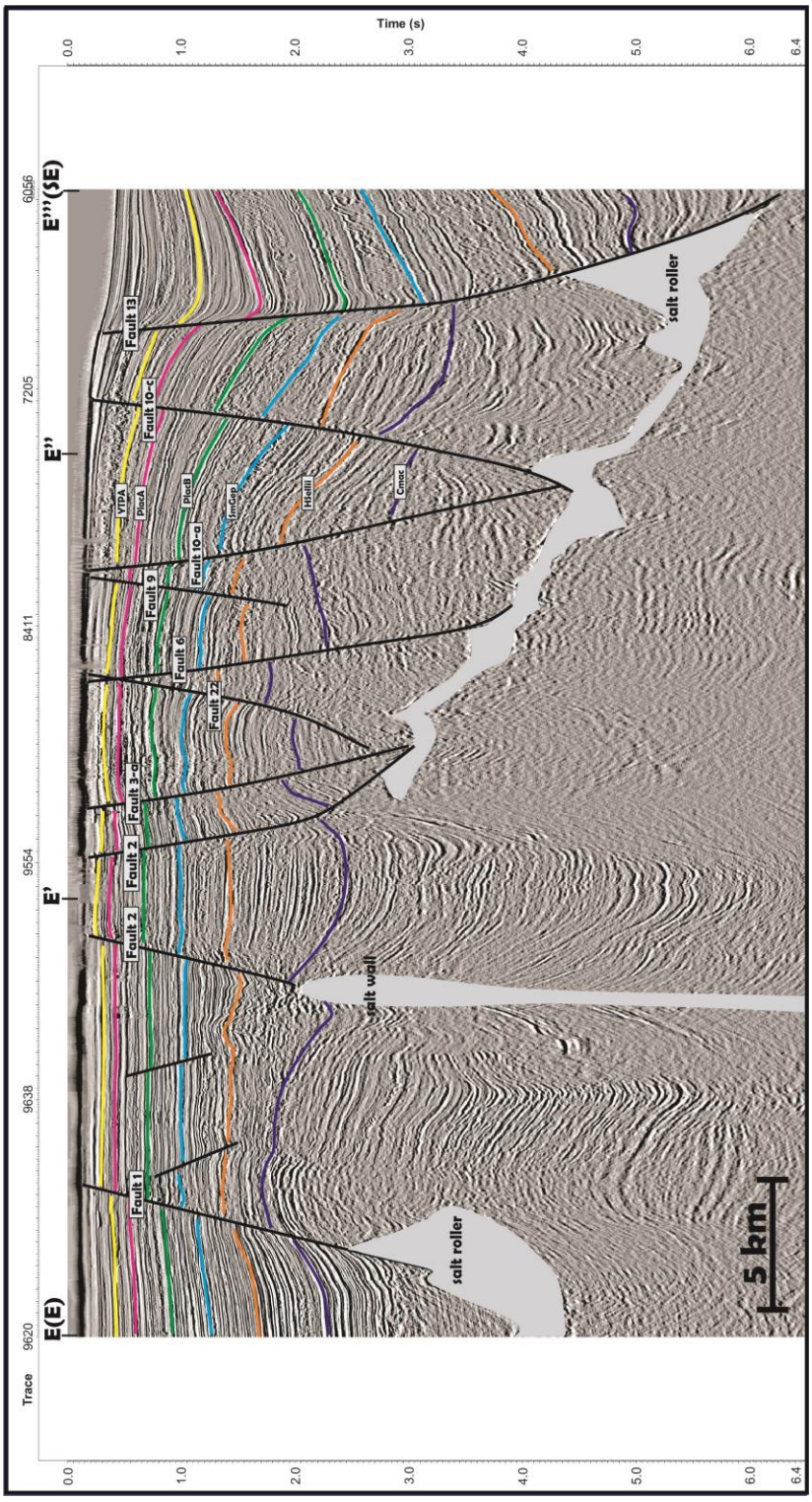

Figure 3.17: Interpreted seismic section of arbitrary line EE’’’. There is a salt wall in the eastern part of the cross section. The salt wall is probably linked to the autochthonous Louann salt. Most of the faults in the cross section sole into a salt sheet.

3.4.5 Cross Section EE’’’

The length of the cross section is 44.5 km and it consists of three segments. The first segment is oriented N44W, the second segment is oriented N30W, and the third segment is oriented N20W.

3.4.5.1 Faults

Fault 1 is an east-dipping, arcuate normal fault. The sediment thickness is greater in the hanging wall and the displacement increases with depth. This fault bounds Minibasin 1 and soles into a salt roller which shows that faulting and salt movement share the same kinematic history.

Fault 2 is a basinward-dipping, arcuate normal fault. The presence of two Fault 2 in the cross section indicates that the cross section crosses Fault 2 twice (Fig. 3.17). The fault has a landward-tilted rollover monocline in its hanging wall with expanded growth sections. The fault soles into a salt layer indicating coeval salt movement and fault nucleation.

Fault 22 is a landward-dipping, arcuate normal fault. The thickness in hanging wall and foot wall are the same and displacement remains constant with depth. Also, this fault does not sole into salt, which might show that its nucleation is after the salt withdrawal.

Fault 3-a is a basinward-dipping, arcuate normal fault. The greater thickness in the hanging wall indicates the synsedimentary growth nature of the fault. The thickness of strata in the hanging wall remains constant and the fault soles into a salt roller. The age of the oldest strata (Cmac) indicates that salt withdrawal occurred during the Pleistocene.

Fault 6 is a basinward-dipping arcuate normal fault and is soling into a salt roller. The strata in the hanging wall thickens landward and this landward thickening is the highest for the older Cmac strata. The increase of the displacement with depth shows the synsedimentary nature of the fault.

Fault 9 is a planar, landward-dipping normal fault. There is no interaction with salt movement as it does not reach any salt layer or salt structure. The thickness of strata remains the same at hanging wall and footwall.

Fault 10-a is a basinward-dipping, arcuate normal fault. This fault bounds Minibasin 3 to the north and it soles into a salt weld. The sedimentary thickness in this minibasin caused the evacuation of salt away from the center and the nucleation of this basin-bounding fault. The displacement increases downward, and the thickness of the strata is greater in the hanging wall.

Fault 10-c is another basin-bounding fault in the cross section (Fig. 3.17). It is a landward-dipping arcuate normal fault. Minibasin 3 is bounded by this fault to the south. The strata on the hanging wall thicken basinward and the displacement increases with

depth. This fault soles into a salt weld and salt withdrawal is believed to have occurred during the Pleistocene because of the age of the older strata in the cross section.

Fault 13 is a basinward-dipping arcuate normal fault with a large triangular salt roller in its footwall. The size of the salt roller can be explained by its depth being greater than the other salt rollers in the cross section. Greater depth means more salt evacuation to this point. The fault is a basin-bounding fault and it coincides with shelf edge where the slope starts to increase. There is a landward-dipping monocline in the hanging wall of the fault and the displacement increases downward.

3.4.5.2 Horizons

The thickness of deposited sediments significantly increases basinward. The younger sediments are affected only by faulting whereas older sediments are folded and, deformed by faulting and salt movement.

3.4.5.3 Salt Structures

Salt rollers and salt walls are the prominent salt structures in this cross section (Fig. 3.17). The salt wall is an elongated upwelling of diapiric salt, commonly forming sinuous, parallel rows in time or depth sections. In this cross section, the salt wall separates two depocenters. There are two different salt sheets in the cross section. The first salt sheet situated to the right is tilted basinward. On the other hand, only just a small part of the

second salt sheet visible to the left of the cross section; therefore, the description of this salt sheet is not possible.

3.4.5.4 Minibasins

Minibasin 3 is situated to the right of the cross section. The basin is bounded by Fault 10-a to the northwest and by Fault 10-c to the southeast. The basin is the hanging wall of Fault 10-c which is a growth fault that soles into a salt roller. The salt flow causes more accommodation space for sediments; therefore sediments in the basin are tilted basinward.

CHAPTER 4: STRUCTURAL EVOLUTION

4.1 Fault Growth (T-z Plots)

A simple graphical technique to analyze the kinematic evolution of growth faults is Throw vs Depth (T-z) plots. Growth faults record the interaction between sedimentation and fault-slip history so are valuable tools to enlighten the kinematic history of the study area. T-z plots are derived from depth converted 3-D high-resolution seismic data.

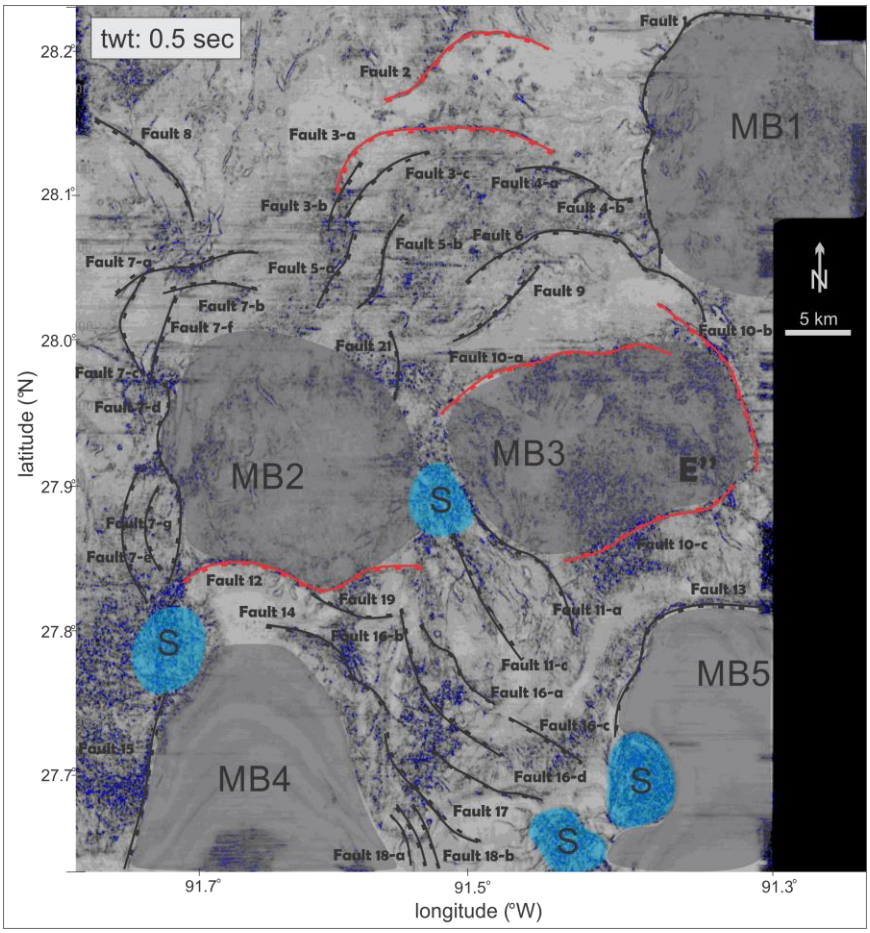

Figure 4.1: Location of faults used to plot T-z charts (Red lines). Faults are chosen from different part of the study area and they have different dipping directions.

The growth period is apparent as the sloping parts of the line and non-growth periods show zero slope in the plot. Not all interpreted faults are included in these plots and only a few representative faults with high enough displacement and length values from northern, southern and central area (basin-bounding faults) are interpreted.

Throw versus depth plots were constructed for all six faults in the study area and show variations in form (Fig. 4.1). Two of them are closely located to each other and are evaluated to see if they share a regional growth history or whether each fault has its individual growth history. In addition to T-z plot, 'fault growth vs depth column' is also created, where depth interval are assigned to either one of three types of fault activity: "rapid growth", "slow growth", and "no growth".

Fault 10-a is a basinward-dipping extensional fault that soles into a salt roller at 4690 m depth. It is one of the basin bounding fault of Minibasin 3. The maximum throw measured for this fault is 507.3 m and the age of this fault is older than 1.5 Ma because this fault cuts the Cmac horizon at 2293 m. The fault has three zero slope intervals between approximately 0.45-0.50 Ma, 0.70-0.80 Ma and 0.92-1.1 Ma. The fault has five growth phases with two slow growths and three rapid growths from the Late Pleistocene to recent. Slow growth intervals are longer than rapid growth intervals (Fig. 4.2).

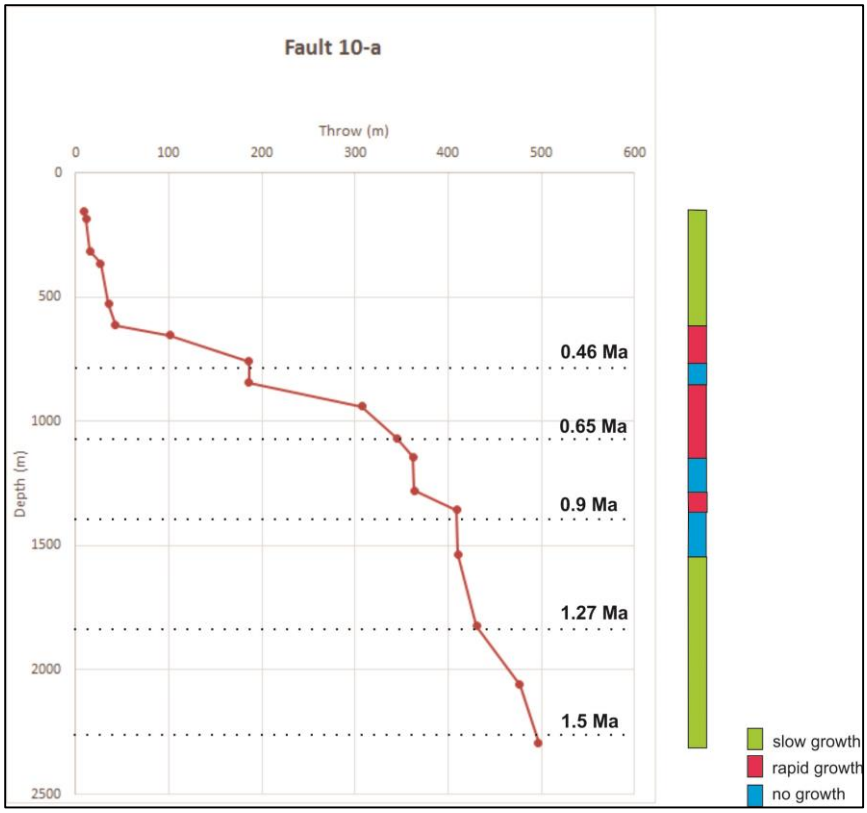

Figure 4.2: T-z plot and growth history plot for Fault 10-a. This fault has two long periods of slow growth, two short periods of growth and three periods of non-growth. Note that all three rapid growth periods are followed by a non-growth period.

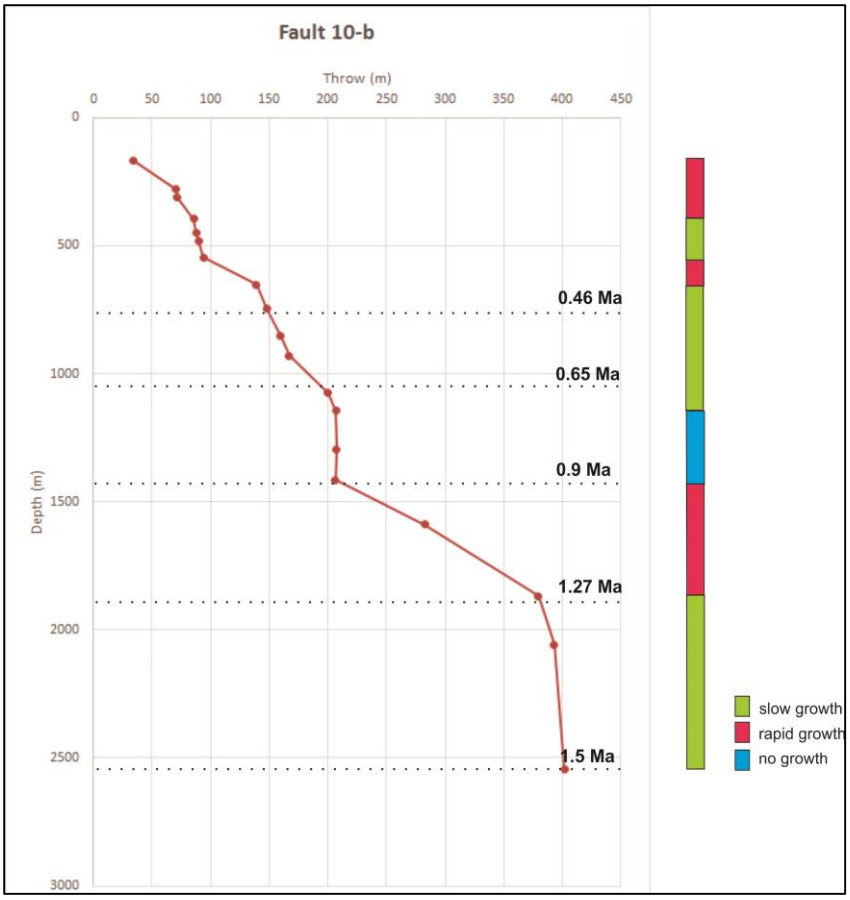

Figure 4.3: T-z plot and growth history column for Fault 10-b. This fault has three periods of rapid growth, three periods of slow growth and one period of no growth. Fault 10-b is southwest-dipping fault so the primary force for its growth could be salt movement.

Fault 10-b is a southwestern-dipping normal fault located at the northeastern edge of Minibasin 3. The fault is soling into a salt diapir at 3126 m depth. The maximum throw measured is 413.2 m and the age of this fault is older than Cmac as it cuts this horizon at 2545 m depth. The fault has only one zero slope interval between 0.65-0.9 Ma. It has three rapid growth and three slow growth intervals from the Pleistocene to recent. Slow growth intervals are longer than rapid growth intervals (Fig. 4.3).

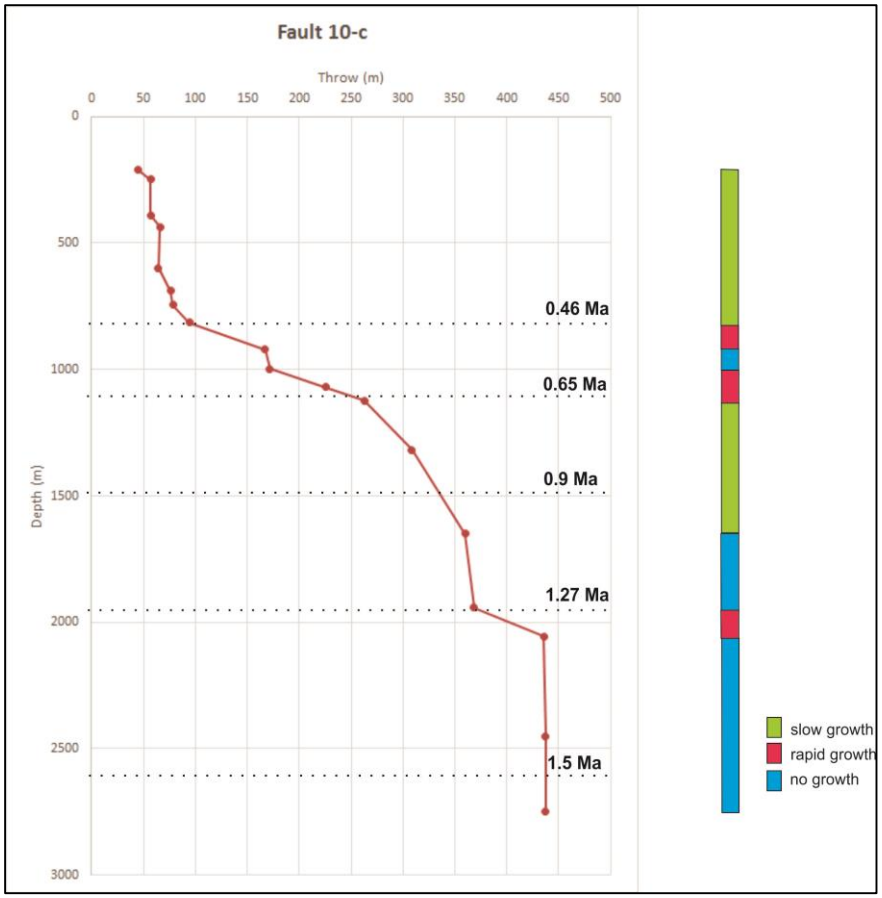

Figure 4.4: T-z plot and growth history column for Fault 10-c. This fault has two periods of slow growth, three periods of rapid growth and three periods of no growth. Fault 10-c is a landward dipping fault so it cannot be related to the regional growth pattern of the study area. This growth history is probably related to the salt movement.

Fault 10-c is a northwestern dipping normal fault located at the south edge of Minibasin 3. The fault is soling into a salt weld at 5267 m depth. The maximum throw measured is 437.5 m and the age of this fault is older than Cmac as it cuts this horizon at 2575 m depth. The fault has three zero slope intervals between 0.52-0.57, 1.1-1.25 and 1.35-1.5 Ma. It has three rapid growth and two slow growth intervals from the Pleistocene to recent. Slow growth intervals are longer than rapid growth intervals and non-growth

interval are longer than rapid growth intervals. Non-growth intervals are followed by rapid growth intervals. (Fig. 4.4).

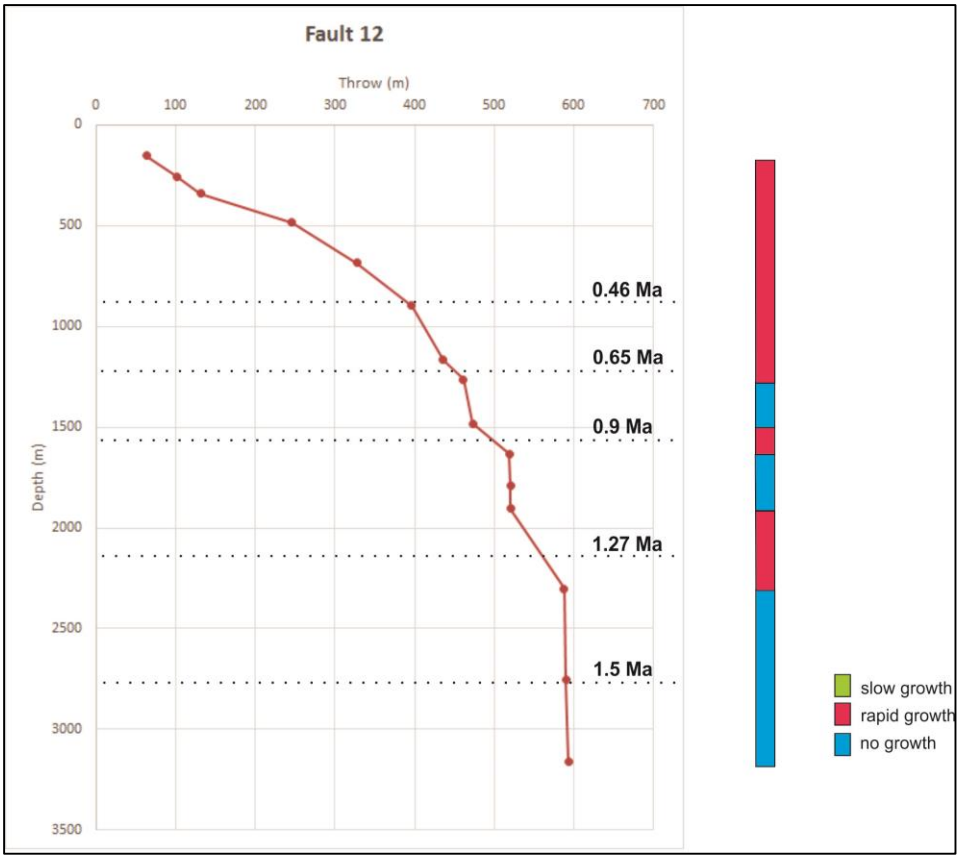

Figure 4.5: T-z plot and growth history column for Fault 12. This fault has three periods of rapid growth and three periods of no growth. There is no slow growth period for this fault, this might be explained with the location of the fault being near the shelf edge.

Fault 12 is a basinward-dipping normal fault located at the southern edge of Minibasin 2 and the northern edge of Minibasin 4. The fault is soling into a salt roller at 4227 m depth. The maximum throw measured is 593.1 m and the age of this fault is older than Cmac as it cuts this horizon at 2790 m depth. The fault has three zero slope intervals between 0.7-0.88, 0.95-1.1 and 1.35-1.5 Ma. It has three rapid growth and no slow growth

intervals from the Pleistocene to recent. (Fig. 4.5). The fact that there is no slow growth in the kinematic history of the fault implies high sediment supply or rapid sediment accumulation. The location of the fault is another explanation for the absence of the slow growth interval. Increased slope because of the shelf edge indicates rapid growth.

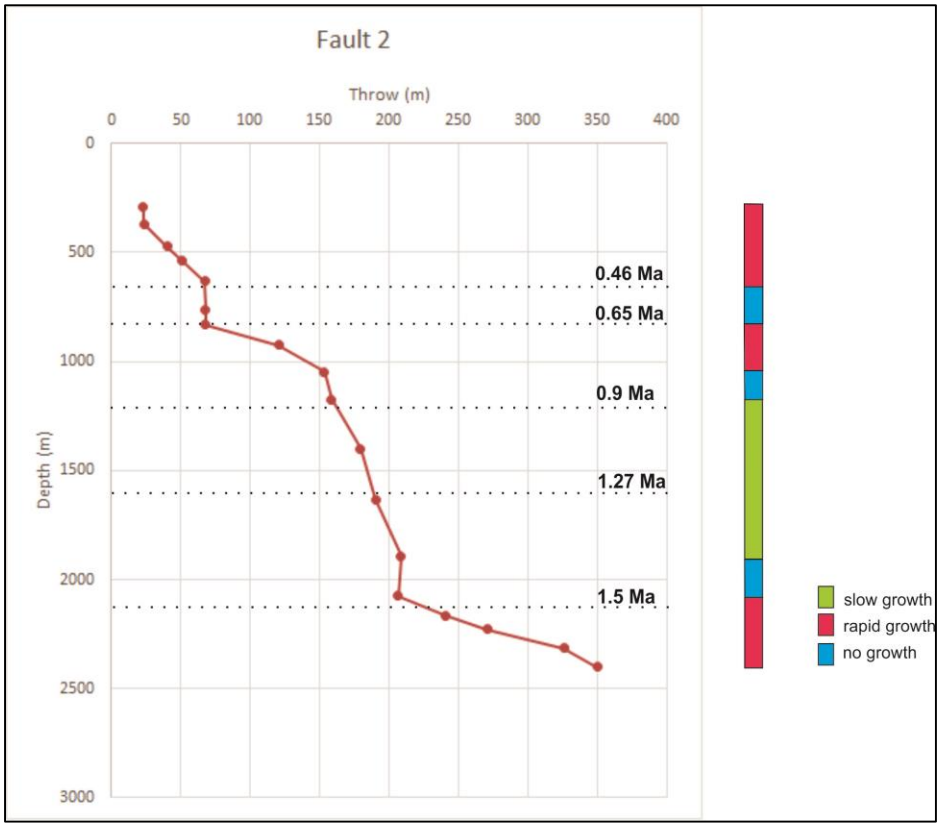

Figure 4.6: T-z plot and growth history column for Fault 2. This fault has three periods of rapid growth, one long period of slow growth and three periods of no growth. This north dipping fault's growth history might be related with the kinematic history of the region.

Fault 2 is a basinward-dipping normal fault located at the northern part of the study area. It is the first fault of a roller fault family defined in Chapter 6. The fault is soling into a salt roller at 2879 m depth. The maximum throw measured is 349.7 m and the age of this fault is older than Cmac because it cuts this horizon at 2112 m depth. The fault has three

zero slope intervals between 0.5-062, 0.78-0.85, 1.4-1.5 Ma. It has three rapid growth and one slow growth intervals from Pleistocene to recent. The slow growth interval is longer than the rapid growth intervals and rapid growth intervals are followed by non-growth intervals (Fig. 4.6). The rapid growth after 1.5 Ma can be explained with the movement of salt creating more accommodation space for sediments. The kinematic of salt movement being similar to the kinematic of faulting form a perfect environment for sediment accumulation.

Fault 3-a is a basinward-dipping normal fault located at the northern part of the study area. The fault is adjacent to Fault 2 and both of them belongs to a roller fault family. The fault is soling into a salt roller at 3077 m depth. The maximum throw measured is 615.1 m and the age of this fault is older than Cmac as it cuts this horizon at 2520 m depth. The fault has two zero slope intervals between 0.85-0.95 and 1.20-1.30 Ma. It has three rapid growth and one slow growth interval from the Pleistocene to recent. Slow growth intervals are longer than rapid growth intervals (Fig. 4.7). The rapid growth after 1.27 Ma can be explained by the same causes mentioned earlier for Fault 2. The similar kinematic timing of faulting and salt movement created more space for sediments to accumulate.

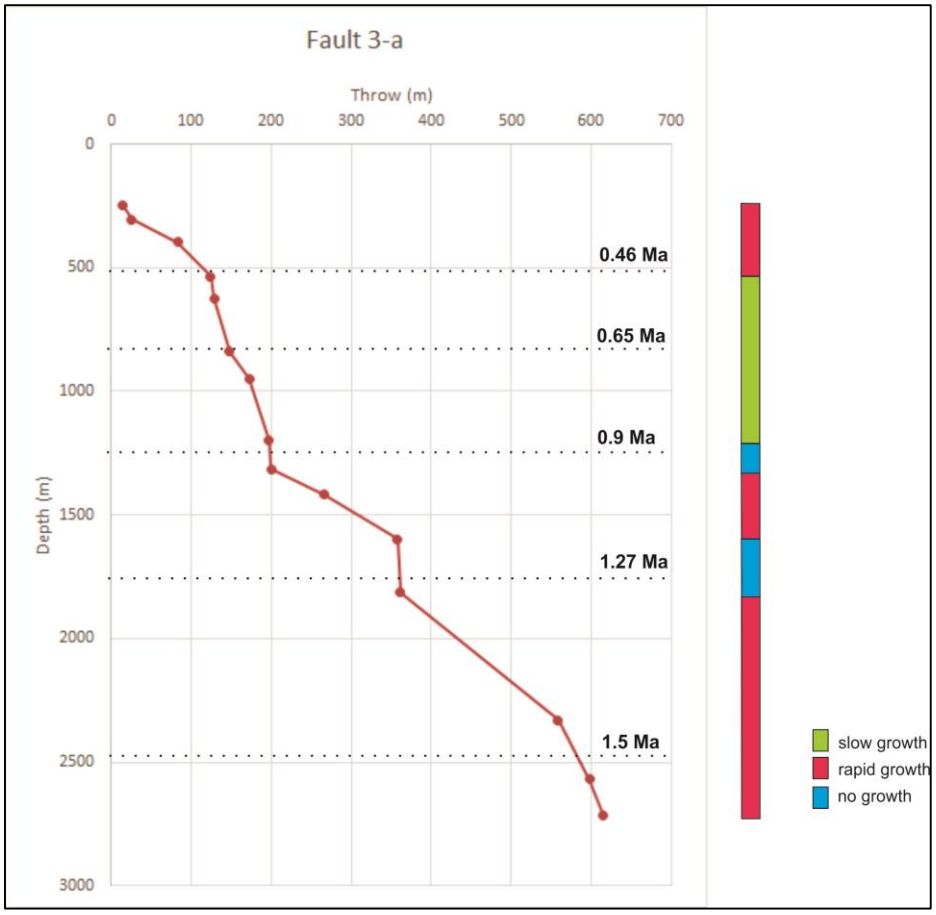

Figure 4.7: T-z plot and growth history column for Fault 3-a. This fault has one period of slow growth, three periods of rapid growth and two periods of no growth. This fault is adjacent to the Fault 2, even though they have similar growth history, they don't have the same slow growth periods.

4.2 Time-Structure Maps

Three time-structure maps are generated for YTPA, PlacA and PlacB horizons. Time–structure maps are useful to identify the relationship between different structures in the study area clearly.

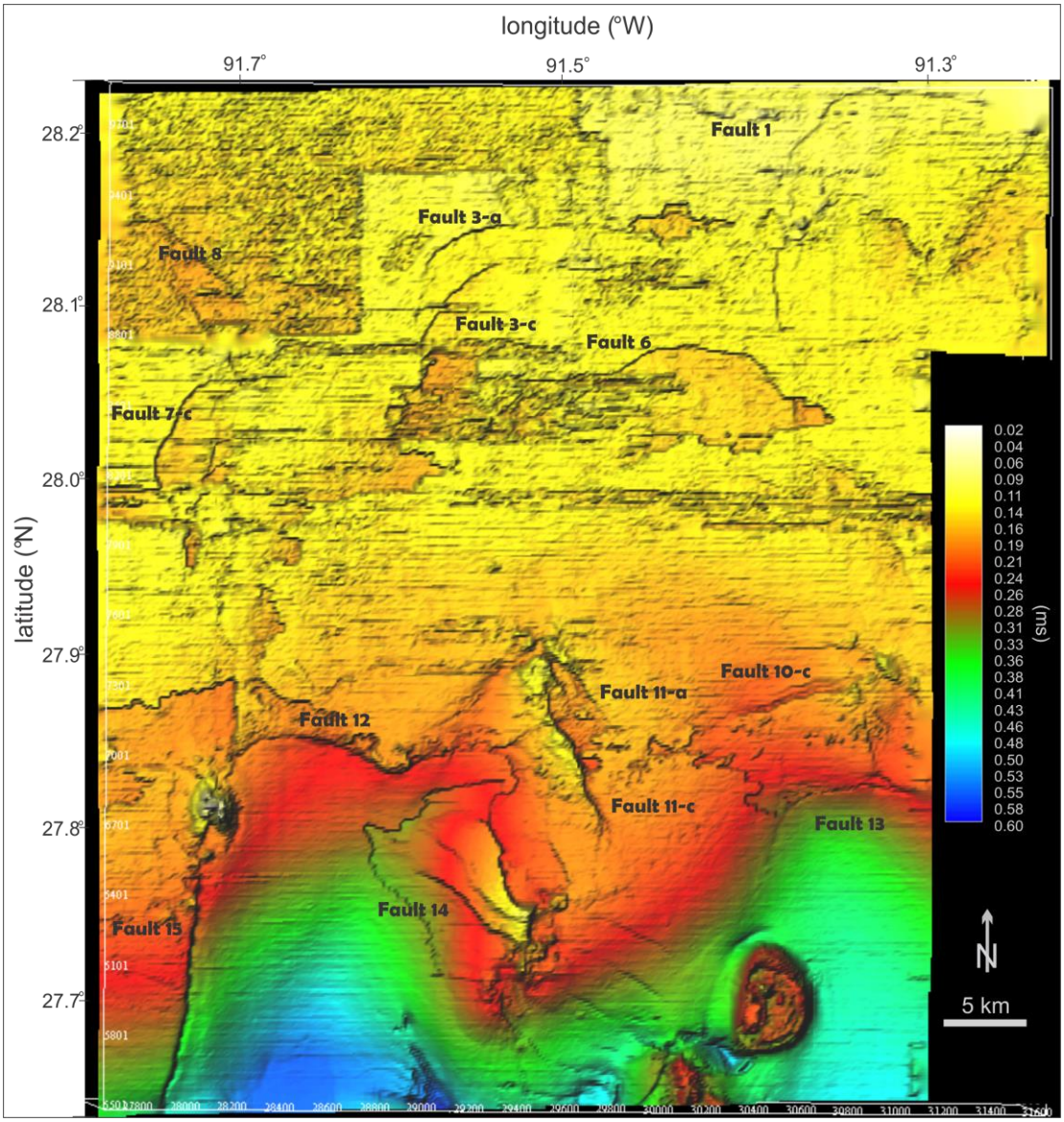

Figure 4.8: Bathymetry of the study area. The map is useful to see active faults and present day structure of the seafloor. Some faults are active and there is one diapir at the surface. These show that faulting and salt movement are still active in the study area.

The bathymetry map shows some key points (Fig. 4.8). There are several faults still active in the northern and southern parts and one diapir that reached the surface in the southeastern part of the study area. The constant depth where Minibasin 2 is located shows that there is no room for sediments and the salt evacuation is ceased. On the other hand,

landward dipping basin bounding Fault 10-c is still active and still provides accommodation space for sediments (Fig. 4.8)

Figure 4.9 shows the time-structure map for YTPA (≤ 0.49 Ma) horizon. The study area is highly faulted and the vast majority of faults are dipping basinward (Fig. 4.9). The northern part of the study area is highly affected by arcuate basinward-dipping normal faults. These basinward-dipping normal faults are called roller fault family as mentioned in the previous chapter. In the south part of the roller fault family there is a roughly circular topographic high caused by the upward movement of the salt. The roller fault family seems to be connected to each other with hard or soft linkage. This phenomenon will be discussed in detail in the next chapter.

Figure 4.10 shows the time-structure map for PlacA (0.49 Ma) horizon. The western part of the study area consists of salt diapirs connected with normal and strike-slip faults to each other. Three salt diapirs are connected by faults dipping either to the west or to the east. Each salt diapir is surrounded by small scale normal faults explained in detail in the next section.

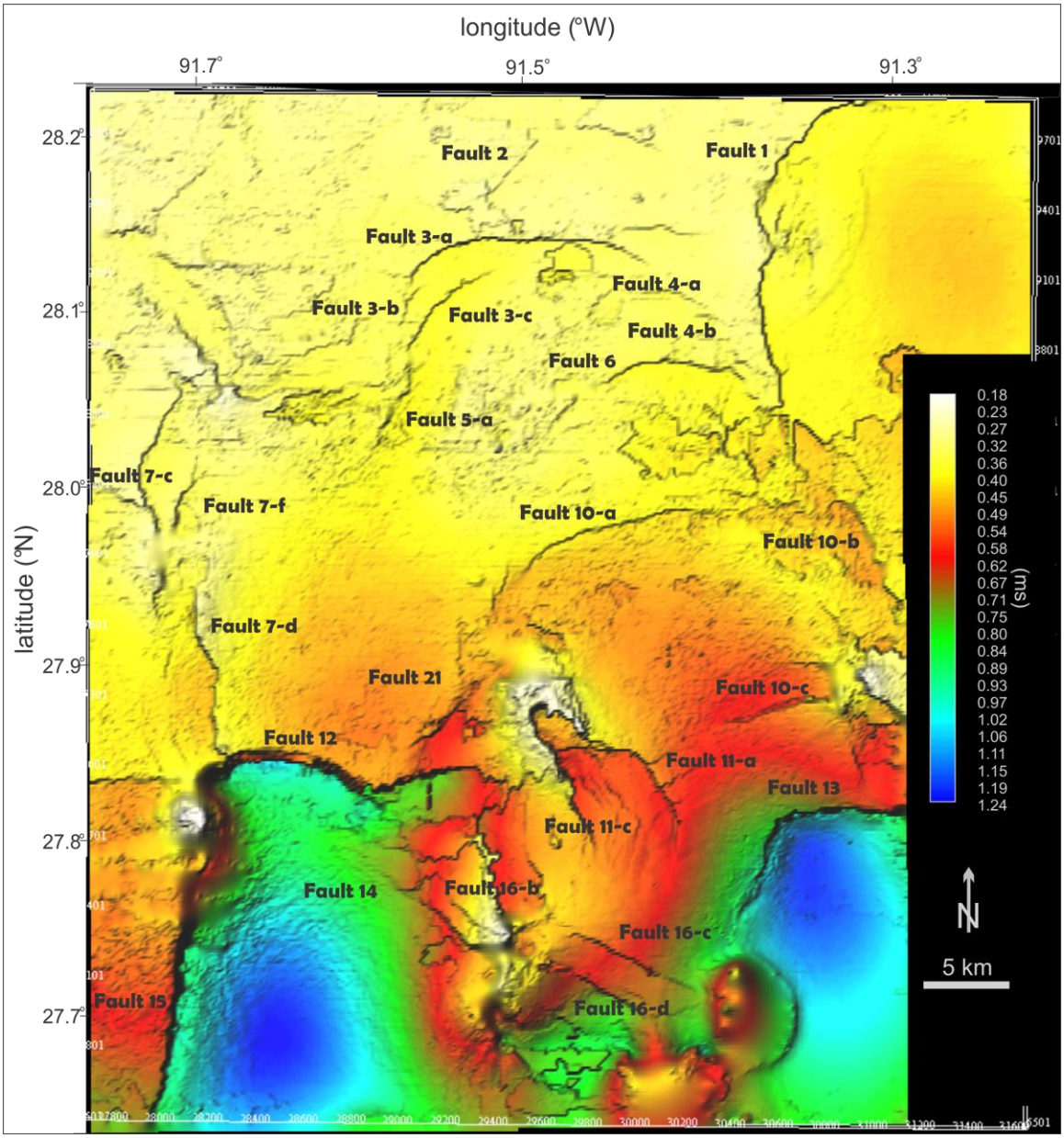

Figure 4.9: Time-structure map of YTPA horizon. The horizon deepens from north to south. The highest areas represent the horizon situated above rising salt structures.

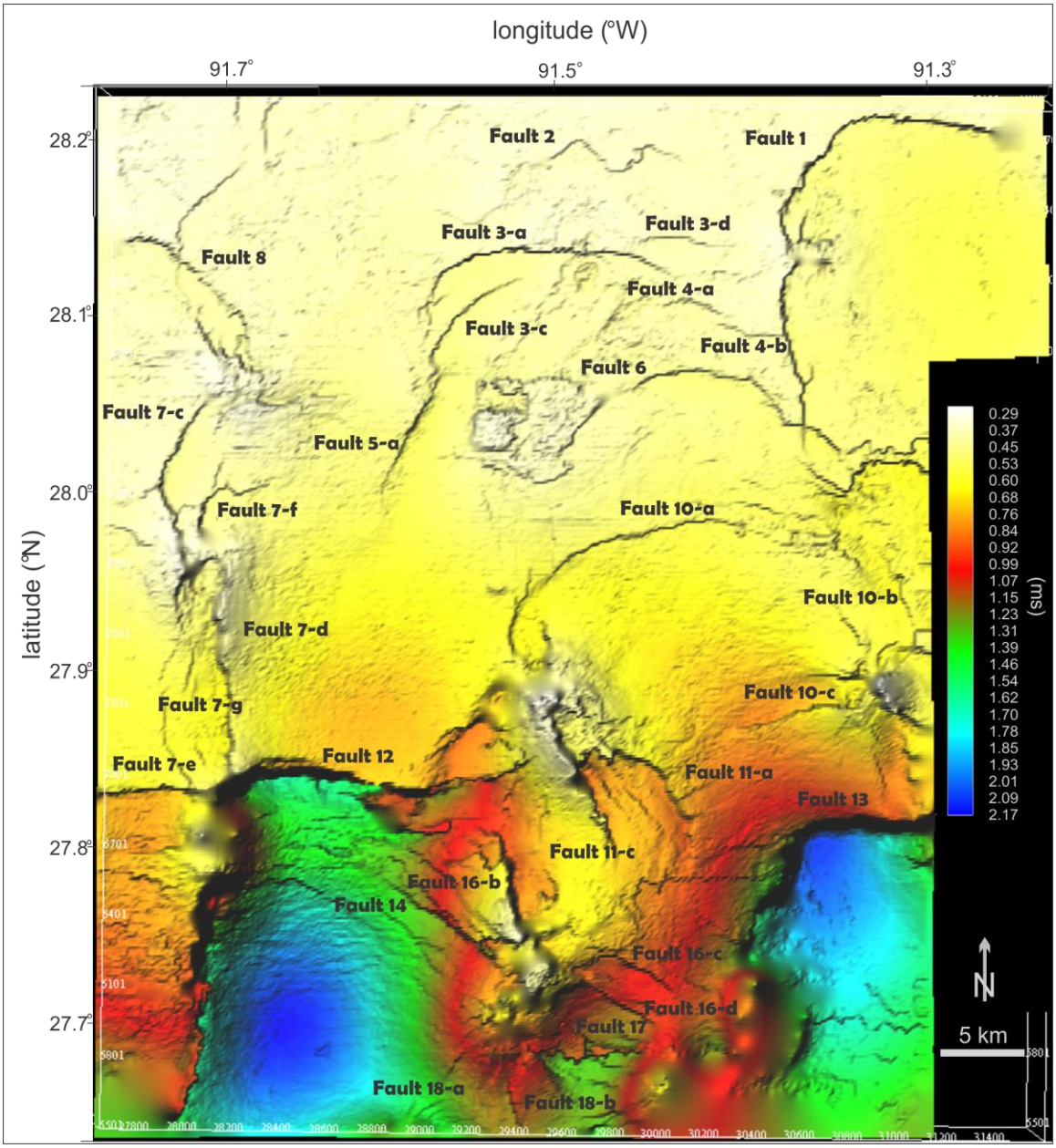

Figure 4.10: Time-structure map of PlacA horizon. The horizon deepens from north to south. The part of the horizon situated between two most southern Minibasins is highly faulted. This faulted part is caused by the rising of a salt diapir below the horizon. As the horizons get deeper, faults' displacement increases as well.

Shelf minibasins (Minibasin 2 and Minibasin 3) are situated in the central part of the map. Both minibasins are bordered by salt diapirs to the west and east (Fig. 4.10). The alignment of salt diapir indicates the possible route of the salt flow. Diapirs situated at the edges of the minibasins indicate that salt flowed to the east and west away from the central part of the minibasin. The flow direction is perpendicular to the regional north-south trend of the study area. This concludes that salt flow is a three dimensional process.

Figure 4.10 shows the time-structure map for PlacB (0.65 Ma). The increasing length of the faults are noticeable in the time-structure map. As the depth increases, their displacement and length increase (Fig. 4.8-11). There is another fault family situated near or above salt diapirs. These are called radial faults and they are small scale faults compared to the regional faults. Clausen et al., (2014) performed an experiment to study fractures formed above rising salt structures and concluded that vertical movement only results in concentric faults. On the other hand, if there is horizontal movement accompanying the vertical movement, radial faulting will result. Concentric patterns in my study area indicate an upward movement of the salt coupled with lateral movement.

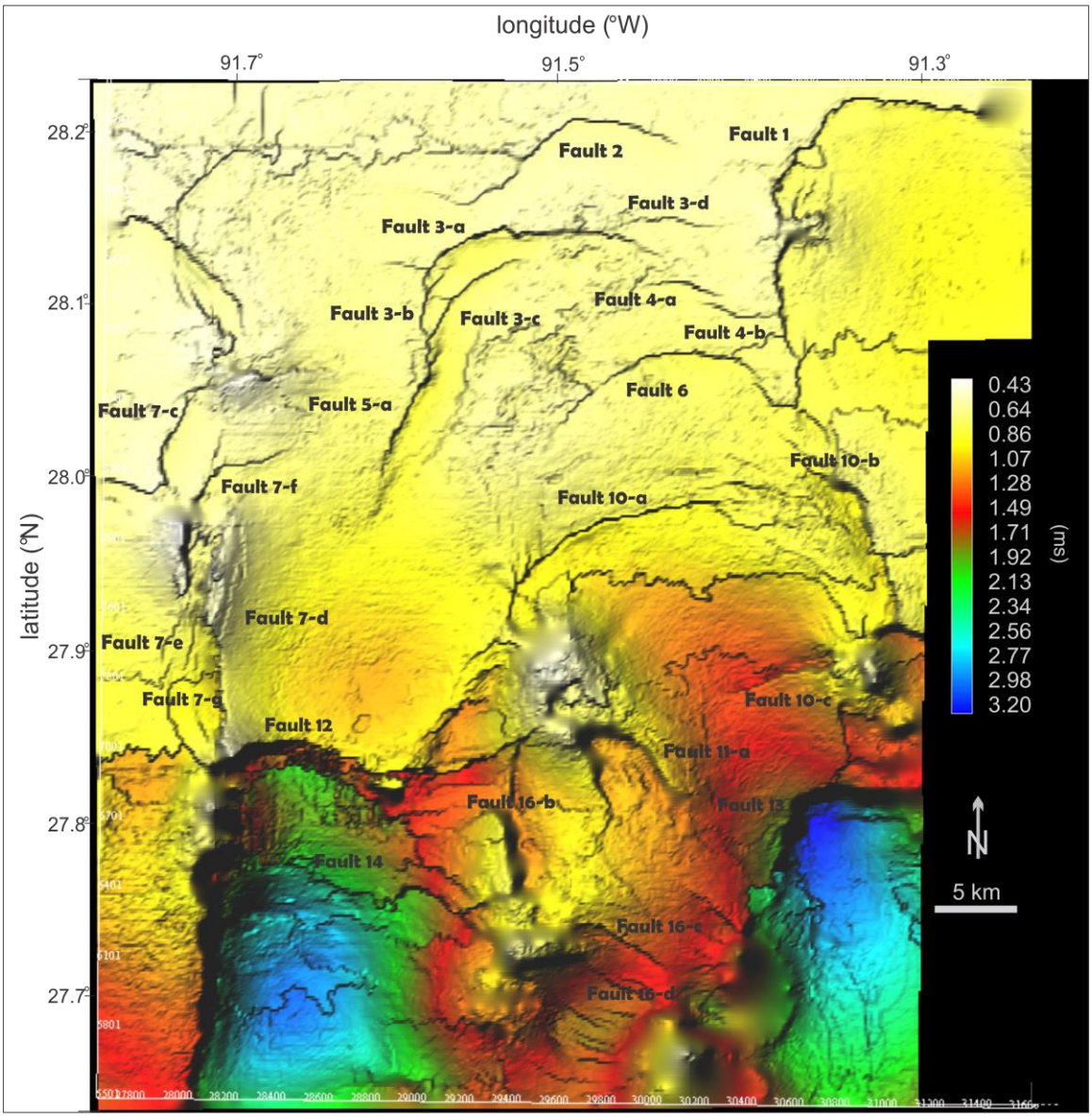

Figure 4.11: Time-structure map of PlacB. The length of faults increases with every deeper horizon. And their displacement increases accordingly. The radial faults become more prominent.

4.3 Isopach Maps

Isopach maps show the thickness between two defined surfaces. In this study, three different isopach maps are generated in order to evaluate the sedimentary thickness change in the study area. Figure 4.11 shows the sedimentary thickness between PlacA (0.49 Ma) and YTPA (<0.49 Ma) horizons. The sedimentary thickness is about 200 m in the northern part and about 800 m in the southern part of the study area.

The sedimentary thickness increases toward the south and reaches the maximum thickness of 1150 m. The sedimentary thickness is about 350 m where Minibasin 2 is located. This increasing sedimentary thickness is attributed to salt withdrawal, since there is no faulting to create more accommodation space for sediments. The minimum thickness in the southern part of the study area corresponds to the thickness of a rising salt diapir above. Since the salt pushes the sediments upwards, their thickness above the diapir thins. The maximum sedimentary thickness is observed where Minibasin 4 and Minibasin 5 are located. This thickness is related to three large faults (Fault 15, Fault 12 and Fault 13) situated at the northern and western edge of the minibasins (Fig. 4.12). The effect of salt movement remains uncertain for these two minibasins because of the depth of the data.

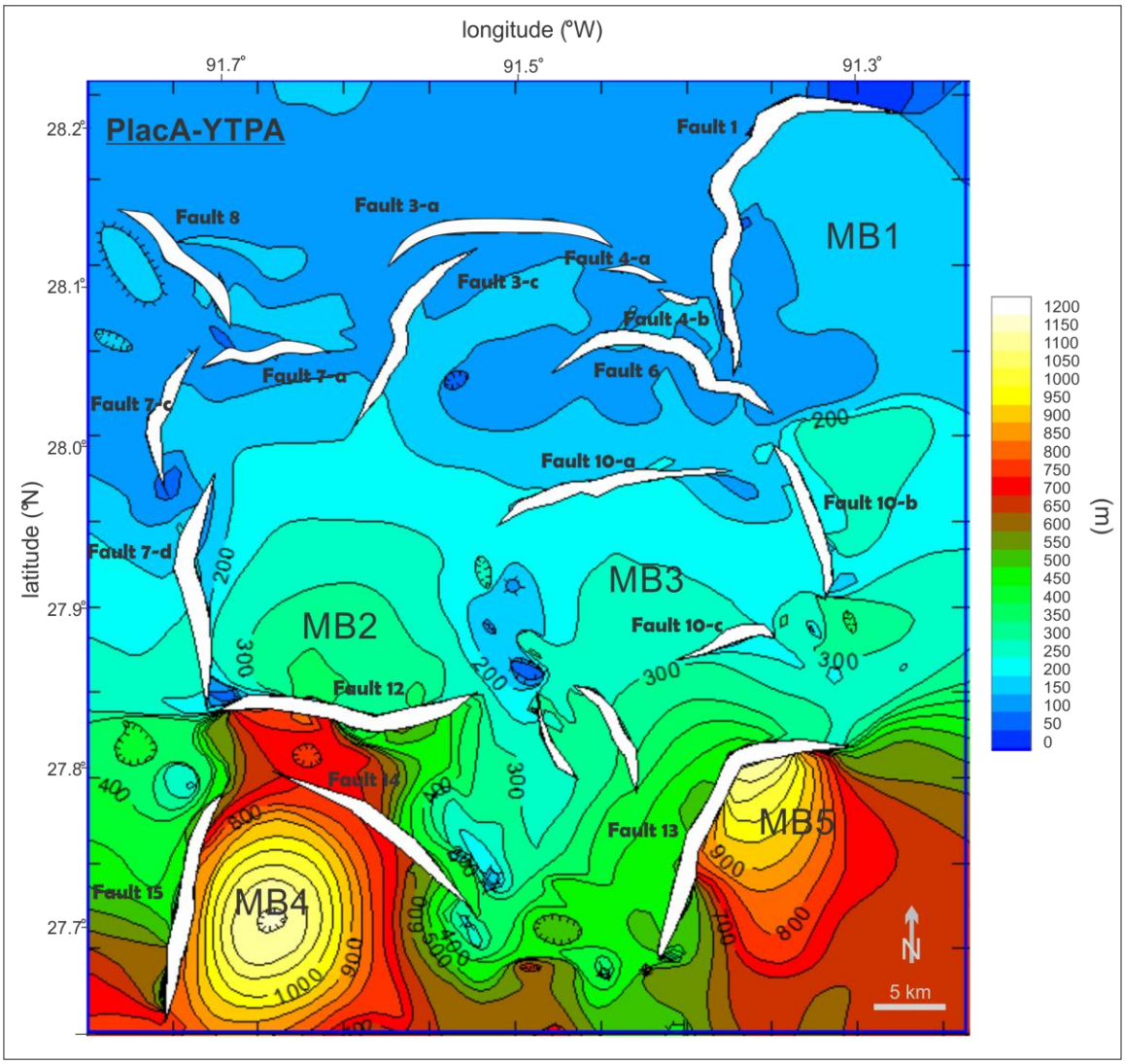

Figure 4.12: Isopach map of PlacA-YTPA. The sedimentary thickness increases toward the southern part of the study area. Faulting and possible salt movement dominate the sedimentary thickness.

Figure 4.13 shows the sedimentary thickness between PlacB (0.65 Ma) and YTPA (<0.49 Ma) horizons. The sedimentary thickness is about 600 m in the northern part and 1600 m at the southern part of the study area. The minimum thickness is observed where there is a salt diapir below the horizons and the maximum thickness is observed to south where minibasin 4 and minibasin 5 exist. The thickness of minibasin 2 is about 700 m and

the thickness of minibasin 3 1000 m. This difference in thickness can be explained by the presence of faulting and salt movement. The thickness of minibasin 2 is suggested to be dominated only by the salt movement because of the lack of evidence of faulting in the fault maps generated in the study area. On the other hand, the thickness of Minibasin 3 is believed to be controlled by both salt movement and faulting. Fault 10-a and Fault 10-b provide more accommodation space in this minibasin. The thickness decreases towards the tips of faults 10-a and 10-b.

Figure 4.14 represents the thickness between PlacB (0.65 Ma) and PlacA (0.49 Ma). The thickness increases from north to south and the thickness in the northern part is about 300 m whereas the thickness in the southern part of the study area is about 900 m. The thickest depocenter is Minibasin 5 which is bounded by Fault 13 to the north. The thickness is primarily controlled by faulting and by salt withdrawal. The contribution of salt withdrawal remains unknown due to the depth of data. The lowest thickness is observed between Minibasin 2 and Minibasin 3 where a salt diapir exists.

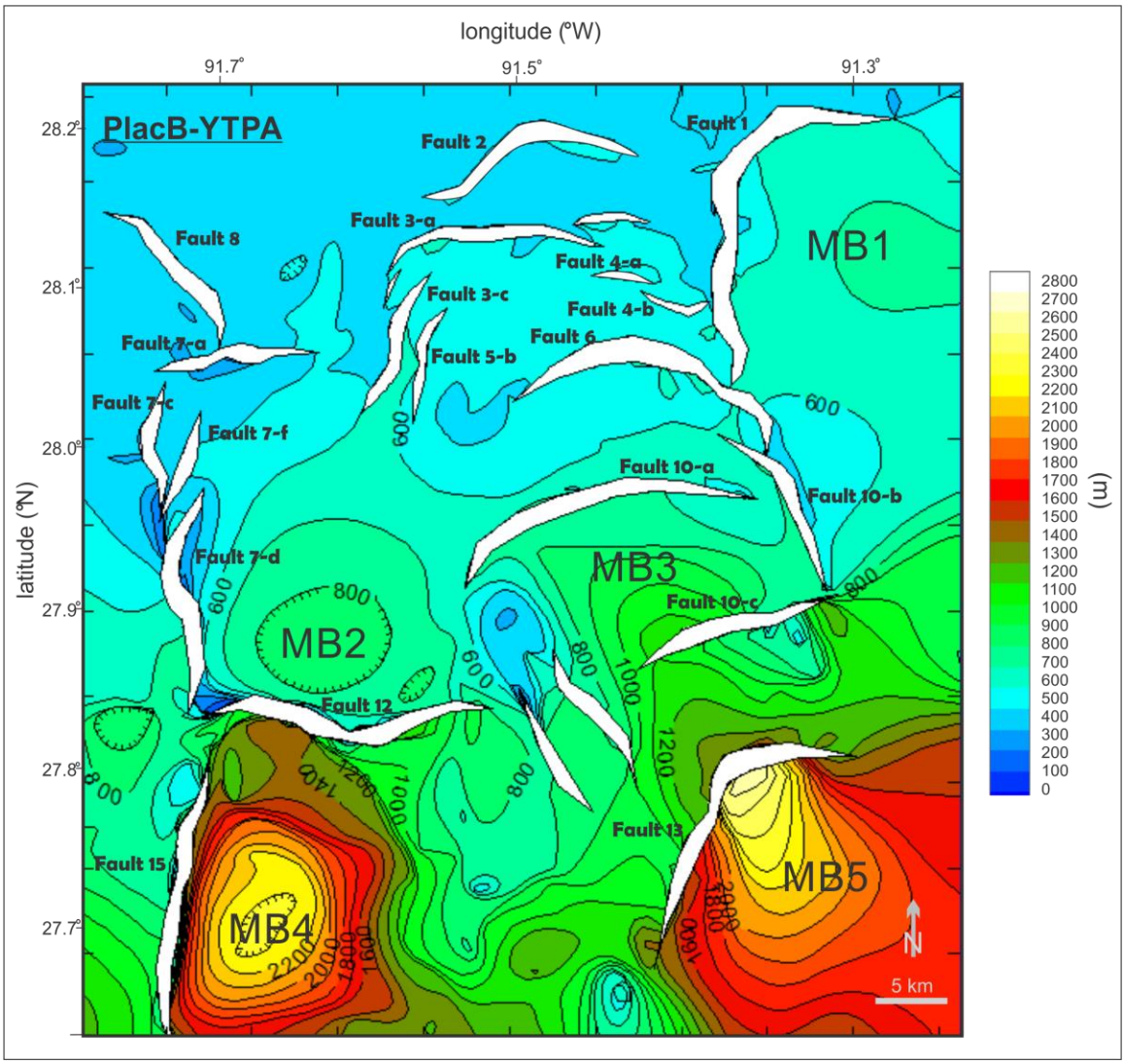

Figure 4.13: Isopach map of PlacB-YTPA. The thickness increases toward the southern part of the study area. Salt withdrawal and faulting couple are responsible for the thickness of Minibasin 3 whereas only salt withdrawal is responsible for the thickness of Minibasin 2.

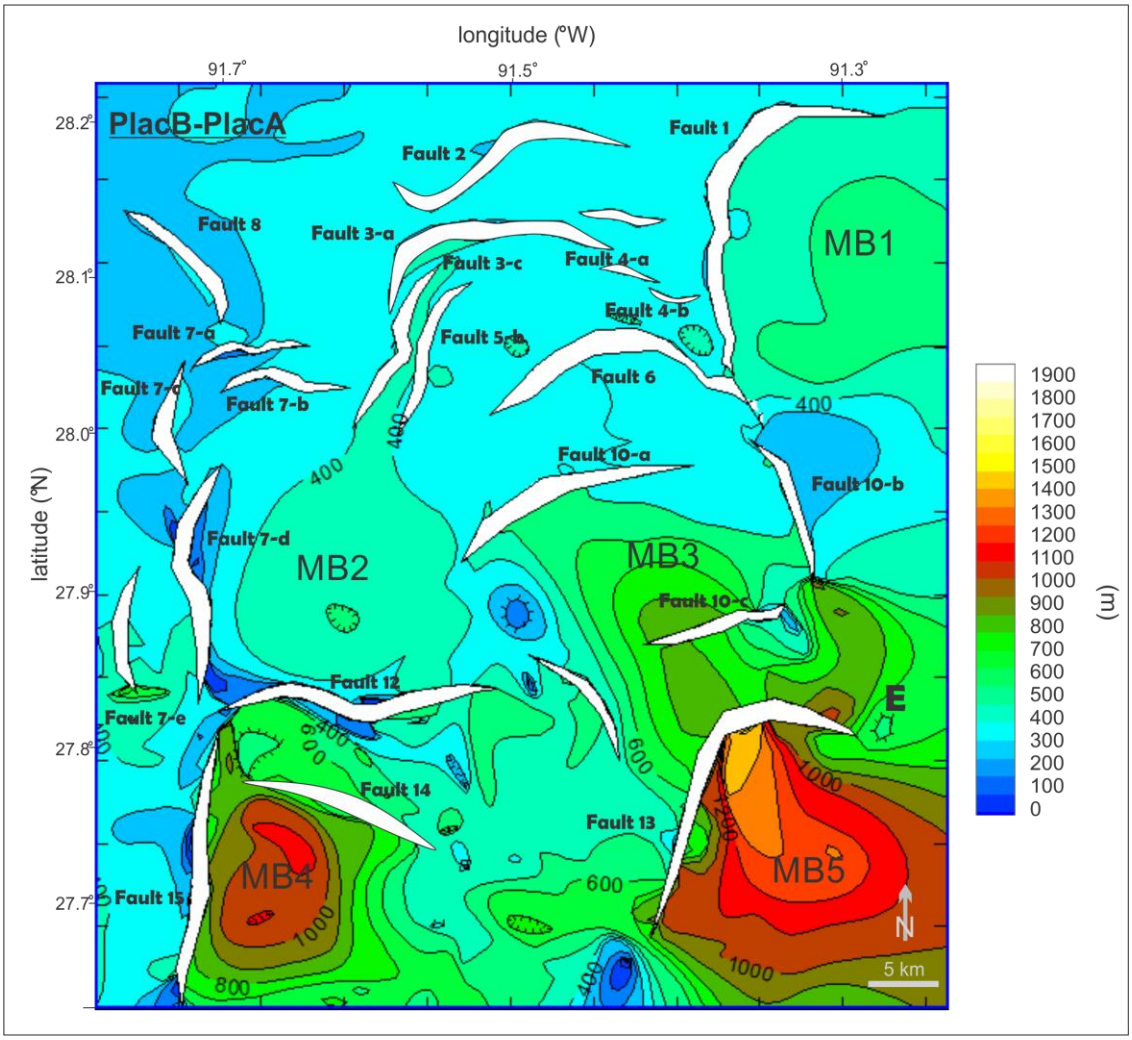

Figure 4.14: Isopach map of PlacB-PlacA. The faulting coupled with sedimentary loading increased the thickness of Minibasin 3 when compared with Minibasin 2 that has no evidence of faulting bordering itself.

4.4 Relay Ramps and Fault Linkage

In order to understand the evolution of fault segment in a context, it is important to evaluate its nature. It is now widely recognized that normal faults are segmented and a large fault is composed of multiple linked fault segments (Peacock, 2002). Four stages are identified to explain the linkage of faults: **Stage 1** is when two faults are not interacting

with each other, **Stage 2** is when two faults are connected to each other with a relay ramp, **Stage 3** is when connecting fractures are deforming the relay ramp, in other words when the relay ramp is breached, and finally **Stage 4** is when the relay ramp is totally destroyed and an irregular shaped single fault is formed (Peacock, 2002). This evolution may occur through time or it may develop spatially, down the dip of the fault zone.

In the study area, time-structure maps show the segmented nature of faults located in the northern part. In the time-structure map of PlacA horizon six relay ramps are visible: (1) relay ramp between Fault 5-a and Fault 3-c, (2) relay ramp between Fault 3-c and Fault 3-a, (3) relay ramp between Fault 3-d and Fault 3-a, (4) relay ramp between Fault 3-a and 4-a, (5) relay ramp between Fault 4-a and Fault 4-b, and (6) relay ramp between Fault 10-a and Fault 10-b. Faults are at Stage 2 with a visible relay ramp. Only the relay ramp between Fault 3-c and Fault 5-a is breached; therefore this implies that the linkage is at Stage 3 (Fig. 4.15).

Time-structure map of PlacB horizon reveals hard linked faults that are connected with a relay ramp at the time-structure map of PlacA horizon. In the shallowest depths, Fault 3-c and Fault 5-a are connected with a relay ramp and they are at Stage 2 of the fault linkage. But in this depth, the relay ramp between these faults is totally destroyed and a hard linked fault is formed (Fig. 4.16). The same hard linkage stage is occurred between Fault 3-a and 3-c. These faults are connected to each other with a relay ramp in the time-structure map of PlacA but now they are hard linked in the time-structure map of PlacB. This means that these faults have spatially different stages of relay ramp evolution. The evolution for these faults is not limited with time but also it continues with depth.

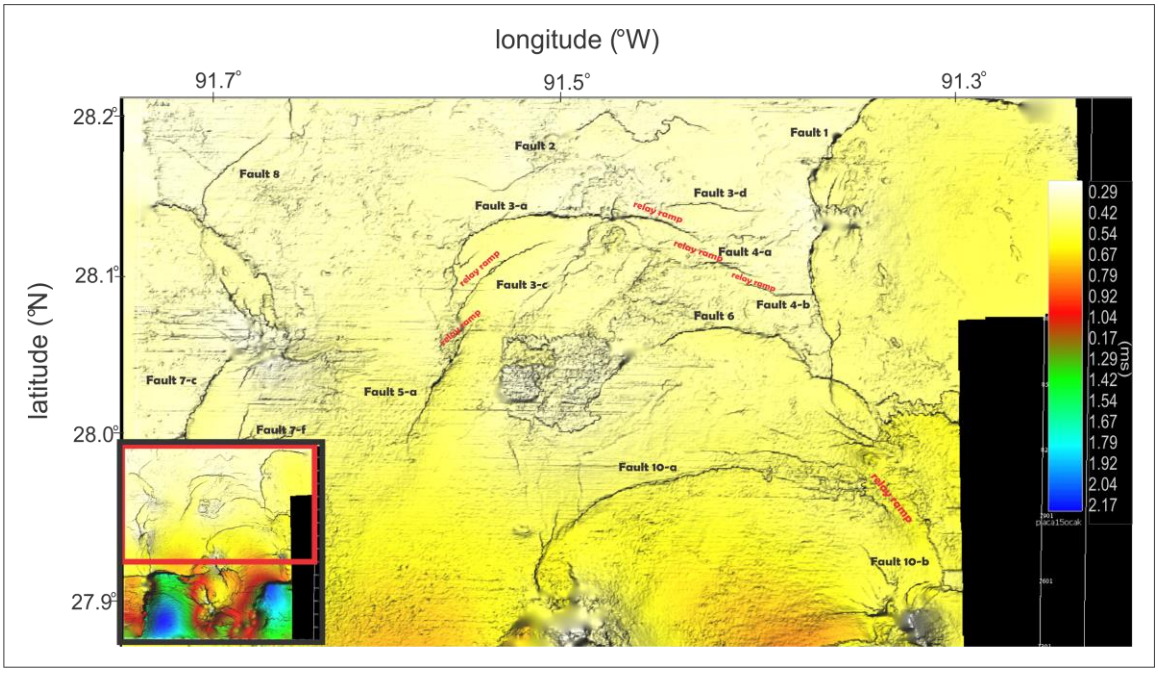

Figure 4.15: Time-structure map of PlacA horizon showing relay ramps and soft linked faults. Six relay ramps are identified in the northern part of the study area. The linkage is defined as Stage 2 which means that the faults are connected to each other with a relay ramp. Red box shows the location of the map.

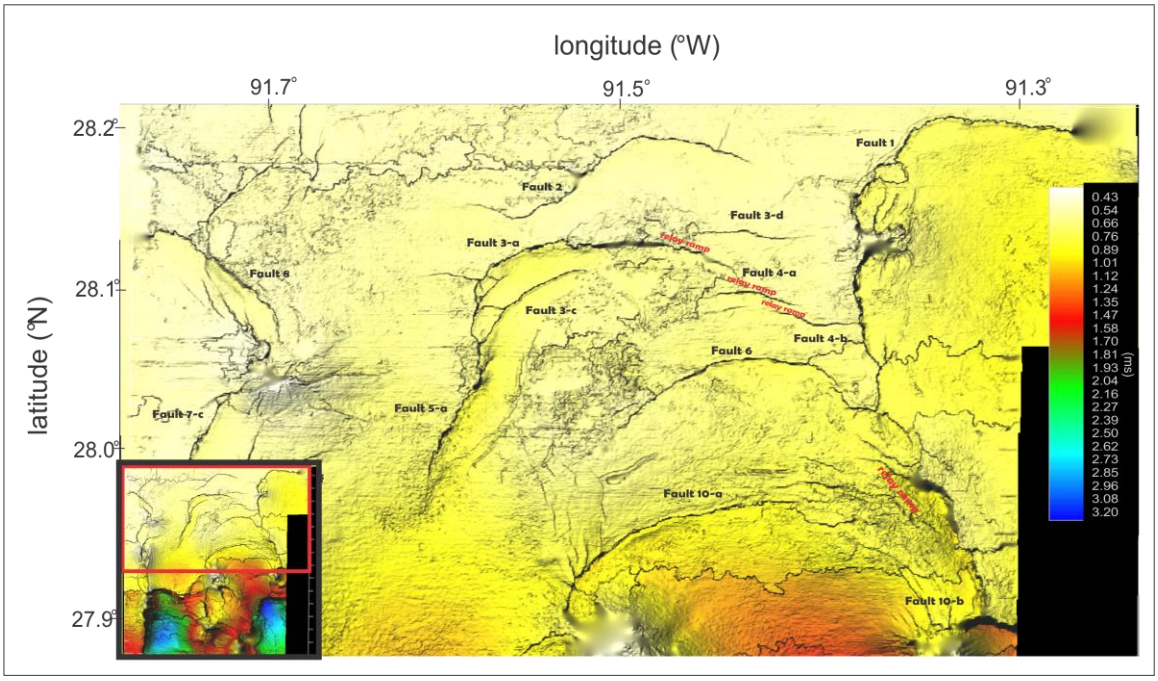

Figure 4.16: Time-structure map of PlacB horizon showing relay ramps and hard linked fault segments. Faults that are soft linked at shallower horizons now are hard linked. With greater depth, it evolves from Stage 2 to Stage 4 defined by Peacock, (2002). Red box shows the location of the map.

4.5 Kinematic Model Explaining the Relationship between Basinward Dipping Normal Faults and Basinward Striking Strike-Slip Fault

In order to understand the relation between Fault 15 which is a basinward striking strike-slip fault and the roller fault family situated in the northern part of the study area, the heave and displacement of each fault are measured using depth converted seismic section. The roller fault family consists of Fault 2, Fault 3a, 3b, 3c and 3d, Fault 4a, 4b, Fault 5a and Fault 6. Table 4.1 shows the value of displacement for each fault. The total displacement is 743 m for roller fault family and the displacement of Fault 15 is 692 m. The comparison between the total displacement of roller fault family versus the

displacement of Fault 15 shows that the motion along Fault 15 is compensated by the total displacement of the roller fault family situated in the northern part of the study area. In other words, basinward dipping normal faults and basinward striking strike-slip fault are kinematically linked to each other (Fig. 4.17).

Table 4.1: The displacement of roller fault family and basinward striking Fault 15

	Fault Name	Displacement (m)	
roller fault family	Fault 2	80 m	total displacement (m): 749 m
	Fault 3a	220 m	
	Fault 3b	25 m	
	Fault 3c	110 m	
	Fault 3d	23 m	
	Fault 4a	31 m	
	Fault 5a	220 m	
	Fault 6	50 m	
	Fault 15	692 m	

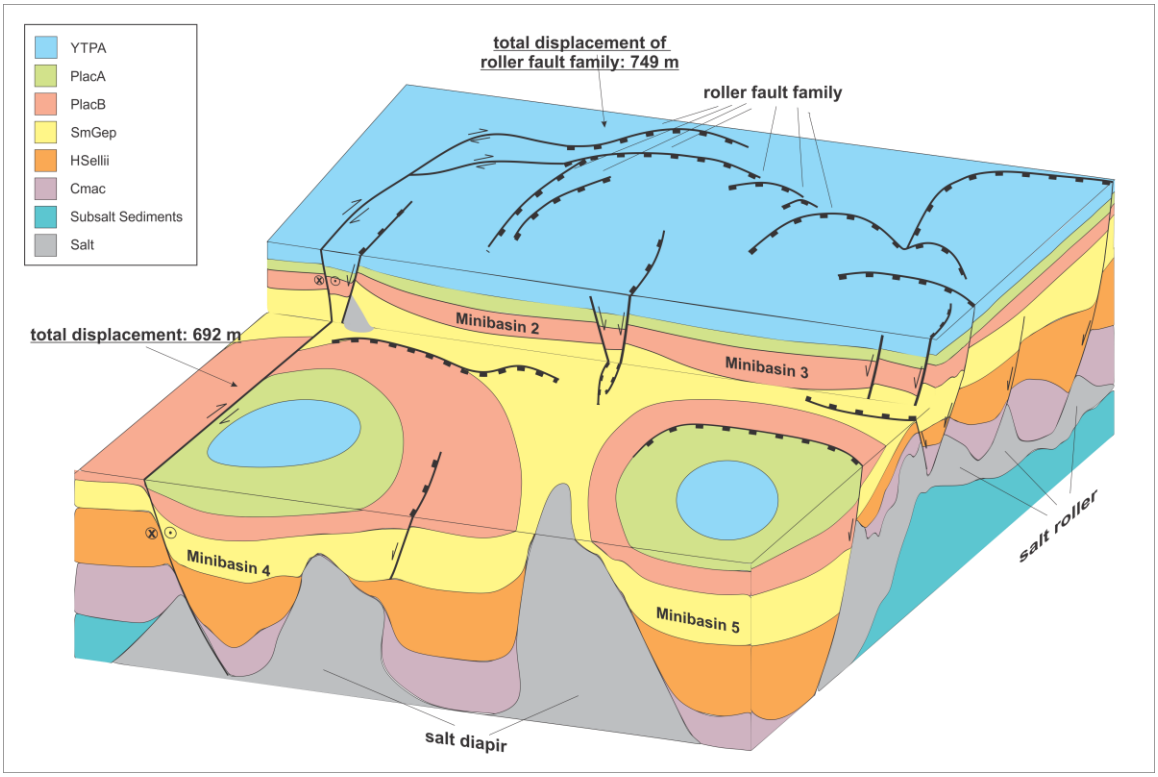

Figure 4.17: Schematic diagram of the study area showing the relationship between normal faults situated in the northern part of the study area and strike-slip fault located in the western part of the study area (Fault 15). The displacement values show that the motion of roller fault family is compensated by the horizontal displacement on the strike-slip fault.

4.6 Minibasin Formation and Evolution

The main cause of a minibasin formation is salt evacuation. Salt evacuation can be related to the instability caused by the slope or the pressure applied by overlying sediments. Interpreted seismic cross sections show that salt flow does not have any preferred direction even though continental shelf has a little slope from north to south. This indicates that the primary cause for minibasin formation is high sediment supply from the coastal area.

High sedimentation creates lateral pressure gradients on underlying salt and mobilizes it, causing salt to flow laterally and basinward. The flow of the salt layer forms a topographic low and this topographic low traps sediments coming from the coastal area. More accommodation space is created as salt continues to move away from the center of the minibasin. The salt evacuation is recognizable with the presence of a salt weld beneath the minibasin.

Once the salt is completely evacuated beneath the minibasin, the formation of new accommodation space terminates and the basin becomes infilled. During the lowstands, the progradation of shelf-margin deltas across the buried minibasins occurs. The sediment bypassing mobilizes the salt and the whole process described above starts again in order to form new minibasins. This cycle shows the basinward trend of younger minibasins in the Gulf of Mexico (Armentrout, 1987).

Rapid evacuation of the salt layer or rapid sediment infilling causes faulting along the minibasin edges. These faults are usually soles into a salt structure (salt roller, salt weld or salt diapir). This implies that the kinematics of faulting and the kinematics of salt evacuation are similar to each other (Fig. 4.18).

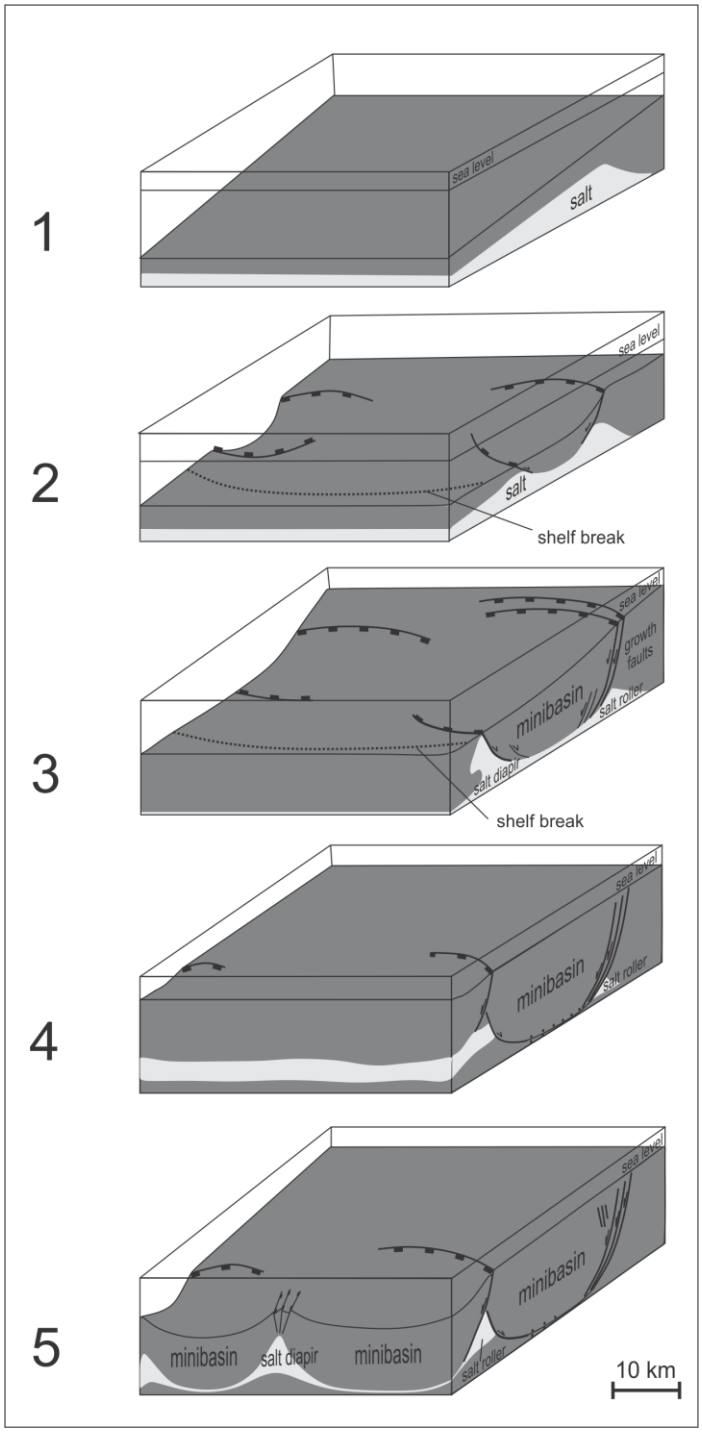

Figure 4.18: Stages of a minibasin evolution. First salt flow is triggered by the slope and then the high sediment supply causes salt to flow and creates accommodation space for sediments. Once the minibasin is infilled, sediment bypass cause the salt to mobilize and this process results in the formation of new minibasins in the basinward direction. Shelf break moves basinward and becomes invisible in later stages.

CHAPTER 5: SUMMARY AND CONCLUSION

Minibasins are common features in the Louisiana shelf and slope and they are critical for understanding both the deformation processes in the area along with petroleum production because most of the hydrocarbon production on the present-day Louisiana shelf is from traps related to shelf minibasins (Sumner et al., 1991). Thus, it is crucial to understand the evolution and interaction of minibasins with faulting and salt structures.

To understand these relationships, the workflow included generating fault maps for four time slices using the similarity attribute. The majority of the normal faults are dipping basinward which implies the gravity-driven nature of the deformation in the study area. Landward-dipping faults are compensation features that form because of subsidence during salt withdrawal. E-W dipping faults are related to intrusion of underlying salt diapirs and are usually radial faults.

Five arbitrary seismic cross sections are interpreted in order to understand the relations between faulting, salt movement, and minibasin formation. The fact that most of the faults sole into a salt structure implies that the kinematics of faulting and the kinematics of salt movement are similar. For basin-bounding faults, I propose that they are formed in response to the salt flowage away from the center of the minibasin leading to syn-depositional subsidence. This implies that the onset of salt evacuation is prior to the nucleation of basin-bounding faults.

Throw vs. Depth plots are created for six different faults that are located in different parts of the study area. The most important feature of these plots is their stepped shapes.

Intervals of increasing throw with depth are followed by intervals of constant throw with depth. Usually rapid growth periods are much shorter than slow growth periods and every rapid growth is followed by a non-growth period. Faults that are close to the shelf break exhibit only rapid and non-growth periods which can be explained with high sediment accumulation periods shown by their increased slope.

Adjacent groups of faults display strikingly different shapes for their T-z plots, with zero gradient intervals occurring commonly at different interval and with different durations even on neighboring pairs of faults. From the interpretation of zero slope intervals as periods of fault inactivity, it can be concluded that because each of the *T-z* plots has at least two zero slope intervals (except Fault 10-b which is a west-dipping, basin-bounding fault), all faults in the study area show polycyclic growth.

In the time-structure maps, they are three different fault styles: 1) basinward-dipping normal faults; 2) landward-dipping normal faults; and 3) radial faults within sedimentary layers overlying rising salt diapirs. Based on previous modeling studies, radial faults indicate that salt diapirs form from both vertical and horizontal salt displacements. Basinward-dipping and basinward-bounding faults create more accommodation space for sediments to fill in the depocenters. Once salt starts to move away from the center of minibasins, sediments start to accumulate and the sudden escape of salt initiates fault nucleation. This explains is why most of the basin-bounding and basinward-dipping faults are growth faults.

Time structure maps show fault linkage and relay ramps for basinward-dipping faults located at the northern part of the study area. In the shallower part, the linkage is at

Stage 2 with the presence of a relay ramp between previously mentioned faults (Peacock, 2002). In the deeper parts, some faults progressed to Stage 4 with a totally destroyed relay ramp. These faults form an irregular shaped single fault and this transition is visible from the time-structure map of PlacA (0.49 Ma) to time-structure map of PlacB (0.65 Ma). This transition shows that the evolution of a fault linkage may develop through time and also spatially down the dip of the fault. The presence of relay ramp in this fault family means that these faults are kinematically linked.

A conceptual block model is proposed to clarify the kinematic relationship between Fault 15 which is a strike-slip fault and the roller fault family situated in the northern part of the study area. The comparison between the total displacement of the fault family and the displacement of the strike-slip fault concludes that the extensional motion of the roller fault family is compensated by the right-lateral motion of Fault 15.

Interpreted seismic sections and time-structure maps show that salt flows laterally or downdip and does not have any primary flow direction. I propose that while the continental shelf slope likely initiates salt flowage, sedimentary loading remains the primary force that controls the salt evacuation in the study area.

Isopach maps generated for three different sequences in minibasins demonstrate the primary influence of salt withdrawal and faulting to provide accommodation space for minibasin sediments. Faulting and salt withdrawal provide the maximum space for sediment to accumulate. Without faulting, salt withdrawal alone would provide only small accommodation space. Another reason for sediment thickness difference in these minibasins might be the location of possible sediment sources compared to the location of

minibasins. One minibasin might be fed only by one source whereas other minibasins might be fed by two or more source situated close to the minibasin.

The bathymetric map of the study area (Fig. 4.8) indicates the presence of active faults and two diapirs reaching to the surface. These observations show that the salt movement and evolution is still continuing in the study area.

The greater thickness of sediments of Minibasin 4 and Minibasin 5 on the shelf compared to Minibasin 2 and Minibasin 3 on the slope has two possible explanations: 1) an effect of active growth faulting results in more accommodation space for sediments; 2) once the salt beneath the minibasin is totally evacuated, the basin is infilled because the creation of accommodation space has ceased leading to the basinward progradation of shelf edge and sediment bypassing to fill younger minibasins situated on the slope. This conclusion is similar to Alexander and Flemings (1995) who suggest that the age of minibasins decreasing basinward due to bypassing.

These conclusions coincide with results from previous studies summarized in the Chapter 1. Rowan and Weimer (1998) stated that salt influence is minimal and that the sediment influence is maximum landward. Moreover, they plotted sediment accumulation rates for six different depocenters situated close to the study area. They concluded that the sedimentation rate was highest between 0.6-0.4 Ma (Rowan and Weimer, 1998). T-z plots shows that all faults except landward dipping Fault 10-c have gone through rapid growth during this time interval. This indicates that rapid deposition is the primary cause for periods of fault motion. McBride (1995) previously concluded that deformation in Gulf of

Mexico continental shelf is mainly controlled by the progradation of sediments over allochthonous salt.

Rowan (1993) mentioned that sediment loading may create a pressure imbalance when there is a relative sea level fall. The sudden increase in sediment supply because of the prograding continental margin may lead to the lateral and vertical flow of the salt. In this study, the interpreted cross sections show that salt can flow not only in the N-S direction but also in the E-W direction.

Yapar (2013) concluded that salt kinematics is the same or at least similar to the fault kinematics. In this study, I concluded that the kinematics of salt is similar to the kinematics of faulting. The kinematics of salt movements precedes faulting in order to initiate the faulting process.

REFERENCES

Alexander, L. L., and Flemings, P. B. (1995). Geologic evolution of a Pliocene-Pleistocene salt-withdrawal Minibasin: Eugene Island Block 330, offshore Louisiana. AAPG bulletin, 79(12).

Armentrout, J. M. (1987). Integration of biostratigraphy and seismic stratigraphy: Pliocene-Pleistocene, Gulf of Mexico. Innovative Biostratigraphic Approaches to Sequence Analysis, 6-14.

Bird, D. E., Burke, K., Hall, S. A., and Casey, J. F. (2005). Gulf of Mexico tectonic history: Hotspot tracks, crustal boundaries, and early salt distribution. AAPG bulletin, 89(3), 311-328.

Bryant, W. R., Lugo, J., Cordova, C., and Salvador, A. (1991). Physiography and bathymetry. The geology of North America. The Gulf of México basin, 2, 1-18.

Buffler, R. T., and Thomas, W. A. (1994). Crustal structure and evolution of the southeastern margin of North America and the Gulf of Mexico basin. Phanerozoic evolution of North American continent-ocean transitions: Boulder, Colorado, Geological Society of America, Decade of North American Geology, Continent-Ocean Transect Volume, 219-264.

Clausen, O. R., Egholm, D. L., Andresen, K. J., and Wesenberg, R. (2014). Fault patterns within sediment layers overlying rising salt structures: A numerical modelling approach. Journal of Structural Geology, 58, 69-78.

Coleman, J. M., Roberts, H. H., and Bryant, W. R. (1991). Late Quaternary sedimentation. The Gulf of Mexico Basin: Boulder, Colorado, Geological Society of America, the Geology of North America, 325-352.

Diegel, F. A., Schuster, F. D. D., Shoup, R. C., Karlo, J. F., and Tauvers, P. R. (1995). Cenozoic structural evolution and tectono-stratigraphic framework of the northern Gulf Coast continental margin. In Salt Tectonics: a Global Perspective: Based on the Hedberg International Research Conference, Bath, UK, September 1993 (Vol. 65, p. 109). AAPG Online Bookstore.

Ewing, T. E. (1991). Structural framework. The Gulf of Mexico Basin: Geological Society of America, the Geology of North America, v. J, 31-52.

Galloway, W. E. (2008). Depositional evolution of the Gulf of Mexico sedimentary basin. Sedimentary basins of the World, 5, 505-549.

Galloway, W. E., Whiteaker, T. L., and Ganey-Curry, P. (2011). History of Cenozoic North American drainage basin evolution, sediment yield, and accumulation in the Gulf of Mexico basin. Geosphere, 7(4), 938-973.

Gore, R. H. (1992) the Gulf of Mexico. Pineapple Press, Inc, Sarasota Florida.

Hudec, M. R., Jackson, M. P., and Schultz-Ela, D. D. (2009). The paradox of Minibasin subsidence into salt: Clues to the evolution of crustal basins. Geological Society of America Bulletin, 121(1-2), 201-221.

Jackson, M. P. A., and Cramez, C. (1989). Seismic recognition of salt welds in salt tectonics regimes. In Gulf of Mexico salt tectonics, associated processes and exploration potential: Gulf Coast Section SEPM Foundation 10th Annual Research Conference (pp. 66-71).

Jackson, M. P., and Galloway, W. E. (1984). Structural and depositional styles of Gulf Coast Tertiary continental margins: application to hydrocarbon exploration.

Jackson, M. P. A. and Talbot, C. J. (1991) A glossary of salt tectonics. In: Geological Circular 91-4, Bureau of Economic Geology, University of Texas at Austin, 44pp.

Konyukhov, A. I. (2008). Geological structure, evolution stages, and petroliferous complexes of the Gulf of Mexico basin. Lithology and Mineral Resources, 43(4), 380-393.

Martin, R. G. (1978). Northern and eastern Gulf of Mexico continental margin: stratigraphic and structural framework. Framework, facies, and oil-trapping characteristics of the upper continental margin: AAPG Studies in Geology, 7, 21-42.

McBride, B. C. (1998). The evolution of allochthonous salt along a megaregional profile across the northern Gulf of Mexico Basin. AAPG bulletin, 82(5B), 1037-1054.

McBride, B. C., Weimer, P., and Rowan, M. G. (1998). The effect of allochthonous salt on the petroleum systems of northern Green Canyon and Ewing Bank (offshore Louisiana), northern Gulf of Mexico. AAPG Bulletin-American Association of Petroleum Geologists, 82(5), 1083.

Peacock, D. C. P. (2002). Propagation, interaction and linkage in normal fault systems. Earth-Science Reviews, 58(1), 121-142.

Peel, F. J., Travis, C. J., and Hossack, J. R. (1995). Genetic structural provinces and salt tectonics of the Cenozoic offshore US Gulf of Mexico; a preliminary analysis. Salt Tectonics, AAPG Memoir, 65, 153-175.

Rowan, M. G. (1993). A systematic technique for the sequential restoration of salt structures. Tectonophysics, 228(3), 331-348.

Rowan, M. G., Hart, B. S., Nelson, S., Flemings, P. B., and Trudgill, B. D. (1998). Three-dimensional geometry and evolution of a salt-related growth-fault array: Eugene Island 330 field, offshore Louisiana, Gulf of Mexico. Marine and petroleum geology, 15(4), 309-328.

Rowan, M. G., Jackson, M. P., and Trudgill, B. D. (1999). Salt-related fault families and fault welds in the northern Gulf of Mexico. AAPG bulletin, 83(9), 1454-1484.

Rowan, M. G., and Ratliff, R. A. (2012). Cross-section restoration of salt-related deformation: Best practices and potential pitfalls. Journal of Structural Geology, 41, 24-37.

Rowan, M. G., and Weimer, P. (1998). Salt-sediment interaction, northern Green Canyon and Ewing bank (offshore Louisiana), northern Gulf of Mexico. AAPG bulletin, 82(5B), 1055-1082.

Salvador, A. (1987). Late Triassic-Jurassic paleogeography and origin of Gulf of Mexico basin. Am. Assoc. Pet. Geol., Bull.; (United States), 71(4).

Salvador, A. (1991). Origin and development of the Gulf of Mexico basin. The Gulf of Mexico Basin, 389-444.

Sawyer, D. S., Buffler, R. T., and Pilger Jr, R. H. (1991). The crust under the Gulf of Mexico Basin. The Gulf of Mexico Basin: Geological Society of America, The Geology of North America, v. J, 53-72.

Seni, S. J. (1992). Evolution of salt structures during burial of salt sheets on the slope, northern Gulf of Mexico. Marine and Petroleum Geology, 9(4), 452-468.

Shoup, R., and Karlo, J., Structural systems of the northwestern Gulf of Mexico; AAPG Student course, 100 pp, 1993.

Sumner, H. S., Robinson, B. A., Dirks, W. K., and Holliday, J. C. (1991). Morphology and evolution of salt/mini-basin systems: Lower shelf and upper slope, central offshore Louisiana. AAPG Bulletin (American Association of Petroleum Geologists); (United States), 75(CONF-910403).

Weimer, P., Varnai, P., Budhijanto, F. M., Acosta, Z. M., Martinez, R. E., Navarro, A. F., and Pulham, A. J. (1998). Sequence stratigraphy of Pliocene and Pleistocene turbidite systems, northern Green Canyon and Ewing Bank (offshore Louisiana), northern Gulf of Mexico. AAPG bulletin, 82(5), 918-960.

West, D. B. (1989). Model for salt deformation on deep margin of central Gulf of Mexico basin. AAPG Bulletin, 73(12), 1472-1482.

Worrall, D. M. and Snelson, S. (1989) Evolution of the northern Gulf of Mexico, with emphasis on Cenozoic growth faulting and the role of salt. In: The Geology of North America --An Overview (Eds A. W. Bally and A. R. Palmer), Vol. A, Geological Society of America, Boulder, CO, pp. 97-138

Wu, S., Bally, A. W., and Cramez, C. (1990). Allochthonous salt, structure and stratigraphy of the north-eastern Gulf of Mexico. Part II: Structure. Marine and Petroleum Geology, 7(4), 334-370.

Yapar, O. (2013). Investigation of the interaction between salt movement, faulting and deposition, using high resolution 3-D seismic data, Eugene Island South Addition, Gulf of Mexico.